Criticality of Nodal Semimetals

Mikolaj D. Uryszek

A dissertation submitted in partial fulfillment
of the requirements for the degree of
Doctor of Philosophy
of
University College London

Departament of Physics
University College London
August 22, 2022

I, Mikolaj Uryszek, confirm that the work presented in this thesis is my own. Where information has been derived from other sources, I confirm that this has been indicated in the thesis.

Abstract

In this thesis we investigate interaction driven quantum phase transitions of semimetals with a point-like Fermi surface. The most famous example of a member of this family is graphene, which at half-filling hosts gapless fermionic excitations that are Dirac like, i.e. disperse linearly. Unlike in conventional metals the density of states vanishes at the Fermi level, which in turn promises novel correlations due to the reduced phase space available to fluctuations. When subject to strong short-ranged interactions these systems undergo a phase transition into a broken symmetry phase where the excitations become gapped. However due to the gapless nature of the fermionic excitations in the semimetallic phase it is not possible to describe the criticality using a Ginzburg-Landau type theory which only contains bosonic order parameter degrees of freedom. The low-energy theory best equipped for these so-called fermionic quantum criticality problems is that of the Yukawa-type effective field theory which couples the dynamical order parameter field to the fermions.

With the use of Renormalisation Group (RG) we study the critical phenomena of the quantum phase transition from a nodal-point semimetal to charge density wave (CDW) insulator. We showcase that the screening of order parameter fluctuations by particle-hole excitations is crucial. Without inclusion of this non-perturbative effect the RG flows contain non-universal dependence on the momentum shell cutoff scheme. We compute the exact critical exponents for the case of Dirac and semi-Dirac fermions in two spatial dimensions up to linear order in $1/N_f$ where N_f is the number of fermionic flavours. Lastly we consider the effects of non-magnetic disorder on a Dirac semimetal to CDW phase transition, and find a new disordered interacting fixed point which gives rise to non-Fermi liquid behaviour. We investigate the scaling of physical observables at this critical fixed point.

Impact Statement

The study of quantum phase transitions of semimetals is key to understanding how their properties behave under a variety of conditions, knowledge without which technological applications won't be developed. Graphene particularly has various excellent properties with which come great opportunities for applications like battery storage, bio-membranes for water filtration, and countless other electronics. Hence the work presented here could be useful to experimentalists within academia and industry alike. Our work which has shed light on the importance of dynamical screening near criticality should be highly relevant to researchers studying quantum phase transitions in strongly correlated materials that exhibit gapless fermionic excitations.

Acknowledgements

Firstly, I would like to thank my supervisor Dr. Frank Krüger for his scientific and pastoral support over these past four years. His passion for physics and teaching made the PhD extremely enjoyable and trouble-free. I am indebted to the numerous hours he spent with me discussing the intricacies of our calculations and the broader picture. Aside from the science, our tennis matches and outings to the pub resulted in my opinion a happier group and a more productive one. Secondly my PhD would have not been the same if not for Elliot Christou. His excellence in research and on the tennis court in my opinion is second to none, and without which I wouldn't have achieved as much as I did.

I would also like to thank Andrew Green, Huanzhi Hu, Adam Walker, and Jennifer Li for fruitful discussions, and numerous shared lunches at UCL. The past four years wouldn't have been as easy and as enjoyable without my housemates - Ben Kolbeck, James Mills and Connor Hall - with whom I shared every high and every low. There are numerous friends I would also like to thank, they are (in alphabetical order)- Joe Ader, Harry Barlow, Alice Berry, Toby Brazier, Peter Brumby, Hugh Collins, Nick Fryman, Lewis Humphreys, Jasper Cattell, Tom Kelly, Olivia Mason, Chris Mathias, Sam Norrington, Olivia Palacci, Jo Paisley, Tom Posa, Wilf Scott, Shant Singh, Iona White and Henry Woods.

I have a special place in my heart for the Race4Rene crew as well as Max and Sophia Zamudio. An Atlantic crossing I will never forget, for René who is always on my mind.

Lastly I would like to thank my parents, Anna and Dariusz, as well as my sister Ula. Without their undying support and love I wouldn't be where I am right now. Their perseverance and hard work set a standard that I hope to achieve.

Contents

List of Figures

Publications

Part of the work presented in this thesis has given rise to the following publications:

1. *"Quantum criticality of semi-Dirac fermions in 2+1 dimensions"*
   M. D. Uryszek, E. Christou, A. Jaefari, F. Krüger, B. Uchoa
   Physical Review B, **100**, 155101 (2019)

2. *"Fermionic criticality of anisotropic nodal point semimetals away from the upper critical dimension: Exact exponents to leading order in* $\frac{1}{N_f}$*"*
   M. D. Uryszek, F. Krüger, E. Christou
   Physical Review Research, **2**, 043265 (2020)

3. *"Interplay of interactions and disorder at the charge density wave transition of two-dimensional Dirac semimetals"*
   M. D. Uryszek, F. Krüger
   Physical Review B, **105**, 075143 (2022)

Chapter 1

Introduction

Understanding the phases of a material and how they might transition from one to another has been at the forefront of scientific pursuit from time immemorial. This is partly due to the fact that phase transitions are ubiquitous in our every day life; liquid water to water vapour or liquid water to ice are two we experience first hand most days. Slightly further away from everyday life, compounds known as the cuprates upon variations of temperature and/or can transition into a number of exotic phases like high temperature superconductivity or into a Mott insulating antiferromagnetic state. Moreover, a thorough understanding of the properties of a material under a variety of conditions is essential to effective application in real world technologies; computer chip makers need to be sure that all of their components will retain their properties over a range of temperatures and currents/voltages.

At a glance the problem of describing the properties and dynamics of 10^{23} particles within a typical system of interest is intractable. Writing down the Schrödinger equation for that many degrees of freedom would be neither possible, nor actually instructive. Knowing the individual positions of the particles would not be helpful in obtaining the thermodynamic properties of the system which we are most interested about. To make the connection from the microscopic to the macroscopic it is imperative to use the language and the theory of statistical mechanics. At the heart of it, is the partition function $\mathcal{Z}$ which encapsulates the possible configurations of all of its degrees of freedom,

$$\mathcal{Z} = \mathrm{Tr}\, e^{-H/k_B T} \tag{1.1}$$

where H is the Hamiltonian of the system, k_B is Boltzmann's constant, T is the temperature of the system, and Tr denotes a sum over all degrees of

freedom. From the partition function it is possible to obtain the free energy $F = -k_B T \log \mathcal{Z}$, from which we are able to calculate the thermodynamic properties like the specific heat capacity, entropy etc., which are its derivatives with respect to external parameters like temperature, magnetic field, and so on.

A phase transition occurs at the point in parameter space where the thermodynamic potential becomes singular[1]. An early classification of phase transitions was proposed by P. Ehrenfest, into either first-order or second-order. The nomenclature comes from lowest order of the derivative of the free energy with respect to an external parameter to be discontinuous across the transition. In practice a more accurate classification defines transitions to be either discontinuous (first-order) or continuous (second and higher orders), the major difference between the two is that the former involves latent heat which is the energy released as you transition from a high-temperature to low-temperature phase. An example of which is the transition from liquid water to ice.

A continuous transitions attains its name from the fact that macroscopic properties of the system do not exhibit a discontinuity across the phase transition. The prototypical example of this is the ferromagnetic-paramagnetic transition of Iron in zero external magnetic field which occurs at 1040K. As you approach this transition from below (i.e. from the ferromagnetic phase) thermal fluctuations destroy the ordering of magnetic moments and the magnetisation of Iron decreases continuously and is identically zero at the transition. The point in parameter space where the phase transition occurs is defined to be the *critical point*.

It is possible to identify a continuous phase transition by its order parameter, a thermodynamic quantity that is zero in the disordered phase, non-zero in the ordered phase, varies continuously across the transition, and tells us about the change in symmetry across the two phases. In the case of Iron the order parameter would be the magnetisation, which encapsulates the breaking of time reversal symmetry in the ferromagnetic phase. The fluctuations of the order parameter are non-zero in both phases, and as you approach the critical point the spatial and temporal correlations of the fluctuations get longer and longer. At the critical point the fluctuations are infinitely corre-

[1]The potential, being a sum of analytic functions, can only become non-analytic in the thermodynamic limit, i.e. as $N \to \infty$ where N is the number of particles in the system. In practice in a typical system we have 10^{27} degrees of freedom which can be taken to be close to the thermodynamic limit.

lated and the spatial ξ and temporal ξ_τ correlation lengths follow a power law,

$$\xi \sim |t|^{-\nu}, \quad \xi_\tau \sim |t|^{-\nu z} \tag{1.2}$$

where t is a tuning parameter for the transition (reduced temperature for classical phase transitions), i.e. at the critical point $t = 0$. The dynamic critical exponent and the correlation length exponent are represented by z and ν respectively. The divergence of both spatial and temporal correlations implies that there is no characteristic scale in the system and that fluctuations occur at all length and time scales. This means that the system is scale invariant, which in turn implies that all observables follow a power law with some critical exponent which then uniquely defines the transition.

While historically phase transitions that occur at non-zero temperature have taken the limelight, as of late there has been vast interest in quantum phase transitions which occur at $T = 0$. The name is derived from the fact there are no thermal fluctuations, and that quantum effects are responsible for the critical behaviour. This means that the phase transition is not driven by temperature but rather by some parameter of the Hamiltonian, e.g. the spin density wave insulator to superconductor phase transition in iron based high-T_c superconductors is driven by the concentration of dopants. As there are no entropy considerations, it follows that there is a macroscopic rearrangement of the ground state of the system across the transition. While it might seem that an understanding of what happens at absolute zero is unhelpful given that it's not possible to reach 0K in experiments nor get close to it without an awful lot of effort, it turns out that the behaviour at the quantum critical point (QCP) has a huge impact on the finite-T regime [1, 4]. This phenomenon has been dubbed the *quantum critical fan*, for it encapsulates three distinct cross-over regimes in the phase diagram with their boundaries resembling a fan, as can be seen in Fig. 1.1. Amazingly, within the quantum critical regime, the critical phenomena at the QCP govern the behaviour of observables at finite T. Specifically the observables exhibit power-law dependence with respect to temperature with critical exponents derived from those at the QCP. Such behaviour persists up to temperatures which are comparable with the microscopic energy scales of the system. These theoretical predictions were also confirmed in an experimental set up [5]. An understanding of criticality at a quantum phase transition can then shed light on the macroscopic behaviour at temperatures that are more accessible, and hence its studies are paramount.

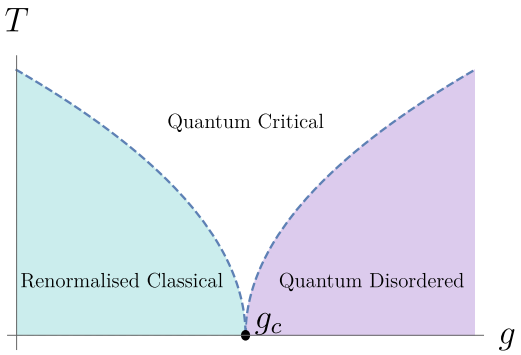

Figure 1.1: A phase diagram of a strongly correlated material with a continuous phase transition at critical value of some Hamiltonian parameter g_c. For $g < g_c$ the material is in a symmetry broken phase, while for $g > g_c$ we are in a high symmetry phase. The behaviour at the QCP leads to scaling behaviour far away in the finite temperature part of the diagram. The existence of the fun is generic for any continuous phase transition. For more details regarding the nature of the three regimes (in the case of the Heisenberg AFM transition in 2D), please consult Ref. [1]

A concept that is helpful in the study of phase transitions of quantum matter is that of *universality*. At the simplest level it tells us that systems with seemingly different microscopic physics, behave in the same way near a phase transition. In fact it is possible to classify each phase transition according to the universality class it belongs. All members in a particular class will posses the same critical exponents. For example, a continuous liquid-to-gas transition possess the same critical exponents as a ferromagnetic transition involving Ising spins [6].

Another fundamental tool is that of mean field treatment of a phase transition, which is the most basic theory to use the order parameter. In it, the interaction between a large number of degrees of freedom is exchanged for the interaction between a single degree of freedom and an averaged coarse grained order parameter. For example in the case of a magnetic transition, we would consider a singular spin interacting with the averaged magnetization of its nearest neighbours. Such a basic picture results in a theory that is solely dependent on a single parameter.

Ginzburg and Landau extended this methodology [7], by assuming a gen-

eralised thermodynamic potential that is a functional of a spatially fluctuating order parameter field. This theory was first developed for superconductivity where the order parameter field can become inhomogeneous in the presence of an external magnetic field. This advance in turn paved way for the Landau-Ginzburg-Wilson order parameter theory of phase transitions which traded Landau's free energy functional for a statistical mechanics action, the critical properties of which were studied using renormalisation group [8].

Recently there has been interest in phase transitions where an order-parameter theory is inadequate to describe the criticality. Namely where fermionic excitations are fundamental to the critical behaviour. Such problems have been dubbed fermionic quantum criticality. One particular avenue of interest is the large family of nodal semimetals where valence and conduction bands touch at a number of discrete points or around closed (nodal) loops in the Brillouin zone. The crossings posses a quantized topological charge which ensures the stability of the fermionic states at the Fermi level. The gapless nature of the excitations means that the fermionic degrees of freedom cannot be simply integrated out and are key in describing the potential phase transitions. The semimetals zero-dimensional Fermi surface, and the vanishing density of states at the nodal points, make them a perfect setting to study criticality beyond the order parameter paradigm.

The simplest members of this family are Dirac and Weyl semimetals [9, 10, 11], which are four-fold and two-fold degenerate at the nodal point respectively and exhibit relativistic dispersion in their vicinity. The most famous example of a Dirac semimetal is graphene [12], which exhibits massless Dirac fermions at half-filling. Other examples of Dirac semimetals include surface states of topological insulators [13, 14], while the more elusive Weyl semimetals have been predicted to occur in pyrochlore iridates by ab initio studies [15].

Due to the topological charge of a nodal point, a transition into a topologically trivial state can only be achieved when a pair of nodal points with opposite topological invariants are merged; at such a topological phase transition the system no longer exhibits full Lorentz symmetry as the dispersion is now linear (relativistic) in one direction and quadratic(Newtonian) in the other. Such excitation has been dubbed as a semi-Dirac fermion [16, 17, 18]. Further ahead semimetals with a quadratic band touching points (QBT) [19] have been found in numerous two and three dimensional materials [20, 21, 22, 23]. More recently semimetals that exhibit chiral structure have been found to host exotic quantum states like multifold fermions which have no analogue

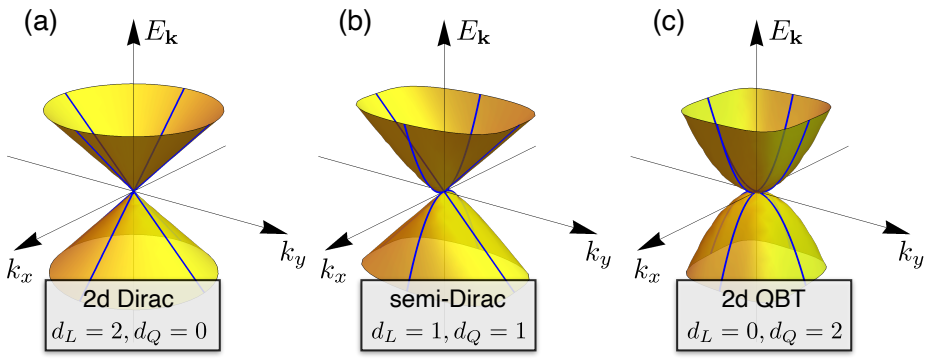

Figure 1.2: Different types of nodal-point semimetals in $d = 2$ spatial dimensions. The quasiparticles at the band-touching point disperse linearly along d_L and quadratically along d_Q directions, $d_L + d_Q = 2$.

in high energy physics [24, 25, 26], as well as long Fermi arc surface states [15, 27, 28, 29].

We can define the family of anisotropic nodal semimetals to contain d_L linear and d_Q quadratic momentum directions in $d = d_L + d_Q$ spatial dimensions, which allows us to interpolate between relativistic Dirac or Weyl fermions and quasiparticles in systems with quadratic band touching (QBT) (see Fig. 1.2).

A common feature of most of the semimetals espoused above, is the vanishing density of states at the nodal points, which follows a modified power law, $\rho(E) \sim |E|^r$, $r = (2d_L + d_Q - 2)/2$. Compared to the case of normal metals where the density of states is constant, this promises novel correlation effects. As such there has been a lot of interest in the phase transitions driven by electron-electron interactions. In the simplest case of monolayer graphene, the 2D Dirac semimetal state has been shown to be stable under weak short-range interactions, however it undergoes a quantum phase transition into a gapped phase at strong coupling [30, 31].

The situation is different in QBT semimetals, where in 3D an arbitrary weak long-range Coulomb interaction renders the system unstable to the spontaneous formation of a topological Mott insulator state [32], while in 2D the long-range Coulomb tail is screened and the non-interacting ground state is unstable to arbitrary weak short-range interactions[33, 34, 35]. The strong anisotropy of semi-Dirac semimetals makes the system particularly

interesting; while it transitions into symmetry broken states under a strong short-ranged interaction[36, 37, 38] it also exhibits exotic, directionally dependent screening effects [39, 40, 41, 42].

1.1 Outline of Thesis

This thesis investigates the fermionic quantum criticality of anisotropic nodal point semimetals in $d = d_L + d_Q$ spatial dimensions that disperse linearly in d_L dimensions, and quadratically in the remaining d_Q dimensions. When subject to strong interactions, these systems are susceptible to semimetal-insulator transitions concurrent with spontaneous symmetry breaking. The gapless nature of the low energy excitations as well as restricted phase space available to them promises novel phenomena that cannot be described by a simple order parameter theory.

Firstly in Chapter 2 we introduce the honeycomb lattice and calculate its dispersion with the use of a tight-binding Hamiltonian describing non-interacting fermions with nearest neighbour hopping. We show that at half-filling the low energy excitations are best described by massless Dirac fermions. We then consider short-range interactions on the honeycomb lattice and obtain an effective field theory for the semimetal to charge density wave (CDW) transition. Lastly we introduce semi-Dirac fermions and write down a general field theory for the family of anisotropic nodal point semimetals.

In Chapter 3 we utilise Landau's free energy approach for classification of phase transitions. Using a path-integral approach we calculate the mean-field critical exponents for the CDW transition for the case of both Dirac and semi-Dirac semimetals. Lastly by allowing small, long-wavelength modulations of the order parameter we calculate the correlation length exponents for the semi-Dirac case and portray its inherent anisotropy.

A modern way of investigating phase transitions in condensed matter systems is the the theory of Renormalisation Group and Wilson's momentum shell implementation of it. As an introduction to the topic, in Chapter 4 we consider the scalar ϕ^4 theory which can describe the magnetic transition of Ising spins on a two dimensional lattice. We calculate the RG equations up to one-loop order, and then use the famous ϵ-expansion to show the existence of the Wilson-Fisher fixed point slightly below the upper critical dimension, and calculate its critical exponents.

While Wilson's momentum shell has had incredible amount of success, its

naive implementation, often performed in the strongly correlated literature, results in inconsistencies. The Gross-Neveu-Yukawa theory of interacting Dirac fermions coupled to a dynamic order parameter field has been known to describe chiral symmetry breaking and spontaneous mass generation in high energy physics, while in condensed matter it describes the Dirac semimetal to insulator transition. The theory posses an interacting fixed point which is Lorentz invariant, however naive calculation of the RG equations at one loop order using a spherical and a cylindrical cutoff scheme results in disparate results. The former retains the relativistic invariance while the latter does not. In Chapter 5 we showcase this inconsistency and then by utilising a soft cutoff approach we portray the importance of Landau damping of order parameter fluctuations by particle-hole excitations. We then perform an RG calculation using a dressed bosonic propagator retaining terms that are $\mathcal{O}(1/N_f)$ where N_f is the number of fermionic flavours. We obtain critical exponents which are in full agreement with the previous literature.

In Chapter 6 we extend our soft cutoff methodology to the case of anisotropic nodal semimetals subject to strong short-range interactions. We consider interactions that go hand in hand with a CDW insulator transition, which in the language of the effective field theory is represented by a scalar order parameter field in the Yukawa action. We once again show that the bare bosonic propagator results in consistencies in the RG, and that using the RPA damped bosonic propagator results in corrections that are cutoff scheme independent. We calculate the RG equations for a general dimension D and then calculate the exact critical exponents for semi-Dirac fermions to leading order in $1/N_f$. Finally we consider the ϵ-expansion around the upper critical line, and compare the two methods.

Disorder is present in any realistic condensed matter system, the possible sources of it are endless, e.g. crystal dislocations, charged impurities, lattice warping. A through understanding of possible symmetry breaking wouldn't be complete without its inclusion. In Chapter 7, we investigate the effect of disorder on the phase transition between a Dirac semimetal and a CDW insulator. Utilising work from previous chapters we include the effect of Landau damping, to calculate the RG equations up to leading order in $1/N_f$ and the disorder "strength". The non-perturbative correction coming from RPA was found to be crucial for the existence of a new interacting disorder fixed.

Lastly in Chapter 8 we summarise our results and conclude with remarks regarding potential future work.

Chapter 2

Topological Nodal semimetals

In Sec. 2.1, we consider a theory of non-interacting fermions on the honeycomb lattice, and show that at half filling the tight-binding dispersion in the vicinity of the Fermi surface is best described by an effective field theory that takes the form of the massless Dirac equation. In Sec. 2.2.1, we go on to formulate the Gross-Neveu-Yukawa theory for the semimetal-to-insulator transition for the case of Dirac fermions on the honeycomb lattice. In Sec. 2.3, we generalise the effective field theory to encapsulate $d = d_L + d_Q$ dimensional anisotropic nodal semimetals with d_L linear, and d_Q quadratic dispersing directions.

2.1 Non-interacting fermions on the honeycomb lattice

In graphene the carbon atoms are arranged on a two-dimensional honeycomb lattice, where the valence and conduction electron bands are formed by $2p_z$ orbitals. The honeycomb is not a Bravais lattice, but rather a bipartite triangular lattice with two sites per unit cell, denoted by A and B (see Fig. 2.1). The primitive unit vectors are $\boldsymbol{a}_1 = \frac{\sqrt{3}a}{2}(1, \sqrt{3}), \boldsymbol{a}_2 = \frac{\sqrt{3}a}{2}(-1, \sqrt{3})$, where a is the distance between the A and B sites in the unit cell. While the nearest-neighbour vectors are $\delta_1 = a(\sqrt{3}, 1)/2$, $\delta_2 = a(-\sqrt{3}, 1)/2$, and $\delta_3 = a(0, -1)$. The dispersion of graphene was first calculated by Wallace [43] with the use of a tight binding approximation, where in the simplest case can be described

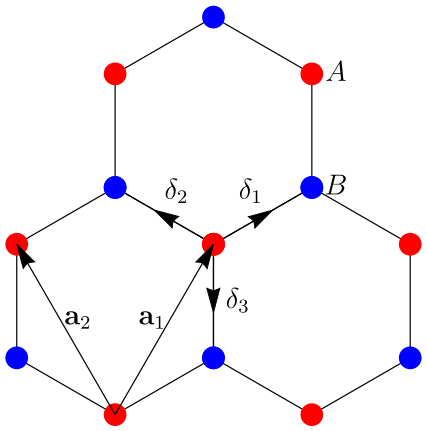

Figure 2.1: The honeycomb bipartite lattice with sublattices A and B, primitive vectors $\boldsymbol{a}_{1,2}$, and nearest-neighbour vectors $\delta_{1,2,3}$.

by a non-interacting hopping Hamiltonian between nearest neighbours,

$$H = -t \sum_{\boldsymbol{r}} \sum_{j=1,2,3} (c_A^\dagger(\boldsymbol{r}) c_B(\boldsymbol{r} + \delta_j) + h.c.), \tag{2.1}$$

where t is the hopping amplitude, the summation is over all nearest neighbours, and $(c_\sigma(\boldsymbol{r}), c_\sigma^\dagger(\boldsymbol{r}))$ are the fermion annihilation and creation operators respectively which act on site $\sigma = A, B$ at position $\boldsymbol{r}$. These second quantized operators follow the standard anticommutation relations.

The Hamiltonian is then transformed to a Fourier basis where $c_\sigma(\boldsymbol{r}) = \frac{1}{\sqrt{N}} \sum_{\boldsymbol{k}}^{BZ} c_\sigma(\boldsymbol{k}) e^{i\boldsymbol{k}\cdot\boldsymbol{r}}$, where the summation is over all momentum modes in the Brillouin Zone which is defined by the reciprocal lattice vectors $\boldsymbol{b}_1 = \frac{2\pi}{3a}(\sqrt{3}, 1)$, and $\boldsymbol{b}_2 = \frac{2\pi}{3a}(-\sqrt{3}, 1)$. This results in,

$$H = -t \sum_{\boldsymbol{k}}^{BZ} \begin{pmatrix} c_A^\dagger(\boldsymbol{k}) & c_B^\dagger(\boldsymbol{k}) \end{pmatrix} H_{\boldsymbol{k}} \begin{pmatrix} c_A(\boldsymbol{k}) \\ c_B(\boldsymbol{k}) \end{pmatrix} \tag{2.2}$$

where

$$H_{\boldsymbol{k}} = v_{\mathrm{F}} \begin{pmatrix} 0 & e^{i\boldsymbol{k}\cdot\delta_1} + e^{i\boldsymbol{k}\cdot\delta_2} + e^{i\boldsymbol{k}\cdot\delta_3} \\ e^{-i\boldsymbol{k}\cdot\delta_1} + e^{-i\boldsymbol{k}\cdot\delta_2} + e^{-i\boldsymbol{k}\cdot\delta_3} & 0 \end{pmatrix} \tag{2.3}$$

where $v_{\mathrm{F}} = 3at/2$ is the Fermi velocity. The matrix $H_{\boldsymbol{k}}$ can now be diagonalised and the corresponding eigenvalues give the dispersion,

$$E_{\pm}(\boldsymbol{k}) = \pm\sqrt{3 + 4\cos\left(\frac{3k_y}{2}\right)\cos\left(\frac{\sqrt{3}k_x}{2}\right) + 2\cos\left(\sqrt{3}k_x\right)} \tag{2.4}$$

where $\boldsymbol{k} = (k_x, k_y)$. Each carbon atom in the two dimensional sheet contributes one electron, which means that the Fermi energy lies exactly at the band touching points where $E(\boldsymbol{k}) = 0$. There are six of these points, all located at the corners of the Brillouin Zone where the density of states vanishes linearly with the energy, as illustrated in Fig. 2.2. However only two of those six are inequivalent, as it is possible to access the other 4 by translations with the reciprocal lattice vectors, $\boldsymbol{b}_1, \boldsymbol{b}_2$. In the literature these two points, $\boldsymbol{K}_{\pm} = \pm\frac{4\pi}{3\sqrt{3}}(1, 0)$, are known as Dirac points (or as valleys). Upon an expansion of Eq. (2.4) around K^+, the dispersion becomes linear as can be seen in Fig. 2.2(a), and the Hamiltonian takes the form of the massless Dirac Hamiltonian,

$$H_{\boldsymbol{k}} = v_{\mathrm{F}}\begin{pmatrix} 0 & k_x - ik_y \\ k_x + ik_y & 0 \end{pmatrix} = v_{\mathrm{F}}\boldsymbol{k}\cdot\boldsymbol{\sigma} \tag{2.5}$$

where $\boldsymbol{\sigma} = (\sigma^x, \sigma^y)$ are the Pauli matrices. The Hamiltonian for the other Dirac point can then be obtained by a time-reversal transformation. Combining the contributions from the two valleys we arrive at the following,

$$H = v_{\mathrm{F}}\int_0^{\Lambda}\frac{d^2\boldsymbol{k}}{(2\pi)^2}\Psi^{\dagger}(\boldsymbol{k})\ \boldsymbol{k}\cdot\boldsymbol{\alpha}\ \Psi(\boldsymbol{k}), \tag{2.6}$$

where

$$\Psi^{\dagger} = (\Psi^{\dagger}_{A,+}, \Psi^{\dagger}_{B,+}, \Psi^{\dagger}_{A,-}, \Psi^{\dagger}_{B,-}) \tag{2.7}$$

is a 4-component spinor, and $\boldsymbol{\alpha} = (\alpha_1, \alpha_2) = (\tau_z \otimes \sigma_x, \tau_0 \otimes \sigma_y)$ where the Pauli matrices σ_i and τ_i $(i = 0, x, y, z)$ act on the sub-lattice (pseudospin) and valley spaces respectively. The constant Λ is the ultraviolet cut-off, up to which the linear approximation of the dispersion is valid.

We see that the energy eigenvalues around the Dirac points are equal to $E(\boldsymbol{k}) = v_{\mathrm{F}}\,|\boldsymbol{k}|$. We have shown that graphene at half-filling exhibits semimetallic behaviour, where the low energy excitations are best described by massless Dirac fermions.

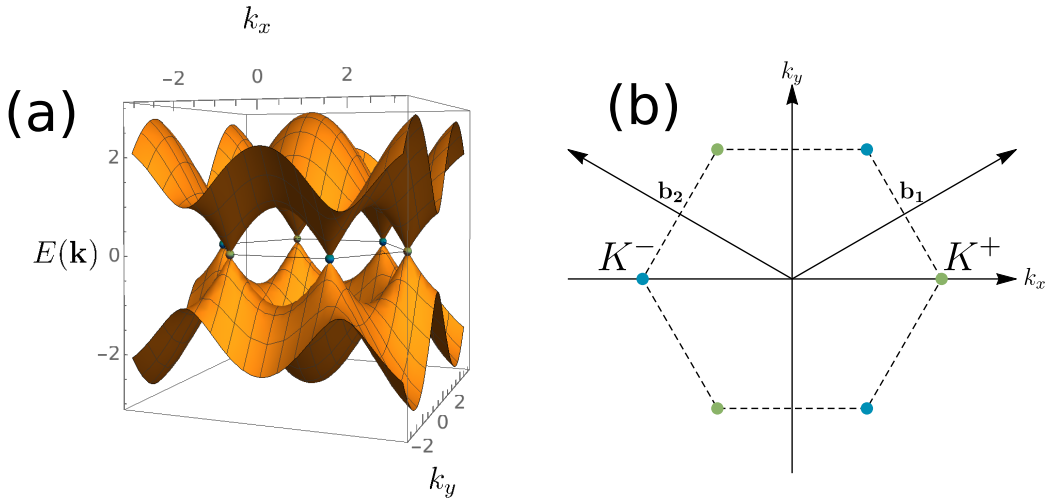

Figure 2.2: (a) The full dispersion of the honeycomb lattice. The Dirac points sit exactly at charge neutrality, and the dispersion in their vicinity is linear in the momentum. (b) The first Brillouin Zone of the honeycomb lattice. The two sets of inequivalent Dirac points are denoted in separate colours.

It is important to note that the emergence of these relativistic quasiparticles results from the inherent symmetries of the honeycomb lattice, rather than it being an artefact of the tight-binding model. The honeycomb lattice posseses, among others, the anti-unitary time reversal symmetry $\mathcal{T}$ which ensures the Hamiltonian is invariant under the exchange of the two sublattices, while the unitary inversion symmetry I ensures invariance under the exchange of the two Dirac points. Effectively the former maps the wavevector $\boldsymbol{k} \to -\boldsymbol{k}$, while the latter maps the position vector $\boldsymbol{r} \to -\boldsymbol{r}$. The Dirac Hamiltonian, must be invariant under both of those symmetries,

$$\mathcal{T} H \mathcal{T}^{-1} = H, \quad I H I^{-1} = H.$$

From these equations we obtain two condtions,

$$\mathcal{T} : H_{\boldsymbol{k}} = H^*_{-\boldsymbol{k}}, \tag{2.8}$$

$$I : \tau_0 \otimes \sigma_x H_{-\boldsymbol{k}} \tau_0 \otimes \sigma_x = H_{\boldsymbol{k}}. \tag{2.9}$$

The combination prohibits a term in Eq.(2.5) that couples to the last Pauli matrix σ_z which would gap the spectrum (note that Eqs.(2.8)-(2.9) are valid

for any Bloch Hamiltonian). A pertubation which is invariant under $\mathcal{T}$ and I then cannot open up a gap but can change the position of Dirac point within the Brilloun Zone [17]. Further hoppings, next-nearest-neighbour etc., will not induce a gap, only will shift the energy of the Dirac points. However with the addition of real spin into the equation, it was shown that intrinisic spin-orbit coupling would open up a gap and transition graphene from a semimetal to a quantum spin Hall insulator [44], however subsequent work found that the gap was of the order 24μeV at the Dirac points and could only be detected at "unrealistically low temperatures"[45, 46]. The nature of the low-energy Dirac excitations in graphene seems to be fundamental.

2.2 Interactions on the honeycomb lattice

We've established that non-interacting spinless fermions on the honeycomb lattice result in a semimetallic state, with a point like Fermi surface. Due to the fact that within the vicinity of the Dirac points the density of states vanishes linearly, Dirac fermions on the honeycomb lattice are a perfect setting to study fermionic quantum criticality, i.e. criticality which cannot be described by a conventional order parameter Ginzburg-Landau-Wilson theory as the nature of the fermions is fundamental to the transition.

The question now is whether the inclusion of electron-electron interactions might induce a first or a second order phase transition into some strongly correlated phase. Specifically we're intersted in interaction-driven phases which gap the Dirac spectrum, and hence are akin to the metal-insulator transition of the Hubbard model which hosts a Mott insulating state. We aim to set up an effective field theory for the description of symmetry breaking phase transtions in a Dirac semimetal.

The simplest interacting tight-binding Hamiltonian on the honeycomb lattice involving spinless fermions contains an inter-site (nearest-neighbour) repulsive interaction with real-valued strength V,

$$H = H_0 + H_{\text{int}} \tag{2.10}$$

$$H_{\text{int}} = V \sum_{\langle \boldsymbol{r}\boldsymbol{r}' \rangle} \hat{n}(\boldsymbol{r})\hat{n}(\boldsymbol{r}'), \tag{2.11}$$

where H_0 is the non-interacting part defined in Eq.(2.1) and the fermion

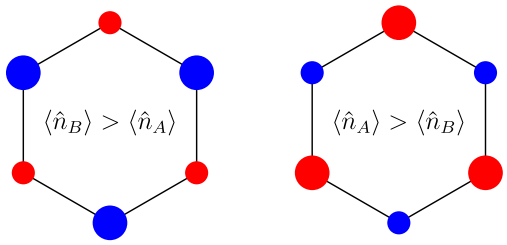

Figure 2.3: An illustration of the charge density wave (CDW) phase on the honeycomb lattice, where the accumulation of charge on one lattice site is more than on the other. The two sublattices A and B are denoted by red and blue colours respectively.

number operator is defined as

$$\hat{n} = \sum_{\sigma=A,B} \hat{n}_\sigma = \sum_{\sigma=A,B} c_\sigma^\dagger c_\sigma. \tag{2.12}$$

As only spinless fermions are considered, the usual Hubbard U term which denotes on-site interaction has been omitted. Further interactions that might extend this Hamiltonian, range from a next-nearest-neighbour intersite interaction to exchange interactions and ring terms. The nature of the interaction will determine the possible phases that the Dirac semimetal might transition into. In this particular case, as we will shortly see, the repulsive nearest-neighbour interaction goes hand in hand with a charge density wave (CDW) instability, which is an insulating state that spontaneously breaks the sublattice symmetry, i.e an imbalance between charge densities on the A and B sublattices. Such a phase transition can be characterised by an order parameter which tracks the difference between charge density on the two lattices; the expectation of which would be zero and non-zero in the semimetal (disordered) and CDW (ordered) phases respectively. The CDW phase can be seen in Fig. 2.3.

In order to obtain the low energy effective theory of the interaction, we take the Fourier transform of Eq.(2.11) and expand around the two Dirac points K and K'. Transforming back to real space (for ease of notation) we

arrive at the following,

$$H_{int} = V \int d^2\boldsymbol{r} \Big\{ \Psi^\dagger_{A,+}\Psi_{A,+}\Psi^\dagger_{B,+}\Psi_{B,+} + \Psi^\dagger_{A,+}\Psi_{A,+}\psi^\dagger_{B,-}\Psi_{B,-} + \Psi^\dagger_{A,-}\Psi_{A,-}\Psi^\dagger_{B,+}\Psi_{B,+} + \Psi^\dagger_{A,-}\Psi_{A,-}\Psi^\dagger_{B,-}\Psi_{B,-} \Big\} \tag{2.13}$$

$$= V \int d^2\boldsymbol{r} \left(\Psi^\dagger_A \tau_0 \Psi_A\right)\left(\Psi^\dagger_B \tau_0 \Psi_B\right). \tag{2.14}$$

The four-fermion interaction can be decoupled into two seperate terms,

$$H_{\text{int}} = \frac{V}{4} \int d^2\boldsymbol{r} \left(\Psi^\dagger \tau_0 \otimes \sigma_0 \Psi\right)^2 - \left(\Psi^\dagger \tau_0 \otimes \sigma_z \Psi\right)^2 \tag{2.15}$$

where the first term can be thought of as the total density on sublattice sites A and B while the second term signifies the difference in densities between the two sites,

$$\begin{gathered} \Psi^\dagger\Psi \sim \hat{n}_A + \hat{n}_B \\ \Psi^\dagger \begin{pmatrix} \sigma_z & 0 \\ 0 & \sigma_z \end{pmatrix} \Psi = \Psi^\dagger \alpha_3 \Psi \sim \hat{n}_A - \hat{n}_B \end{gathered} \tag{2.16}$$

where we have defined $\alpha_3 = \tau_0 \otimes \sigma_z$. Taking into consideration only the momentum modes near the Dirac points, the quantum mechanical action corresponding to the interacting Hamiltonian at low energies can be written as

$$S = \int_0^\beta d\tau \int d\boldsymbol{r}\ \mathcal{L}(\tau, \boldsymbol{r}) \tag{2.17}$$

with the effective Lagrangian density $\mathcal{L}$ defined to be,

$$\mathcal{L} = \Psi^\dagger \left(\delta_\tau - \imath \alpha_i \delta_i\right) \Psi + \tilde{V}(\Psi^\dagger\Psi)^2 - \tilde{V}(\Psi^\dagger \alpha_3 \Psi)^2, \tag{2.18}$$

where τ is the imaginary time, and $\beta = 1/T$ the inverse temperature. While the total density term $(\Psi^\dagger\Psi)^2$ will be shown to percipitate nothing but a redefinition of the chemical potential, the latter four-fermion term will drive, under sufficiently storng interactions, a continuous phase transtion from the semimetal state to a CDW phase. A different form of the four fermion term could come about from considering different types of interactions at the lattice level. Already the inclusion of a next-nearest-neighbour repulsive interaction results in a much richer phase diagram, which includes charge modulated phases similar to the CDW state mentioned here as well as Kekulé bond order phase [47, 48].

2.2.1 Gross-Neveu-(Yukawa) Model

The form of the Lagrangian density derived in Eq.(2.18) is one example of a broader group of models called the Gross-Neveu (GN) models [49] which describe spontaneous breaking of chiral symmetry in high-energy physics.

We now introduce the imaginary time path integral representation of the partition function,

$$\mathcal{Z} = \int D[\Psi^\dagger, \Psi] e^{-\int d\tau d\boldsymbol{x} \mathcal{L}}, \tag{2.19}$$

where $\mathcal{L}$ for this situation is the Gross-Neveu Lagrangian density,

$$\mathcal{L} = \Psi^\dagger \left(\delta_\tau - i\alpha_i \delta_{x_i}\right) \Psi + g_{ab} (\Psi^\dagger M_a \Psi)(\Psi^\dagger M_b \Psi). \tag{2.20}$$

The parameter g_{ab} denotes the strength of the four-fermion interaction that is local in space and time, and M_a and M_b are 4×4 matrices. For a discussion of symmetry allowed interactions consult Ref. [31].

When studying symmetry breaking transitions, it is advantegous to cast the problem in a different light using the Hubbard Stratonovich transformation. The aim of said transformation is to bring the Lagrangian into quadratic term in the fermionic fields Ψ's. This is first done by decoupling the quartic term in a "channel" where the expectation of a billinear is nonzero in the ordered phase. For example, for a s-wave singlet superconducting instability the decoupling will be in the Cooper channel $\langle \Psi_{\boldsymbol{k}} \alpha_2 \Psi_{-\boldsymbol{k}} \rangle$ [2]. The decoupling is followed by the introduction of an auxilarry bosonic field ϕ that is conjugate to the channel. The final result after integration is a Ψ billinear coupled to a single auxilarry field ϕ.

This methodology will be now portrayed for the effective field theory denoted in Eq.(2.18) which describes a a quantum phase transition from a Dirac semimetal to a charge density wave (CDW) insulator where the sublattice symmetry is broken. This corresponds to a spontaneous symmetry breaking of a Z_2 Ising (pseudo)spin degree of freedom, which belongs to the chiral Ising GNY universality class [49, 50]. We will use the decoupling shown first in Eq.(2.15), which is in the "charge" channel. Tackling the total density term first, we introduce an auxilary field $\chi \sim \Psi^\dagger \Psi$ with the use of the Gaussian integral identity for real fields, $1 \approx \int dx\ e^{-x^2}$,

$$\exp\left[-\tilde{V}\left(\Psi^\dagger\Psi\right)^2\right] = \int D\left[\chi\right] \exp\left[-\frac{\chi^2}{4\tilde{V}} - \tilde{V}\left(\Psi^\dagger\Psi\right)^2\right]. \tag{2.21}$$

Performing a variable transformation, $\chi \to \chi + 2i\tilde{V}\left(\Psi^\dagger\Psi\right)$, we arrive at the following identity,

$$\exp\left[-\tilde{V}\left(\Psi^\dagger\Psi\right)^2\right] = \int D\left[\chi\right]\exp\left[-\frac{\chi^2}{4\tilde{V}} - i\chi(\Psi^\dagger\Psi)\right]. \tag{2.22}$$

The result is that the four-fermion total density interaction term has been traded for a fermion billinear coupled to the auxillary field χ. It is worth pointing out that the Hubbard-Stratonovich transformation is exact, no information is lost in the process, simply the picture is now of a composite boson-fermion theory. The mixed term $\chi\Psi^\dagger\Psi$ enters in the same way as the chemical potential, hence it can be absorbed by the redefinition $\tilde{\mu} = \mu + i\langle\chi\rangle$.

The transformation for $(\Psi^\dagger\alpha_3\Psi)^2$ follows the same process, where a real scalar bosonic field $\phi \sim \Psi^\dagger\alpha_3\Psi$ is introduced which is equivalent to an order parameter for the CDW state. The dimensionality of the order parameter field depends on the phase it's destined to describe. For a spin density wave instability, the order parameter would be three dimensional. The full Hubbard-Stratonovich transformation of Eq.(2.18) results in the following Lagrangian density,

$$\mathcal{L} = \Psi(\delta_\tau - iv\boldsymbol{\alpha}\cdot\boldsymbol{\partial})\Psi + \frac{1}{2}\left(-\partial_\tau^2 - c^2\boldsymbol{\partial} + m^2\right)\phi^2 + g\phi\Psi^\dagger\alpha_3\Psi, \tag{2.23}$$

where $\boldsymbol{\partial} = (\partial_x, \partial_y)$, m^2 is the bosonic mass term which as we'll see in the next chapter acts as the tuning parameter for the phase transtion(i.e. $\sim V - V_c$). The parameter g is known as the "Yukawa" coupling, which delineates the strength of interaction between the boson and fermions. The fermionic and bosonic velocities are denoted by v and c respectively. The structure of the dispersion of the bosonic field is a consequence of ϕ being a real scalar field which places a constraint on the leading functional form. By symmetry, analytical terms that are odd in momentum or frequency are not allowed.

The Yukawa coupling anti-commutes with the non-interacting Lagrangian and thereby fully gaps the fermionic quasiparticle spectrum in the broken-symmetry phase, as can be seen in Fig.2.2.1,

$$E(\boldsymbol{k}) = \pm\sqrt{v^2\boldsymbol{k}^2 + g^2\langle\phi\rangle^2}, \tag{2.24}$$

maximizing the condensation energy gain.

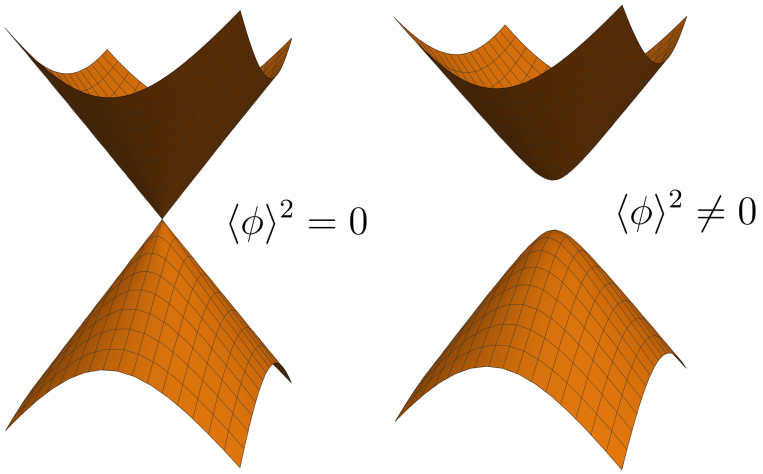

Figure 2.4: Illustration of the Dirac spectrum in the Dirac and the CDW phases, where the order parameter is zero and non-zero respectively/

We now present the "graphene" representation of the α's using Dirac matrices. Identifying

$$\gamma_0 = \alpha_3 = \tau_0 \otimes \sigma_z = \begin{pmatrix} \sigma_z & 0 \\ 0 & \sigma_z \end{pmatrix} \tag{2.25}$$

we redefine the fermionic field,

$$\Psi\gamma_0 = \bar{\Psi} \tag{2.26}$$

so that our interaction term becomes

$$\phi\Psi^\dagger\alpha_3\Psi \to \phi\bar{\Psi}\Psi. \tag{2.27}$$

This motivates the following defintion,

$$\gamma_1 = i\alpha_3\alpha_1 = \begin{pmatrix} \sigma_y & 0 \\ 0 & -\sigma_y \end{pmatrix}, \quad \gamma_2 = i\alpha_3\alpha_2 = \begin{pmatrix} \sigma_x & 0 \\ 0 & \sigma_x \end{pmatrix} \tag{2.28}$$

The Clifford algebra is complete with the definition of two anticommuting γ matrices,

$$\gamma_3 = \begin{pmatrix} 0 & \sigma_y \\ \sigma_y & 0 \end{pmatrix}, \quad \gamma_5 = \begin{pmatrix} 0 & -i\sigma_y \\ i\sigma_y & 0 \end{pmatrix}. \tag{2.29}$$

The Dirac γ matrices anticommute $\{\gamma_\mu, \gamma_\nu\} = 2\delta_{\mu\nu}$ for $\mu, \nu = 0, \ldots, 5$. Hence the Gross-Neveu-Yukawa (GNY) Lagrangian defined in imaginary time τ using the γ matrix representation takes the following form,

$$\mathcal{L}_{\text{GNY}} = \bar{\Psi}\left(\partial_\tau \gamma_0 + v\boldsymbol{\partial}\cdot\boldsymbol{\gamma} + g\phi\right)\Psi + \frac{1}{2}\phi(-\partial_\tau^2 - c^2\boldsymbol{\partial}^2 + m^2)\phi + \lambda\phi^4. \quad (2.30)$$

The inclusion of the ϕ^4 vertex is a result of the inclusion of the most relevant (in the RG sense) bosonic interaction allowed by symmetry. The Lagrangian can be defined for a general d-spatial dimension where then $\boldsymbol{\gamma} = (\gamma_1, \cdots, \gamma_d)$ and $\boldsymbol{\partial} = (\partial_1, \cdots, \partial_d)$.

2.3 Anisotropic nodal semimetals

Graphene is a member of a larger family of nodal semimetals. Other members include semimetals where crossings are of the semi-Dirac type, or are quadratic in nature.

2.3.1 Semi-Dirac semimetal

The former excitation first reported in Ref.[17] occurs at a phase transition between a Dirac semimetal and a trivial band insulator. While in the case of the nearest-neighbour tight-binding model on the honeycomb lattice the Dirac points were located at the high symmetry points in the corners of the Brillouin Zone, it is possible to change the location of the Dirac points by varying the lattice parameters. In the derivation in Sec.2.1 we assumed that the hopping parameters along each nearest-neighbour had the same magntitude, however if some assymetry were induced then two Dirac points could be moved from $\boldsymbol{K}_\pm$ to some new position $\boldsymbol{D}_\pm$. Upon sufficient variation it is feasible that the two points might merge when $\boldsymbol{D}_+ = \boldsymbol{D}_- = -\boldsymbol{D}_+$, which happens at four points within the first BZ, $\boldsymbol{D}_+ = \{\boldsymbol{b}_1 + \boldsymbol{b}_2, \boldsymbol{b}_1, \boldsymbol{b}_2, \boldsymbol{0}\}/2$, where $\boldsymbol{b}_{1,2}$ are the reciprocal lattice vectors. Expanding Eq.(2.4) around any of these points, we find that at linear order the contribution in one direction vanishes, and an expansion up to secord order is required. This results in the non-interacting Hamiltonian for the semi-Dirac excitation,

$$H = \int_0^\Lambda \frac{d^2\boldsymbol{k}}{(2\pi)^2}\Psi^\dagger(\boldsymbol{k})\left(v_f k_x \sigma^x + \left(\frac{k_y^2}{2m^*} + \Delta\right)\sigma^y\right)\Psi(\boldsymbol{k}) \quad (2.31)$$

where the dispersion is obtained through diagnolisation,

$$E_{\boldsymbol{k}} = \pm\sqrt{(v_f k_x)^2 + \left(\frac{k_y^2}{2m^*} + \Delta\right)^2}. \tag{2.32}$$

where as before v_f is the Fermi velocity, $1/m^*$ is the curvature of the dispersion in the y-direction, and the Pauli matrices σ act on the sublattice space. For $\Delta < 0$ the dispersion contains two relativistic Dirac points $\boldsymbol{D}_\pm = \left(0, \pm\sqrt{2m(-\Delta)}\right)$, while for $\Delta > 0$ the dispersion has an energy gap Δ. Hence Δ tunes a transition between a Dirac semimetal and a band insulator. At $\Delta = 0$, the system undergoes a topological Lifshitz transition, corresponding to the merging of two Dirac points. At this point the system exhibits quasiparticle excitations that disperse quadratically along the direction the Dirac points were merged, and linearly in the other direction. Similarly to the pure Dirac case, the density of states vanishes at the semi-Dirac point, however with a modified dependence on the energy, i.e. $\mathrm{DOS}(E) \sim \sqrt{|E|}$. This means that the density of states near the nodal point is enhanced compared with the Dirac case, which could result in novel behaviour.

2.3.2 Family of nodal semimetals

We can generalise the above continuum field theory to classify a d-dimensional member of the family of anisotropic nodal semimetals by the number of d_L linear and d_Q quadratic dispersing directions such that $d = d_L + d_Q$, e.g. a 2D semi-Dirac semimetal would be characterised by $d_L = 1$ and $d_Q = 1$. The non-interacting Lagrangian for such a family would then take the following form,

$$\mathcal{L}_0 = \bar{\Psi}\left(\partial_\tau \gamma_0 + \boldsymbol{\partial}_L \cdot \boldsymbol{\gamma}_L + (i v_Q^2 \boldsymbol{\partial}_Q^2 + \Delta)\gamma_Q\right)\Psi \tag{2.33}$$

where we have defined $\boldsymbol{\partial}_L = (\partial_1, \ldots, \partial_{d_L})$ and $\boldsymbol{\partial}_Q = (\partial_{d_L+1}, \ldots, \partial_{d_L+d_Q})$. The parameter v_Q is related to the curvature of the quadratic dispersion. The linear momenta couple to $\boldsymbol{\gamma}_L = (\gamma_1, \ldots, \gamma_{d_L})$, which together with γ_0 and γ_Q form a set of mutually anti-commuting gamma matrices, $\{\gamma_\mu, \gamma_\nu\} = 2\delta_{\mu\nu}$. To incorporate short-ranged interactions, we can follow the same scheme that was laid out in Sec.2.2. The fermionic effective field theory is gained from

coarse-graining appropriate interactions coming from the lattice model, upon which a Hubbard Stratonovich transformation is performed to obtain the full interacting Lagrangian written in the Yukawa language of fermions coupled to a dynamical order parameter field,

$$\mathcal{L} = \mathcal{L}_0 + g\phi\bar{\Psi}\Psi + \frac{1}{2}\left(-\partial_\tau^2 - c^2\boldsymbol{\partial} + m^2\right)\phi^2 + \lambda\phi^4, \tag{2.34}$$

In this thesis, we consider a scalar order parameter field only. Such an Ising order parameter, which is coupled to the σ^z Pauli matrix which in turn anti-commutes with the non-interacting Hamiltonian, breaks the sub-lattice symmetry and fully gaps the fermionic spectrum in the broken symmetry phase.

$$E(\boldsymbol{k}) = \sqrt{\boldsymbol{k}_L^2 + (v_Q^2\boldsymbol{k}_Q^2 + \Delta)^2 + g^2\langle\phi\rangle^2}, \tag{2.35}$$

where $\boldsymbol{k}_L = (k_1, \ldots, k_L)$, $\boldsymbol{k}_Q = (k_{d_L+1}, \ldots, k_{d_L+d_Q})$, and $\boldsymbol{k} = (\boldsymbol{k}_L, \boldsymbol{k}_Q)$.

The parameter Δ tunes the system through a topological phase transition from a nodal-surface semimetal ($\Delta < 0$) to a trivial band insulator ($\Delta > 0$). The nodes for $\Delta < 0$ are given by the d_Q dimensional sphere $\boldsymbol{k}_Q^2 = -\Delta/v_Q^2$ for $\boldsymbol{k}_L = 0$. The experimentally most relevant cases are nodal line semimetals for $d_Q = 2$ and semimetals with a pair of isolated Weyl points for $d_Q = 1$.

Since all quadratic directions couple to the same matrix γ_Q the dispersion remains radially symmetric in the d_Q subspace. A different class of semimetals can be defined in terms of spherical harmonics that couple to different γ matrices [32, 34]. Such theories, which could describe rotational symmetry breaking (nematic transitions) in the d_Q subspace, are not considered in this thesis.

Chapter 3

Mean-field theory of the CDW transition

In this section we utilise Landau's free energy approach to study the phase transition from a Dirac/semi-Dirac semimetal to a charge density wave (CDW) insulator. The method for the mean-field free energy starting from a path integration formulation follows closely arguments laid out in Chapter 4 of [51].

The original work presented in this section first appeared in *Quantum criticality of semi-Dirac fermions in 2+1 dimensions*, M. D. Uryszek, E. Christou, A. Jaefari, F. Krüger, B. Uchoa, Physical Review B, **100**, 155101 (2019)[37].

3.1 Landau's free energy

Landau's theory of phase transitions is centred around the concept of a local order parameter ϕ and a free energy functional F. At a the critical point of a phase transition the thermodynamic potential and its derivatives are non-analytic (when expressed in terms of external parameters only). Landau's idea was to re-express the potential in terms of the order parameter, $F(T, \cdots) \rightarrow F(T, \cdots, \phi(T, \cdots))$, which itself is analytic (and small) near the transition. The free energy could then be Taylor expanded in terms of ϕ, collecting all terms allowed by symmetry.

$$F = F_0 + \frac{a}{2}\phi^2 + \frac{b}{4}\phi^4 + \mathcal{O}(\phi^6). \tag{3.1}$$

Landau then stipulated that the equilibrium state of the system would be given by some of the order parameter that minimizes the free energy, i.e. ϕ^* such that $\partial F(\phi)/\partial\phi|_{\phi^*} = 0$. The free energy would technically be a functional and the derivative a functional derivative. However as a first step it is vital to consider the simplest solution, i.e. one where the order parameter ϕ is static in time and space. This is the so called mean-field solution.

3.1.1 Dirac fermions

In this section the mean-field solution for the CDW phase transition of Dirac fermions will be presented using the functional field formulation. We start off with the partition function for GNY theory in two spatial dimensions, with the mean-field ansatz $\phi(\boldsymbol{r}, \tau) \to \phi_0$,

$$\mathcal{Z} = \int \mathcal{D}\left[\bar{\Psi}, \Psi\right] e^{-\mathcal{S}\left[\bar{\Psi},\Psi\right]}, \tag{3.2}$$

$$\mathcal{S}\left[\bar{\Psi}, \Psi\right] = \sum_n \int_0^\Lambda \frac{d^2\boldsymbol{k}}{(2\pi)^2} \Psi^\dagger(\omega_n, \boldsymbol{k}) \left(-i\omega_n + \boldsymbol{k}\cdot\boldsymbol{\sigma} + g\phi_0\right) \Psi(\omega_n, \boldsymbol{k}) \tag{3.3}$$

$$+ \sum_n \int_0^\Lambda \frac{d^2\boldsymbol{k}}{(2\pi)^2} \frac{m^2\phi_0^2}{2} \tag{3.4}$$

The Hamiltonian in the above action is diagonalised with the use of a unitary transformation, which also prompts a transformation of the fermionic fields $U^\dagger\Psi \equiv \eta$. The result is an action that is diagonal in the single particle energy eigenstates,

$$\mathcal{Z} = \int \mathcal{D}\left[\eta_a^\dagger, \eta_a\right] \exp\left(-\frac{m^2\beta\Lambda}{2(2\pi)^2}\phi_0^2 - \sum_n \int_0^\Lambda \frac{d^2\boldsymbol{k}}{(2\pi)^2}\, \eta_{a,n}^\dagger(-i\omega_n + \varepsilon_a(\boldsymbol{k}))\eta_{a,n}\right) \tag{3.5}$$

where $a = \pm$ and $\varepsilon_a(\boldsymbol{k}) = a\sqrt{|\boldsymbol{k}|^2 + (g\phi_0)^2}$. Now changing the sum over the Matsubara frequencies to a product using properties of exponentials, we then integrate out the fermionic fields. This is trivial since the diagonalisation has decoupled the fields, and we can use Wick's theorem. This results in the following partition function,

$$\mathcal{Z} = e^{-\frac{m^2\beta\Lambda}{2(2\pi)^2}\phi_0^2} \prod_n \int_0^\Lambda \frac{d^2\boldsymbol{k}}{(2\pi)^2}(-i\omega_n + \varepsilon_a(\boldsymbol{k})) \tag{3.6}$$

The free energy is related to the partition function by the following, relation $F = -T\log(\mathcal{Z})$, we arrive at the following equation for the free energy,

$$F = \frac{m^2\Lambda}{2(2\pi)^2}\phi_0^2 - T\sum_n \int_0^\Lambda \frac{d^2\boldsymbol{k}}{(2\pi)^2}\log\left(-i\omega_n + \varepsilon_a(\boldsymbol{k})\right) \tag{3.7}$$

The Matsubara sum can be done with the use of contour integration and a suitably chosen distribution function (in this case the Fermi-Dirac distribution) to arrive at the following,

$$F = \frac{m^2\Lambda}{2(2\pi)^2}\phi_0^2 - T\int_0^\Lambda \frac{d^2\boldsymbol{k}}{(2\pi)^2}\log\left(1 + e^{-\beta\varepsilon(\boldsymbol{k})}\right). \tag{3.8}$$

In the zero temperature limit the integral can be approximated by an integral over the occupied energy band, which in the case of charge neutrality, is just the lower band,

$$F = \frac{m^2\Lambda}{2(2\pi)^2}\phi_0^2 - \int_0^\Lambda \frac{d^2\boldsymbol{k}}{(2\pi)^2}\sqrt{|\boldsymbol{k}|^2 + (g\phi_0)^2} \tag{3.9}$$

$$= \frac{m^2\Lambda}{2}\phi_0^2 + \frac{g^3|\phi_0|^3}{3} - \frac{\left(\Lambda^2 + (g\phi_0)^2\right)^{3/2}}{3}. \tag{3.10}$$

The appearance of a $|\phi_0|^3$ term is a signature that already at mean-field level the phase transition from a Dirac semimetal to a CDW insulator is distinct from the ordinary Ising transition. The free energy is no longer an analytic function of the order parameter. Physically the non-analytic term arises from the gapless nature of the fermionic excitations.

Near the phase transition we can take ϕ_0 to be small and therefore $\Lambda \gg g\phi_0$. Using this expansion we can calculate ϕ_0 which minimizes the free energy,

$$\frac{\partial F}{\partial \phi_0} = 0 \implies \phi_0\left(\Lambda(m^2 - g^2) + g^3|\phi_0|\right) = 0. \tag{3.11}$$

Hence we see that if $m^2 > g^2$ we are in the disordered phase where $\langle\phi_0\rangle = 0$, i.e the Dirac semimetal phase, while if $m^2 < g^2$ then $\langle\phi_0\rangle \neq 0$ and the system is in the broken symmetry phase which in this case is the CDW state. This illustrates why the bosonic mass $m^2 \sim g_{(c)}^2$ can be thought of as the tuning parameter for the transition. The mean-field order parameter exponent β can be obtained from the relation $\phi_0 \sim |(V_c - V)/V_c|^{\beta_{\text{MF}}}$ where

V is a parameter which drives the transition, in our case g^2. Hence for the Dirac semimetal to CDW insulator transition, we find that the mean-field order parameter exponent $\beta_{\rm MF}^{\rm Dirac} = 1$, which is distinct from the exponent for the Ising transition where $\beta_{\rm MF} = \frac{1}{2}$.

3.1.2 Semi-Dirac Fermions

We now present the same calculation but for the case of a semi-Dirac semimetal. Accounting for the difference in the non-interacting dispersion compared to the Dirac case, Eq.(3.9) becomes,

$$F_{\rm SD} = \frac{m^2\Lambda}{2(2\pi)^2}\phi_0^2 - T\int_{k_L^2+k_Q^4\leq\Lambda^2}\frac{dk_L dk_Q}{(2\pi)^2}\sqrt{k_L^2+k_Q^4+(g\phi_0)^2}, \tag{3.12}$$

where as before k_L denotes the linear momentum direction, and k_Q denotes the quadratic direction. Carrying out the integral one obtains

$$F_{\rm SD} = a(\delta g)\phi_0^2 + b|\phi_0|^{\frac{5}{2}} + \mathcal{O}(\phi_0^4). \tag{3.13}$$

with $\delta g = (g_c^2 - g^2)/g_c^2$ and $a, b > 0$. As in the case of relativistic Dirac fermions, the mean-field free energy contains a non-analytic term, $|\phi_0|^{\frac{5}{2}}$, which once again arises from the gapless nature of the excitations as well as from the vanishing density of states at the nodal point. Minimizing $F_{\rm SD}(\phi_0)$ with respect to ϕ_0 one obtains $|\phi_0| \sim |\delta g|^{\beta_{\rm SD}}$ with $\beta_{\rm SD} = 2$.

It's possible to further extend the description of this phase transition by allowing the order parameter to vary in space, i.e. $\phi_0 \to \phi = \phi_0 + \delta\phi(\boldsymbol{r})$, where $\delta\phi(\boldsymbol{r})$ is some small, long-wavelength modulations of the order parameter away from the mean-field configuration. Then this so-called Ginzburg-Landau free energy would be a *functional* of the order parameter, and would depend on its gradients.

For the case of semi-Dirac, an expansion in small $\boldsymbol{k}$ momentum of the modulations, would give rise to terms [52]

$$q_L^2\sqrt{|\phi|}, \quad q_Q^2|\phi|^{\frac{3}{2}}. \tag{3.14}$$

From these we can estimate the correlation lengths ξ_L and ξ_Q along the linear and quadratic dispersing directions respectively. Since

$$\xi_L^{-2}|\phi_0|^{\frac{1}{2}} \simeq \xi_Q^{-2}|\phi_0|^{\frac{3}{2}} \simeq |\delta g|\phi_0^2 \tag{3.15}$$

by dimensional analysis, that leads to the quantum critical scaling

$$\xi_L^2 \sim |\phi_0|^{-\frac{3}{2}} |\delta g|^{-1} \sim |\delta g|^{-(1+\frac{3}{2}\beta_{\rm MF})}, \tag{3.16}$$

and

$$\xi_Q^2 \sim |\phi_0|^{-\frac{1}{2}} |\delta g|^{-1} \sim |\delta g|^{-(1+\frac{1}{2}\beta_{\rm MF})}. \tag{3.17}$$

Using $\beta_{\rm MF} = 2$, this simple scaling analysis of the mean-field free energy yields the correlation length exponents $\nu_L = 2$ and $\nu_Q = 1$.

The anisotropic scaling of the correlation length along the linear and quadratic directions could have very interesting implications for ordered phases in the vicinity of the quantum critical point. In general, the order parameter becomes relatively softer to spatial modulations along the direction where the quasiparticles have parabolic dispersion, and more rigid in the other direction, permitting the emergence of modulated order and stripe phases [52]. In the superconducting case, the system may effectively respond to a external magnetic field as a type II superconductor in one direction and as a type I in the other [52]. This unconventional state could stabilize stripes of magnetic flux rather than conventional vortex lattices.

Chapter 4

Introduction to Perturbative Renormalisation Group

In this chapter we introduce the concepts behind the theory of Renormalisation Group in Sec. 4.1. Then we use Wilson's momentum shell implementation to analyse the ϕ^4 theory near the upper critical dimension in Sec. 4.2. The famous ϵ-expansion is also introduced.

4.1 RG basic concepts

Here we introduce the theory of Renormalisation Group (RG) of phase transitions as first formulated by Wilson [8, 53], a detailed explanation of the concept can be found in Refs. [6, 54].

In condensed matter we are usually concerned with physics at low energies and large length scales, as the long-distance behaviour of a correlation function contains information about any symmetry breaking and therefore the underlying phase. The theory of RG aims to access the low energy behaviour by a successive decimation of short-distance/high-energy degrees of freedom, followed by a rescaling of the theory such that the long-distance behaviour remains unchanged. This effectively results in a "flow" of the coupling constants of the theory. Following this so called "RG" flow to longer and longer length scales, the couplings will flow to asymptotic values (known as fixed points). If the values of the couplings at this fixed point are zero or infinite then it corresponds to a stable phase. If on the other hand the solution to the flow equations is finite then the fixed point corresponds to a

continuous phase transition. Thus with the use of the decimation of high energy modes, and rescaling of momenta and fields we aim to find and classify RG fixed points.

RG transformation

At a critical point between a disordered and an ordered phase the correlation length ξ diverges (for an infinite sized system), and so any two points are infinitely correlated (i.e. there is no intrinsic length scale in the system), hence under a scale transformation

$$\tau' = \tau e^{-z\ell}, \quad x_i' = x_i e^{-\ell} \tag{4.1}$$

we would expect the system to be invariant. Here the factor of z, known as the dynamical exponent, serves to account for any difference in scaling between the spatial directions, x_i, and the imaginary time, τ.

For infinitesimal transformations it is valuable to introduce the notion of a *scaling dimension* of a parameter X, where under the transformation in Eq. (4.1), it scales as

$$X' = X e^{[X]\delta\ell}, \tag{4.2}$$

which defines $[X]$. The scaling dimension allows to characterise the nature of a small perturbation of the parameter to a particular RG fixed point. The sign of the scaling dimension classifies whether the parameter is a relevant ($[X] > 0$), irrelevant ($[X] < 0$), or a marginal ($[X] = 0$) perturbation. Hence a fixed point is said to be stable if all symmetry breaking perturbations at the critical point are irrelevant, and unstable if there is at least one relevant perturbation.

Momentum-shell RG

In the momentum shell formulation of RG, there are three steps: (a) we are interested in long-distance physics so the degrees of freedom are separated into slow modes $\psi_<(\boldsymbol{k})$ where $|\boldsymbol{k}| < \Lambda e^{-\delta\ell}$ and fast modes $\psi_>(\boldsymbol{k})$ where $\Lambda e^{-\delta\ell} < |\boldsymbol{k}| < \Lambda$ (b) integrate out the fast modes while preserving the form of the action, i.e. renormalise the set of couplings $\{g_i\}$ (c) rescale the slow fields and the momenta up to the original kinematic region. Under a successive infinitesimal decimation of the fast modes within the above cycle, the flow

of the couplings can be described by a set of coupled differential equations,

$$\frac{d}{d\ell} g_i = f(\{g_i\}) \tag{4.3}$$

which are in the literature known as the β-equations. The solution of these flow equations will lead to critical points and their characteristics.

Critical exponents

While at the phase transition the correlation length diverges, in its vicinity it follows a power law,

$$\xi \sim |g - g_c|^{-\nu} \tag{4.4}$$

where g is a dimensionless coupling of the underlying Hamiltonian that tunes through the critical point where $g = g_c$, and ν is the correlation length exponent. Additional power laws define other critical exponents, like the order parameter exponent β; phase transitions that posses identical critical exponents are said to be in the same universality class.

4.2 ϕ^4 theory of phase transitions

We now illustrate Wilson's momentum shell renormalisation group procedure for the simplest interacting field theory that describes a phase transition, i.e. the theory of a single fluctuating scalar field ϕ in d-dimensions known as the ϕ^4 theory. It's partition function is given by,

$$\mathcal{Z} = \int \mathcal{D}[\phi(k)] e^{-\mathcal{S}[\phi(k)]} \tag{4.5}$$

where the action in momentum space is

$$\mathcal{S} = \mathcal{S}_\phi + \mathcal{S}_\lambda \tag{4.6}$$

$$\mathcal{S}_\phi = \frac{1}{2} \int_0^\Lambda \frac{d^d \boldsymbol{k}}{(2\pi)^d} \left(k^2 + m^2\right) \phi^2(\boldsymbol{k}) \tag{4.7}$$

$$\mathcal{S}_\lambda = \lambda \int_0^\Lambda \prod_{i=1,2,3,4} \frac{d^d \boldsymbol{k}_i}{(2\pi)^d} \phi(\boldsymbol{k}_1)\phi(\boldsymbol{k}_2)\phi(\boldsymbol{k}_3)\phi(\boldsymbol{k}_4) \times \\ \times \delta(\boldsymbol{k}_1 + \boldsymbol{k}_2 + \boldsymbol{k}_3 + \boldsymbol{k}_4) \tag{4.8}$$

where $\boldsymbol{k} = (k_1, \cdots, k_d)$ is a d-dimensional vector, $k^2 = |\boldsymbol{k}|^2$, and Λ is the UV cut-off which is inversely proportional to the lattice constant $\sim \frac{1}{a}$.

There are a plethora of models which after coarse graining take the form of the ϕ^4 theory - generally any system whose long-range behaviour can be described by a scalar order parameter. The simplest model is that of the classical d-dimensional Ising model, which itself describes the magnetic transition of Ising spins on a lattice.

4.2.1 Tree level scaling

We first define the elementary RG transformation rules, i.e. how the momenta and the bosonic field rescale,

$$\boldsymbol{k}' = \boldsymbol{k} e^{-\delta\ell} \tag{4.9}$$

$$\phi(\boldsymbol{k}) = \phi'(\boldsymbol{k}') e^{-\Delta_\phi \delta\ell/2} \tag{4.10}$$

where the critical dimension $\Delta_\phi = [\phi\phi] + \eta_\phi$ contains the tree-level information as well as the anomalous rescaling.

Requiring that the $\int k^2\phi^2$ is invariant under the RG transformation, sets $[\phi\phi] = -(d+2)$, while a similar calculation results in $[m^2] = 2$. This means that under the successive decimation of high energy modes, the bosonic mass will keep increasing in value, i.e. it is a relevant coupling under the RG flow. Worth noting that this is the case for any spatial dimension d. As showcased in Sec. 3.1, the bosonic mass acts at the tuning parameter for the transition.

Meanwhile the tree level scaling of the quartic term $[\lambda] = 4 - d$, tells us that the interaction is relevant in $d < 4$, marginal in $d = 4$, and irrelevant in $d > 4$. This sets the upper critical dimension of this action to be four spatial dimensions, as when we're above it the ϕ^4 term is irrelevant and can be discarded, and the critical exponents are of mean-field character.

4.2.2 Cumulant Expansion

We now separate the bosonic fields, into fast $\phi_>$ and slow fields $\phi_<$, which are defined over $|\boldsymbol{k}| < \Lambda e^{-d\ell}$ and $\Lambda e^{-d\ell} < |\boldsymbol{k}| < \Lambda$ respectively. The action then takes the form,

$$\mathcal{Z} = \int \mathcal{D}[\phi_<, \phi_>] e^{-\mathcal{S}[\phi_<] - \mathcal{S}[\phi_>] - \mathcal{S}_{\text{int}}[\phi_<, \phi_>]} \tag{4.11}$$

where $\mathcal{S}_{\text{int}}$ mixes the fast and the slow fields. The aim now is to integrate out the fast fields, in order to obtain an action in terms of the slow fields only. To achieve this we take the average with respect to the fast fields,

$$\mathcal{Z} = \int \mathcal{D}[\phi_<] e^{-\mathcal{S}[\phi_<]} \left\langle e^{-\mathcal{S}_{\text{int}}[\phi_<, \phi_>]} \right\rangle_> \tag{4.12}$$

where $\langle \cdots \rangle_>$ denotes an average with respect to the fast fields. As it's not trivial to perform an average of an exponential, a perturbative expansion in the coupling λ is performed. The average of the resulting Taylor series can be then evaluated using Wick's theorem.

$$\mathcal{Z} = \int \mathcal{D}[\phi_<] e^{-\mathcal{S}[\phi_<]} \left\langle \sum_{n=1}^{\infty} \frac{(-1)^n (\mathcal{S}_{\text{int}})^n}{n!} \right\rangle_> \tag{4.13}$$

Each term in the series can be represented by a Feynman diagram, with n external legs which represent the slow fields. By re-exponentiating the average it is then possible to use the linked-cluster theorem to exchange the sum over all possible diagrams to a sum of diagrams that are connected (con.) and one particle irreducible (1PI).

$$\mathcal{Z} = \int \mathcal{D}[\phi_<] \exp\left\{ -\mathcal{S}[\phi_<] + \left\langle \sum_{n=1}^{\infty} \frac{(-1)^n (\mathcal{S}_{\text{int}})^n}{n!} \right\rangle_>^{\text{1PI, con.}} \right\} \tag{4.14}$$

$$= \int \mathcal{D}[\phi_<] \exp\left\{ -\underbrace{(\mathcal{S}[\phi_<] + \delta\mathcal{S}[\phi_<])}_{\mathcal{S}'} \right\} \tag{4.15}$$

Essentially it is now possible to organise the series in the number of internal loops of the Feynman diagrams as higher loops will come with higer powers λ. At one loop order, the perturbative corrections for the ϕ^4 theory, Eq.(4.6), would take the following form,

$$\delta\mathcal{S}_{\text{one loop}} = \langle \mathcal{S}_\lambda \rangle_> - \frac{1}{2} \langle \mathcal{S}_\lambda^2 \rangle_>. \tag{4.16}$$

The two corrections are reproduced diagramatically in Fig. 4.2.3 where as we'll see the bosonic mass m^2 and the quartic interaction strength term λ are renormalised, $m^2 \to (m^2)'$ and $\lambda \to \lambda'$,

$$\mathcal{S} \to \mathcal{S}' = \int (k^2 + (m^2)')\phi^2 + \lambda' \int \phi^4. \tag{4.17}$$

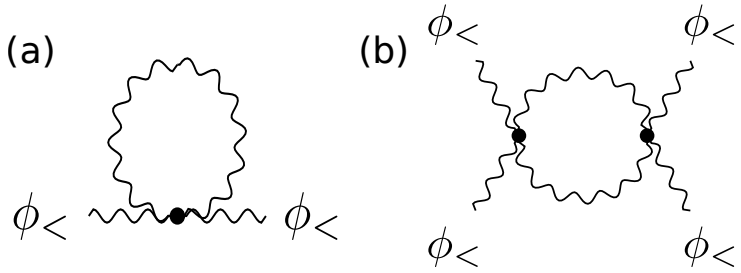

Figure 4.1: Diagrams that contribute at one-loop level to the renormalisation of the ϕ^4 action. (a) $\langle \mathcal{S}_\lambda \rangle$: contains two external legs, which means that it renormalises the bosonic propagator, a zero momentum diagram means that only the bosonic mass is impacted (b) $\langle \mathcal{S}_\lambda^2 \rangle$: renormalises the quartic term, evaluated at zero external momentum.

4.2.3 RG at one-loop order

We now present the perturbative RG calculation up to one loop order. To calculate the corrections the following bosonic propagator is used,

$$\langle \phi(\boldsymbol{k})\phi(\boldsymbol{q})\rangle = G_\phi(\boldsymbol{k})\delta(\boldsymbol{k}+\boldsymbol{q}) = \frac{\delta(\boldsymbol{k}+\boldsymbol{q})}{k^2+m^2} \tag{4.18}$$

The diagram in Fig. 4.2.3(a) evaluates to

$$\langle \mathcal{S}_\lambda \rangle = 6\lambda \int_0^{\Lambda e^{-\delta\ell}} |\phi(\boldsymbol{k})|^2 \frac{d^d\boldsymbol{k}}{(2\pi)^d} \int_{\Lambda e^{-\delta\ell}}^{\Lambda} G_\phi(\boldsymbol{q}) \frac{d^d\boldsymbol{q}}{(2\pi)^d} \tag{4.19}$$

where ϕ's are the slow fields defined over $|\boldsymbol{k}| < \Lambda e^{-d\ell}$, and the factor of 6 comes from the number of combinations the fast fields can be contracted. There is no external momenta in the shell integral, hence the correction couples to and renormalises the zero momentum term, i.e. the bosonic mass. In the limit that $d\ell \ll 1$, the shell integral over the bosonic propagator is trivial and results in the following correction

$$\langle \mathcal{S}_\lambda \rangle = \frac{1}{2}\int |\phi(k)|^2 \; 12 S_d \frac{\Lambda^d d\ell}{\Lambda^2+m^2}\lambda. \tag{4.20}$$

Here S_d denotes the surface area of a d-dimensional unit sphere,

$$S_d = \frac{1}{(2\pi)^d}\frac{2\pi^{d/2}}{\Gamma(d/2)} \tag{4.21}$$

Hence we find the change in the bosonic mass,

$$(m^2)' = m^2 + 12 S_d \frac{\Lambda^d d\ell}{\Lambda^2 + m^2} \lambda. \tag{4.22}$$

Now coupling this correction with the last step of the RG process, i.e. rescaling up to the original momentum range, we arrive (using the fact that $[m^2] = 2$) at the RG equation for the bosonic mass,

$$\frac{dm^2}{d\ell} = 2m^2 + 12 S_d \frac{\Lambda^d}{\Lambda^2 + m^2} \lambda \tag{4.23}$$

To complete the renormalisation group treatment, we tackle the (b) diagram in Fig.4.2.3,

$$-\frac{1}{2}\langle \mathcal{S}_\lambda^2 \rangle = -36 S_d \frac{\Lambda^d d\ell}{(\Lambda^2 + m^2)^2} \lambda^2 \int_0^{\Lambda e^{-\delta\ell}} \frac{d^d \boldsymbol{k}_i}{(2\pi)^{4d}} \phi(\boldsymbol{k}_1)\phi(\boldsymbol{k}_2)\phi(\boldsymbol{k}_3)\phi(-\boldsymbol{k}_1 - \boldsymbol{k}_2 - \boldsymbol{k}_3) \tag{4.24}$$

after rescaling ($[\lambda] = 4 - d$), we arrive at the RG equation for the ϕ^4 term

$$\frac{d\lambda}{d\ell} = (4 - d)\lambda - 36 S_d \frac{\Lambda^d}{(\Lambda^2 + m^2)^2} \lambda^2 \tag{4.25}$$

Equations (4.23) and (4.25) are the so-called β-equations for the running parameters of our theory.

4.2.4 Fixed points of the RG flow

As we will see the system of coupled equations supports two fixed points, i.e. points for which the RG flow is stationary. The trivial (Gaussian) fixed point for which both the bosonic mass m^2 and quartic interaction λ are zero.

However when we consider what happens away from the Gaussian fixed point we run into a problem. We have computed the flow using a perturbative expansion in λ and considered only diagrams up to one-loop order. However below the upper critical dimension such considerations might not be valid anymore as the quartic interaction is relevant and the RG flow increases λ, especially near the physical dimension of interest $d = 3$.

Wilson and Fischer in their famous paper [55] investigated the flow with the use of a controlled small parameter ϵ which denotes the deviation from the upper critical dimension,

$$\epsilon \equiv 4 - d. \tag{4.26}$$

While the shell integrals depend on d the number of dimensions, there is no constraint on whether it's continuous or discrete. Close to the upper critical we are then able take $\epsilon \ll 1$ and retain terms of $\mathcal{O}(\epsilon)$, which results in the following flow equations

$$\frac{dm^2}{d\ell} = 2m^2 + 12S_4 \frac{\Lambda^4}{\Lambda^2 + m^2}\tilde{\lambda} + \mathcal{O}(\epsilon^2) \tag{4.27}$$

$$\frac{d\tilde{\lambda}}{d\ell} = \epsilon\tilde{\lambda} - 36S_4 \frac{\Lambda^4}{(\Lambda^2 + m^2)^2}\tilde{\lambda}^2 + \mathcal{O}(\epsilon^2) \tag{4.28}$$

where we've redefined $\tilde{\lambda} = \Lambda^{-\epsilon}\lambda$. The ϵ-expansion also motivates the expansion in the number of loops of Feynman diagrams, e.g. two-loop diagrams scale as ϵ^2. These coupled RG equations support two fixed points, the previously mentioned Gaussian fixed point as well as the celebrated Wilson-Fisher fixed point,

$$m_*^2 = -\frac{1}{6}\Lambda^2\epsilon, \quad \tilde{\lambda}_* = \frac{2\pi^2}{9}\epsilon. \tag{4.29}$$

As long as ϵ is small, then the value of the quartic interaction at the fixed point will be small as well, ensuring the self-consistency of the expansion.

Stability of fixed points

To gain an understanding of the RG flow, it is imperative to investigate it in the vicinity of the fixed points. This can be done so by linearising the RG equations. Let $K_* = (m_*^2, \tilde{\lambda}_*)$ denote the critical values of the couplings, such that near the fixed point $K = K_* + \delta K$. The flow is then

$$\beta_\alpha(K) = \frac{dK}{d\ell} = \frac{d\left(K_* + \delta K\right)}{d\ell} = \frac{d(\delta K)}{d\ell} = \left.\frac{d\beta_\alpha(K)}{dK}\right|_{K_*} \delta K \tag{4.30}$$

where β_α is the beta-equation (RG flow) for the coupling α. For the case of the Wilson-Fisher fixed point the stability matrix is,

$$\frac{d}{dl}\begin{pmatrix}\delta m^2 \\ \\ \delta\tilde{\lambda}\end{pmatrix} = \begin{pmatrix} 2 - \dfrac{\epsilon}{3} & \dfrac{(6+\epsilon)\Lambda^2}{4\pi^2} \\ \\ 0 & -\epsilon \end{pmatrix}\begin{pmatrix}\delta m^2 \\ \\ \delta\tilde{\lambda}\end{pmatrix}, \tag{4.31}$$

Diagonalising the matrix, we find two eigenvalues

$$\mu_1 = 2 - \frac{\epsilon}{3} + \mathcal{O}(\epsilon^2), \quad \mu_2 = -\epsilon + \mathcal{O}(\epsilon^2), \tag{4.32}$$

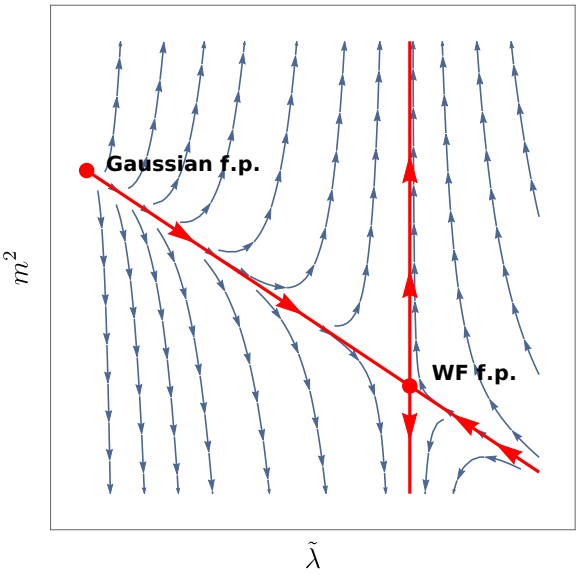

Figure 4.2: The flow diagram of the RG equations for the ϕ^4 theory. The Gaussian fixed point where $(m^2, \tilde{\lambda}) = (0, 0)$ is unstable to both the bosonic mass and the quartic interactions. While the Wilson-Fisher fixed point where $(m^2, \tilde{\lambda}) = (-\frac{1}{6}\Lambda^2\epsilon, \frac{2\pi^2}{9}\epsilon)$ has one relevant direction and one irrelevant.

with new respective eigencouplings $w_{1,2}$, which are linear combination of the original couplings m^2 and $\tilde{\lambda}$, the behaviour of which near the critical points is governed by the flow equation $dw_i/d\ell = \mu_i w_i$. Hence we see that as μ_2 is negative for any ϵ, the coupling w_1 will always flow back to the Wilson-Fisher fixed point, i.e. it's an irrelevant pertubation. This means that the theory near the fixed point reduces to just the flow of one relevant coupling, namely w_2. This can be seen clearly in Fig. 4.2.4.

We can then associate this relevant coupling with the reduced temperature $w_2 \sim t = |T - T_c|/T_c$ which measures the deviation away from criticality and is the relevant direction at the classical Wilson Fisher point. As we move away from the fixed point we introduce a length scale into the system, commonly known as the correlation length, which scales as

$$\xi \sim t^{-\nu} = t^{-1/\mu_2}. \tag{4.33}$$

Hence we find that the correlation length exponent is

$$\nu = \frac{1}{\mu_1} = \frac{1}{2} + \frac{\epsilon}{12} + \mathcal{O}(\epsilon^2). \tag{4.34}$$

The critical exponent for the scaling of the specific heat is given by the "hyperscaling relation", $\alpha = 2 - d\nu$,

$$C \sim t^{-\alpha} \quad \text{where} \quad \alpha = \frac{\epsilon}{6} + \mathcal{O}(\epsilon^2). \tag{4.35}$$

Further critical exponents require calculation of higher loop diagrams, which enable the renormalisation of the momenta terms in the bosonic propagator. This in turn allows for the calculation of the bosonic anomalous dimension η_ϕ, from which the rest of the critical exponents follow.

While we've only established the existence of the Wilson-Fisher fixed point for small ϵ, it is instructive to consider what happens at the the dimension of interest to us, i.e. $d = 3$ for which $\epsilon = 1$. Qualitatively we might think that the picture of an interacting fixed point persists even as the pertubation theory breaks down. Sophisticated techniques like conformal bootstrap and ϵ-expansions up to fifth order in ϵ have confirmed this suspicion [56, 57, 58, 59, 60]. Moreover, amazingly the one-loop critical exponents evaluated at $\epsilon = 1$ are quite close to more accurate values evaluated with the aforementioned methods. This portrays the power of the ϵ-expansion.

Chapter 5

RG approach to interacting Dirac fermions

The original work presented in this Chapter first appeared in *Fermionic criticality of anisotropic nodal point semimetals away from the upper critical dimension: Exact exponents to leading order in* $\frac{1}{N_f}$, M. D. Uryszek, F. Krüger, E. Christou, Physical Review Research, **2**, 043265 (2020)[38].

5.1 Introduction

The discovery of topological insulators has led to an explosion of research into topological aspects of electronic band structures in two and three dimensions [13, 14]. In the so-called nodal-point semimetals, valence and conduction bands touch at a number of discrete points in the Brillouin zone. The most fundamental members of this family are Weyl or Dirac semimetals [9, 10, 11], which exhibit relativistic low-energy excitations that are protected by topology and symmetry.

Semimetals with point-like Fermi surfaces provide the simplest setting to study fermionic quantum criticality. Quantum phase transitions can be driven by sufficiently strong short-range electron-electron interactions in the underlying lattice model. Depending on the nature of the microscopic interactions, this can lead to various types of symmetry breaking, resulting in rich phase diagrams with antiferromagnetic, charge-density wave, and bond-ordered phases, as studied in great detail for extended Hubbard models on the honeycomb lattice [61, 47, 62, 63, 48, 64, 65, 66, 67, 68]. Irrespective of

the particular order, the spontaneous symmetry breaking generically leads to the opening of a gap in the fermion spectrum and is therefore concurrent with semimetal-insulator transitions.

The universality of a particular transition can be studied using an effective field theory that is derived through a Hubbard-Stratonovich decoupling of the interaction vertex in the relevant channel, followed by the conventional coarse graining procedure. This results in a dynamical bosonic order-parameter theory which is coupled to the gapless fermion excitations. In the purely relativistic case of Dirac fermions, this is known as the Gross-Neveu-Yukawa (GNY) theory [30, 31, 69], which describes chiral symmetry breaking and spontaneous mass generation in high-energy physics [49, 50]. The coupling between the order parameter fields and the gapless Dirac fermions leads to novel fermion-induced critical behavior that falls outside the Landau-Ginzburg-Wilson paradigm of a pure order parameter description [70].

Wilson's momentum shell implementation of the theory Renormalisation Group (RG) has been extremely successful in discerning the existence of critical points of phase transitions and in calculating their properties. e.g. critical exponents. It's most famous approach being the ϵ-expansion; a framework first developed by Wilson and Fisher [55], that has been effective in systems near the upper critical dimension (UCD). However without going to high loop order and resummation of divergent series the expansion is unlikely to be controlled when $\epsilon \sim \mathcal{O}(1)$. This is a pressing problem as most interesting condensed matter systems are away from the upper critical dimension where quantum fluctuations are strong.

An alternative perturbative approach within the naive momentum shell framework has been to work directly in the physical dimension and generalise to a large number N_f of fermionic flavours. At which point one can either integrate out the fermions to obtain an effective action in the order parameter [71, 72], or naively perturb in $1/N_f$ in the composite fermion and boson picture. The former approach is not applicable to systems that host gapless fermionic and bosonic excitations at the critical point (i.e. systems that exhibit fermionic quantum criticality), as obtained bosonic action is non-analytic [73]. While the latter naive approach has resulted in disparate results across nodal-point semimetal literature [74, 75].

The correct procedure within the large N_f formulation (which has not always been followed in the nodal-point semimetal field) is to compute bosonic and fermionic self-energies in a self-consistent scheme and to use the dressed dynamical propagators as input in subsequent RG calculations, as explained

in Ref. [40]. Such an approach was commonly used to understand quantum critical behaviour of metals [76, 77, 78, 79, 80, 81, 82, 83], although it was later shown that the $1/N_f$ expansion fails at higher-loop order in systems with a full two-dimensional Fermi surface [84].

The necessity to use a dressed boson propagator is not a mere technical issue. It is intimately linked to the phenomenon of Landau damping of order-parameter fluctuations by gapless electronic particle-hole excitations. This damping is known to completely change the long-wavelength behaviour of the system, leading to distinct critical behaviour. In itinerant ferromagnets, long-range spatial correlations associated with the Landau damping of the order parameter field generate a negative, non-analytic contribution to the static magnetic susceptibility, rendering the Hertz-Millis-Moriya theory [71, 72] unstable towards first-order behaviour or incommensurate order [85].

We demonstrate that the use of an incorrect bosonic IR propagator gives rise to non-universal results that depend on the UV cutoff scheme. In turn, enforcement of cutoff independence leads to the correct scaling form of the bosonic IR propagator, which is given by the full RPA fermion loop resummation.

Using the soft cutoff approach with the dressed order-parameter propagator, we compute the exact critical exponents for relativistic Dirac ($1 < d = d_L < 3$) fermions to leading order in $1/N_f$, and to all loop orders.

In this chapter we tackle the isotropic relativistic (i.e. Dirac) case to illustrate the problem of unphysical cutoff dependence, to introduce the methodology of our approach in a simplified setting, and to demonstrate that our approach reproduces the critical exponents obtained by conformal bootstrap [86, 87, 88] and other methods [89, 90, 91]. The anisotropic case will be investigated in Chapter 6.

Firstly, in Sec. 5.3 we analyse the tree level scaling of the GNY theory of Dirac fermions, generalised to large number N_f of fermion flavours. Then in Sec. 5.5 we show that perturbative momentum shell RG leads to non-universal, cut-off dependent results, as it does not correctly account for this non-analytic structure. In turn in Sec. 5.5, using a completely general soft cut-off formulation, we demonstrate that the correct IR scaling of the dressed bosonic propagator can be deduced by enforcing that results are independent of the cut-off scheme. Using the soft cut-off RG with the dressed dynamical RPA boson propagator, in Sec. 5.6 we compute the exact critical exponents and compare with previous literature. Lastly, in Sec. 5.7 we look at the connections between the ϵ-expansion and the soft-cut off approach near the

upper critical dimension.

5.2 GNY theory of Dirac fermions

For ease of reading we lay out the GNY action in momentum space and in $D = d + 1$ dimensions, where d denotes the number of spatial dimensions (for the Lagrangian see Eq. (2.30)),

$$S = S_\Psi + S_\phi + S_g + S_\lambda, \tag{5.1}$$

$$S_\Psi = -i \int dk\ \bar{\Psi}(\omega, \boldsymbol{k})\,(\omega\gamma_0 + v\boldsymbol{k}\cdot\boldsymbol{\gamma})\,\Psi(\omega, \boldsymbol{k}) \tag{5.2}$$

$$S_\phi = \frac{1}{2}\int dk\ (\omega^2 + c^2|\boldsymbol{k}|^2 + m^2)|\phi(\omega, \boldsymbol{k})|^2 \tag{5.3}$$

$$S_g = \frac{g}{\sqrt{N_f}}\int dkdq\ \phi\,(\Omega, \boldsymbol{q})\,\bar{\Psi}\,(\omega + \Omega, \boldsymbol{k} + \boldsymbol{q})\,\Psi(\omega, \boldsymbol{k}) \tag{5.4}$$

$$S_\lambda = \lambda \int \prod_{i=1,2,3,4} dk_i\ \phi(k_1)\phi(k_2)\phi(k_2)\phi(k_4)\delta(k_1 + k_2 + k_3 + k_4). \tag{5.5}$$

where the measure is defined as

$$\int dk = \int_{-\infty}^{\infty} \frac{d\omega}{2\pi} \int_0^\Lambda \frac{d^d\boldsymbol{k}}{(2\pi)^d} \tag{5.6}$$

and v and c are the fermionic and bosonic velocities respectively, and $\delta(k_i + \cdots)$ is the standard Dirac-delta distribution. To gain analytic control we have generalised to N_f-component Dirac fields, $\Psi = (\Psi_1, \cdots, \Psi_{N_f})$. The Dirac γ matrices anticommute, $\{\gamma_\mu, \gamma_\nu\} = 2\delta_{\mu\nu}$ for $\mu, \nu = 0, \cdots, d$ where $\boldsymbol{\gamma} = (\gamma_1, \cdots, \gamma_d)$ and the identity matrix is implicit. From this it follows that $\mathrm{Tr}(\gamma_\mu\gamma_\nu) = N_f\delta_{\mu\nu}$. Using this convention, the case of spinless fermions on the honeycomb lattice corresponds to $d = 2$ and $N_f = 4$, where it is customary to use the "graphene" representation, presented in Eqs. (2.25) - (2.29). We could then generalise to N flavours of these four-component fermions using $\gamma_\mu \to \gamma_\mu \otimes I_N$ where I_N is the N-dimensional identity matrix, such that $N_f = 4N$. The order parameter mass m^2 is an RG relevant perturbation that tunes through the quantum critical point $m^2 \sim V_c - V$. In contrast, although the Yukawa coupling g and the self-interaction λ are relevant at the non-interacting (Gaussian) fixed point, they are understood to flow to an infrared fixed point (g_*, λ_*) in the critical plane $m^2 = 0$.

5.3 Tree-Level Scaling

We start the scaling analysis by defining the transformation of momenta and frequency,

$$\omega' = \omega e^{-z\delta\ell}, \quad \boldsymbol{k}' = \boldsymbol{k} e^{-\delta\ell}, \tag{5.7}$$

where z is the dynamical exponent. We define the rescaling of the fields as

$$\Psi(k) = \Psi'(k') e^{-\Delta_\Psi \delta\ell/2}, \tag{5.8}$$

$$\phi(k) = \phi'(k') e^{-\Delta_\phi \delta\ell/2}, \tag{5.9}$$

where $\Delta_\Psi = [\bar{\Psi}\Psi] + \eta_\Psi$ and $\Delta_\phi = [\phi\phi] + \eta_\phi$ are the critical dimensions of the fermionic and bosonic fields, respectively. Requiring that the full action, Eq. (5.1), is invariant under the above field and momentum rescaling, we arrive at the following tree-level dimensions,

$$\begin{gathered} \left[\bar{\Psi}\Psi\right] = -(d+2z), \quad [\phi\phi] = -(d+3z) \\ [v] = z-1, \quad [c] = z-1, \quad [g] = \frac{3z-d}{2}, \quad [\lambda] = 3z-d, \end{gathered} \tag{5.10}$$

where the fermionic and bosonic field rescaling was chosen such that the frequency terms in S_Ψ and S_ϕ respectively were invariant, as is the convention. We see that at tree-level if $z = 1$ then both the fermion and boson velocities are marginal, and the theory is Lorentz invariant at the Gaussian fixed point. Whereas the Yukawa vertex g and the ϕ^4 vertex are both relevant perturbations at the non-interacting fixed point for $d < 3$, and irrelevant for $d > 3$. Hence $d = 3$ is called the upper critical dimension, where if above it the critical exponents reduce to their mean-field values.

5.4 Breakdown of naive Wilson RG

Momentum shell RG as first espoused by Wilson has been highly successful in bosonic theories like the well known ϕ^4 theory and in problems near the upper critical dimension. However as we will show, the naive formulation breaks down for the case of Dirac fermions coupled to an Ising order parameter away from the upper critical dimension. The GNY model at the quantum critical point possesses an emergent Lorentz invariance in $1 < d < 3$ that is characterised by a dynamical exponent $z = 1$ and a global terminal velocity, as has been observed with both the one-loop $\epsilon = 3 - d$ expansion of the

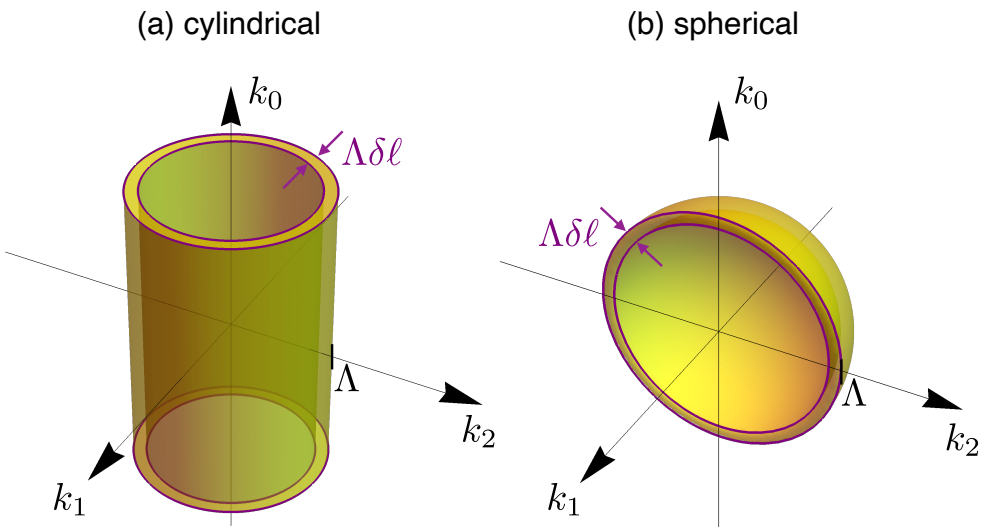

Figure 5.1: Wilson's infinitesimal shell RG integration schemes in $d = 2$ spatial dimensions, at the cutoff scale Λ: (a) cylindrical and (b) spherical. Here k_0 and $\boldsymbol{k} = (k_1, k_2)$ denote frequency and momenta, respectively.

effective Gross-Neveu-Yukawa (GNY) field theory [31] and lattice quantum Monte Carlo [69]. Here we analyse the GNY theory in $1 < d < 3$ dimensions, using Wilson's momentum-shell RG with two different cutoff schemes, as shown in Fig. 5.1. Although the universal long-wavelength behaviour should be independent of the choice of the cutoff scheme, we demonstrate that this is not the case within the perturbative momentum-shell framework. Using the cylindrical scheme in Fig. 5.1(a), where the UV cutoff only acts on the spatial momentum directions and frequency is integrated over the whole real axis, we find an apparent violation of emergent Lorentz invariance. On the other hand, treating frequency and momenta on an equal footing and imposing an isotropic spherical cutoff in $D = d + 1$ space-time dimensions, as shown in Fig. 5.1(b), we do find emergent Lorentz invariance. To illustrate the breakdown of Lorentz invariance, it is sufficient to only study the flow of the Fermi velocity v and the order parameter velocity c in the vicinity of the GNY fixed point. We obtain the velocity RG equations at one-loop order, using Wilson's momentum-shell RG. In this approach, modes of highest energy near the ultraviolet cutoff scale Λ, corresponding to infinitesimal shells in Matsubara frequency ω and momentum $\boldsymbol{k} = (k_1, \ldots, k_d)$, are integrated out.

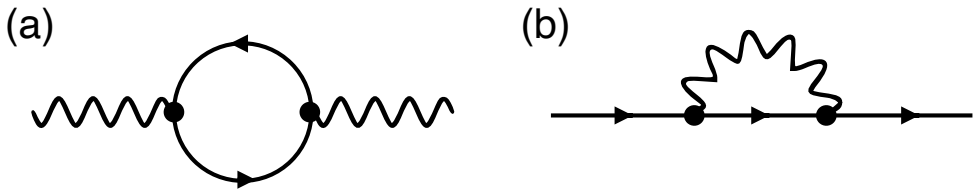

Figure 5.2: One-loop self energy Feynman diagrams for the velocity RG equations. The fermion propagator is denoted by the arrowed line. The order parameter boson propagator is denoted by the wavy line.

We consider the shell schemes displayed in Fig. 5.1,

$$\text{(a) cylinder:} \quad -\infty < \omega < \infty, \quad \Lambda e^{-\delta\ell} < |\boldsymbol{k}| < \Lambda, \tag{5.11}$$

$$\text{(b) sphere:} \quad \Lambda e^{-\delta\ell} < \sqrt{\omega^2/v^2 + \boldsymbol{k}^2} < \Lambda. \tag{5.12}$$

This is followed by the rescaling transformation as espoused in Eq. (5.7).

The quantum corrections are calculated from the one-loop fermion and boson self energy diagrams displayed in Fig. 5.2.

Using the cylindrical cutoff scheme, the resulting RG equations for the velocities are given by

$$\left(\frac{dv}{d\ell}\right)_{\text{cyl}} = v\left(z - 1 - g^2\frac{2(v-c) - (d-3)c}{2N_f vc(v+c)^2}\right), \tag{5.13}$$

$$\left(\frac{dc}{d\ell}\right)_{\text{cyl}} = c\left(z - 1 - g^2\frac{d(c^2-v^2) - (d-3)v^2}{16dv^3c^2}\right), \tag{5.14}$$

where we have made the rescaling $S_d\Lambda^{d-3}g^2 \to g^2$. Here S_d denotes the surface area of the d-dimensional unit sphere,

$$S_d = \frac{1}{(2\pi)^d}\frac{2\pi^{\frac{d}{2}}}{\Gamma(d/2)}. \tag{5.15}$$

On the other hand, using the spherical cutoff scheme in $D = d+1$ dimensions, we obtain the velocity RG equations

$$\left(\frac{dv}{d\ell}\right)_{\text{sph}} = v\left(z - 1 - g^2\frac{I_1\left(\frac{c}{v}\right) - I_0\left(\frac{c}{v}\right)}{N_f v^3}\right), \tag{5.16}$$

$$\left(\frac{dc}{d\ell}\right)_{\text{sph}} = c\left(z - 1 - g^2\frac{(D-2)(c^2-v^2)}{2Dv^3c^2}\right), \tag{5.17}$$

where we have made the rescaling $S_D \Lambda^{D-4} g^2 \to g^2$ and defined the angular integrals $I_\mu(x)$ over the D-dimensional unit sphere ($\hat{k}_0^2 + \hat{\boldsymbol{k}}^2 = 1$),

$$I_\mu(x) = \frac{1}{S_D (2\pi)^D} \int d\hat{\Omega} \frac{1 - 2\hat{k}_\mu^2}{\hat{k}_0^2 + x^2 \hat{\boldsymbol{k}}^2}. \tag{5.18}$$

From inspection of the (a) cylindrical (5.13, 5.14) and (b) spherical (5.16, 5.17) RG equations in $d < 3$, it is clear that $z = 1$ and $c = v$ (for finite g) is not a fixed point solution for (a), but is a solution for (b). Therefore the putative emergent Lorentz invariance ($z = 1$, $c = v$) is violated for (a), but is satisfied for (b). This is the case even for $N_f \to \infty$ where the solution for (a) is $z = 1$, $c = v(2 - 3/d)$. Naturally, each scheme will obtain a different set of critical exponents. However, for the $\epsilon = 3 - d$ expansion, where $g_*^2 \propto \epsilon$, Lorentz invariance emerges for both shell schemes, which also share the same set of critical exponents. The fact that Lorentz invariance emerges in the spherical scheme is a manifestation of the scheme itself, where already a symmetry between the momentum and the frequencies has been hard encoded.

This discussion demonstrates that away from the upper critical dimension, the perturbative loop expansion can lead to physically distinct conclusions at the same critical fixed point. Seemingly, the notion of universality breaks down, and the results depend on the way the cutoff RG scheme is implemented. We resolve this apparent pathology in the next section, where we identify the conditions for quantum corrections that are independent of the RG scheme.

5.5 Soft cutoff approach

Here we apply a completely general soft cutoff RG scheme to obtain the conditions for quantum corrections to be independent of the cutoff scheme, and therefore universal. We prove that for interacting Dirac fermions Eq. (5.1) away from the upper critical dimension, cutoff independent corrections are only obtained with a non-analytic order parameter propagator that scales as k^{d-1} in d spatial dimensions.

Remarkably, such dynamics arise from Landau damping by the gapless fermionic excitations, which is captured by the RPA resummation of fermion loop diagrams. Crucially, this non-perturbative effect is a product of the IR ($k \to 0$) modes that are not typically accessible by perturbative means, such as the integration over infinitesimal shells.

With the soft cutoff RG procedure, we demonstrate the emergence of Lorentz invariance and calculate the GNY critical exponents in general dimensions to leading order in N_f. We find exact agreement with previous results using the large N_f conformal bootstrap [87, 92] and the critical point large N_f formalism [89, 90, 91].

5.5.1 General cutoff function

Following Refs. [93, 94, 95, 96, 97], we introduce the ultraviolet cutoff by means of a completely general, smooth, soft cutoff function,

$$\begin{aligned} A(z) &\sim \exp(-z^n) \quad (n > 0), \\ A(z \to 0) &= 1, \quad A(z \to \infty) = 0. \end{aligned} \tag{5.19}$$

Within this description, the hard cutoff function is captured by $n \to \infty$. The soft cutoff procedure is implemented by augmenting the fermion and boson propagators with the cutoff function at the cutoff scale Λ,

$$G_{\Psi,\phi}(k) \to G_{\Psi,\phi}(k) A\left(\frac{a_\mu k_\mu^2}{\Lambda^2}\right) = G_{\Psi,\phi}(k) A_k, \tag{5.20}$$

where we define the $D = d + 1$ dimensional $k_\mu = (\omega, \boldsymbol{k}) = (k_0, \boldsymbol{k})$ (the Matsubara frequency has been redefined $\omega = k_0$ for notational simplicity) and we use implicit summation over repeated $\mu, \nu = 0, \ldots, d$, such that $k^2 = k_\mu k_\mu$. In the following we use the A_k notation for simplicity.

Although implicitly captured by the general definition of A, we explicitly include a_μ to make reference to the different cutoff schemes introduced in Sec. 5.4: the cylindrical RG scheme corresponds to $a_0 = 0$, $a_{\mu\neq 0} = 1$, whereas in the spherical scheme $a_0 = 1/v^2$, $a_{\mu\neq 0} = 1$.

The quantum corrections to RG equations are then obtained by taking the logarithmic derivative in the cutoff scale $\Lambda \frac{d}{d\Lambda}$ of the one-particle irreducible vertex functions. This is equivalent to the derivative $\frac{d}{d\ell}$ in the shell scheme with $\ell = \log(\Lambda/\Lambda_0)$.

5.5.2 Cutoff independence

Whilst Dirac fermions are fundamental objects that propagate as

$$G_\Psi(k) = i \frac{k_0 \gamma_0 + v \boldsymbol{k} \cdot \boldsymbol{\gamma}}{k_0^2 + v^2 \boldsymbol{k}^2}, \tag{5.21}$$

the *effective* order parameter fields are not, and hence we should not necessarily expect them to adhere to the bare analytic dynamics of Eq. (5.3). Instead, we define a general homogeneous form of the boson propagator (at $m^2 = 0$),

$$G_\phi(k) = \frac{G_\phi(\hat{k})}{y^{n_\phi}}, \tag{5.22}$$

where $k = y\hat{k}$ with $\hat{k}^2 = 1$.

Now we determine the required scaling form of G_ϕ (through a constraint on n_ϕ) to achieve cutoff scheme independent RG equations. To do so, it is sufficient to calculate the quantum corrections from the one-loop fermion self energy diagram in Fig. 5.2(b),

$$\frac{d}{d\ell}\Sigma(q) = -\Lambda\frac{d}{d\Lambda}\frac{g^2}{N_f}\int_k G_\Psi(k+q)A_k G_\phi(k)A_k, \tag{5.23}$$

where $\int_k = \int_{-\infty}^{\infty} d^Dk/(2\pi)^D$. Notice that the external q dependence has been excluded from the cutoff function, and instead A only regulates the internal k integral. This is perfectly consistent with the conventional procedure in the hard cutoff RG.

After expanding the right-hand side of Eq. (5.23) to linear order in the external q_μ, taking the logarithmic derivative and enacting the transformation $k = y\hat{k} = \tilde{y}\Lambda\hat{k}$, we obtain

$$\frac{d}{d\ell}\Sigma = \frac{4iq_\mu\gamma_\mu}{\Lambda^{n_\phi+2-D}}\int_{\hat{\Omega}}\int_0^\infty \frac{\tilde{y}^D d\tilde{y}}{\tilde{y}^{n_\phi+1}}(2\hat{k}_\mu^2 - 1)a_\nu\hat{k}_\nu^2\hat{G}_\phi A' A, \tag{5.24}$$

where $A = A(\tilde{y}^2 a_\mu \hat{k}_\mu^2)$, $\hat{G}_\phi = G_\phi(\hat{k})$ and $\int_{\hat{\Omega}}$ is the $(D-1)$ dimensional angular integral scaled by $(2\pi)^D$. Note that in the above we have rescaled units such that $v = 1$. It is simple to extract the cutoff independence by insisting that the result does not contain the UV cutoff scale Λ, which provides the constraint,

$$n_\phi = D - 2 = d - 1. \tag{5.25}$$

Imposing this constraint, the radial integral can be evaluated for a general A and will result in a correction that is independent of a_μ (i.e. spherical or cylindrical schemes). In contrast, if the constraint is not satisfied, the integral in Eq. (5.24) will depend on the explicit form of the cut-off function A, and cannot possibly contribute to universal phenomena.

In fact, cutoff independence of a quantum correction to the RG equations that corresponds to a diagram with N internal D-dimensional momenta can be determined by inspection of the scaling in the global radial coordinate y, $k_1 = y\hat{k}_1$, $k_2 = yx_2\hat{k}_2, \ldots k_N = yx_N\hat{k}_N$. Such a quantum correction is independent of the cutoff scheme, and therefore universal, if the integrand scales as $1/y$. This follows from the identity

$$\Lambda \frac{d}{d\Lambda} \int_0^\infty \frac{dy}{y} \prod_i A^{n_i} \left(\frac{y^2 f_i}{\Lambda^2} \right) = 1, \tag{5.26}$$

for positive integers n_i and non-trivial angular functions
$f_i = f_i(\hat{\Omega}_1, \ldots, \hat{\Omega}_N, x_2, \ldots x_N)$.

Finally, we should reiterate that *any* RG scheme (Wilson's momentum shell, minimal subtraction, etc.) is applicable, provided the n_ϕ condition that ensures cutoff independence is satisfied.

5.5.3 Cutoff independent RPA propagator

That $n_\phi = D - 2$ should not be a surprise. This result is in agreement with the familiar form $G_\phi^{-1} \sim k$ in two spatial dimensions [98, 99, 100, 79] and naturally arises at the $N_f \to \infty$ GNY fixed point, at which there is a large $\mathcal{O}(1)$ correction to the scaling of the order parameter field, $\eta_\phi = 4 - D$. This is a consequence of the one-loop fermion diagram in Fig. 5.2(a), indicating that it is a Landau damping phenomena from the gapless fermionic excitations. Accounting for the anomalous scaling, the propagator $G_\phi^{-1} = k^{2-\eta_\phi}$ satisfies the condition for cutoff scheme independence.

Away from the upper critical dimension, the cutoff independent propagator is non-analytic and so is not perturbatively renormalisable. This suggests that a non-perturbative solution is required.

To self-consistently account for the damped boson dynamics, and to achieve cutoff independence, we use the non-perturbative RPA re-summation of fermion loops, which is shown diagrammatically in Fig. 5.3(a), to obtain the dressed boson propagator

$$G_\phi^{-1}(q) = G_{\phi,0}^{-1}(q) + \Pi(q), \tag{5.27}$$

where $G_{\phi,0}^{-1}(q) = q_0^2 + c^2 \boldsymbol{q}^2 + m^2$ is the bare boson propagator. The bosonic self energy

$$\Pi(q) = \frac{g^2}{N_f} \int_k \mathrm{tr}\, G_\Psi(k+q) G_\Psi(k), \tag{5.28}$$

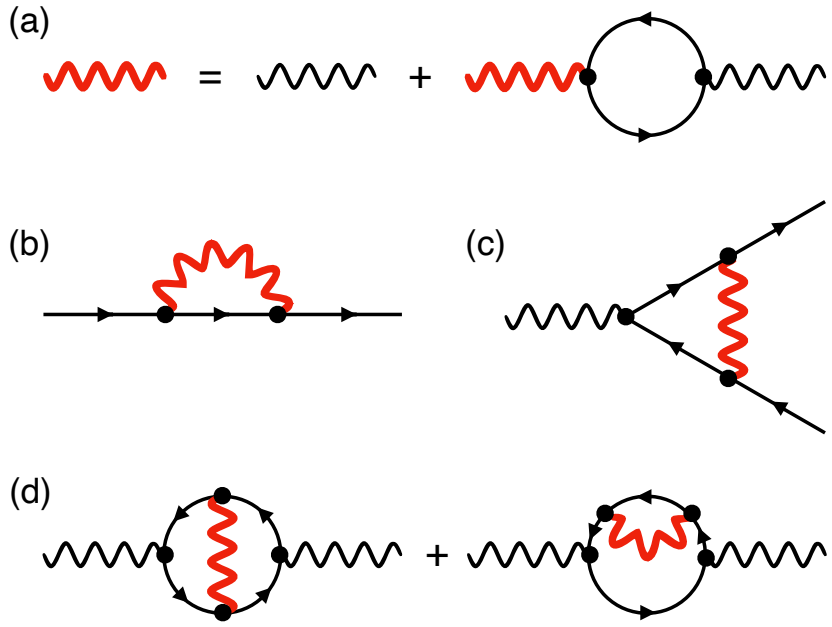

Figure 5.3: Feynman diagrams for large N_f theories. (a) The bold way line represents the RPA boson propagator of the order parameter field. The fermion loops are integrated over the full range of modes and are self-consistently re-summed to infinite order. This results in a non-analytic Landau damped propagator that satisfies cutoff scheme independence. (b) The fermion self energy renormalises the fermion propagator (arrowed straight line). (c) The vertex correction renormalizes the Yukawa coupling g. (d) The two loop diagrams renormalise the boson mass, and contribute to the correlation length exponent.

is calculated by integrating over the full range of modes. Crucially, Π includes the IR ($k \to 0$) modes that are not accounted for in Wilsonian shell schemes, and results in the non-analytic propagator (see Appendix B.1)

$$G_\phi^{-1}(k) = \frac{g^2 S_D \alpha_D}{v^{D-1}} (k_0^2 + v^2 \boldsymbol{k}^2)^{\frac{D-2}{2}} + m^2, \tag{5.29}$$

where

$$\alpha_D = -\frac{\pi}{2\sin(\frac{\pi D}{2})} \frac{\Gamma(D/2)^2}{\Gamma(D-1)}. \tag{5.30}$$

Note that the IR scaling of the dressed RPA boson propagator (5.29) satisfies the condition of cutoff independence, Eq. (5.25). We have neglected the sub-leading momentum terms in $G_{\phi,0}^{-1}(k)$ since these terms are irrelevant in an RG sense. Formally, the RPA contribution dominates in the large N_f limit, which is evident after making the rescaling $g^2 \to g^2 N_f$.

The Landau damped dynamics affects the scaling of the effective order parameter field. At tree level, we have the following equation that governs the scaling of the Yukawa coupling and the bosonic field,

$$4 + 2\,[g] + [\phi\phi] = 0. \tag{5.31}$$

Choosing g to be marginal, we find that crucially, the quartic self interaction $\lambda\phi^4$, Eq. (5.5), is rendered irrelevant at tree-level, and so is neglected in the following. This is a common feature of the "interaction driven scaling" [84] of gapless fermionic systems.

5.6 Large N_f RG equations

We now perform an RG analysis of the large N_f field theory

$$L = \bar{\Psi} \left(\partial_\tau \gamma_0 + v \boldsymbol{\partial} \cdot \boldsymbol{\gamma} + \frac{g}{\sqrt{N_f}} \phi \right) \Psi + \frac{1}{2} \phi\, G_\phi^{-1} \phi, \tag{5.32}$$

using the soft cutoff scheme to calculate the diagrams in Figs. 5.3(b)-(d) to leading order in N_f. Here $G_\phi(k)$ (5.29) is the fully dressed bosonic propagator that is obtained by the RPA re-summation depicted in Fig. 5.3(a). As demonstrated in Sec. 5.5.3, $G_\phi(k)$ has the correct IR scaling that ensures cutoff independence. This makes the evaluation of radial integrals trivial since

we can simply use the radial integral identity, Eq. (5.26). The remaining angular integrals of the one loop diagrams are elementary and can be carried out analytically. Here we only present the results. Details of the calculation, e.g. on the evaluation of the angular integrals in general dimension, can be found in Appendix B.2.
For the fermionic self-energy diagram, Fig. 5.3(b), we obtain

$$\begin{aligned}\frac{d}{d\ell}\Sigma(q) &= -\Lambda\frac{d}{d\Lambda}\frac{g^2}{N_f}\int_k G_\Psi(k+q)G_\phi(k)A_k^2 \\ &= -i\frac{D-2}{\alpha_D D N_f}(q_0\gamma_0 + v\boldsymbol{q}\cdot\boldsymbol{\gamma}),\end{aligned} \tag{5.33}$$

with α_D defined in Eq. (5.30). The vertex correction, which is show in Fig. 5.3(c) and which renormalizes the Yukawa coupling g, is equal to

$$\begin{aligned}\frac{d}{d\ell}\Xi &= \Lambda\frac{d}{d\Lambda}\frac{g^3}{\sqrt{N_f}^3}\int_k G_\Psi^2(k)G_\phi(k)A_k^3 \\ &= -\frac{1}{\alpha_D N_f}\frac{g}{\sqrt{N_f}}.\end{aligned} \tag{5.34}$$

We further evaluate the two-loop diagrams in Fig. 5.3(d) for zero external momentum and frequency but finite boson mass $m^2 \neq 0$, since they contain quantum corrections of order $1/N_f$ that renormalize m^2,

$$\begin{aligned}\frac{d}{d\ell}\tilde{\Pi} &= \Lambda\frac{d}{d\Lambda}\frac{g^4}{N_f^2}\int_{k,q} G_\phi(q)A_q \times \mathrm{tr}\Big[\\ &\quad G_\Psi(k+q)G_\Psi(k+q)G_\Psi(k)G_\Psi(k)A_{k+q}^2A_k^2 \\ &\quad +2G_\Psi(k+q)G_\Psi(k)G_\Psi(k)G_\Psi(k)A_{k+q}A_k^3\Big] \\ &= \frac{D-1}{\alpha_D^2 N_f \sin(\frac{\pi D}{2})}\frac{\pi\Gamma(\frac{D}{2})^2}{\Gamma(D-1)}m^2.\end{aligned} \tag{5.35}$$

Details of the calculation of the two-loop diagrams can be found in Appendix B.3.

The RG equations are obtained by combining quantum corrections and

rescaling contributions (see Eq. (5.7-5.9)),

$$\frac{dv}{d\ell} = v\Big[-(D+z+\Delta_\Psi)+\frac{D-2}{\alpha_D D N_f}\Big], \tag{5.36}$$

$$\frac{dg}{d\ell} = g\Big[2(1-D-z)-\Delta_\Psi-\frac{\Delta_\phi}{2}-\frac{1}{\alpha_D N_f}\Big], \tag{5.37}$$

$$\frac{dm^2}{d\ell} = m^2\Big[-(D-1+z+\Delta_\phi) + \frac{D-1}{\alpha_D^2 N_f \sin(\frac{\pi D}{2})}\frac{\pi\Gamma(\frac{D}{2})^2}{\Gamma(D-1)}\Big], \tag{5.38}$$

subject to the constraint

$$\Delta_\Psi = 1-D-2z+\frac{D-2}{\alpha_D D N_f}, \tag{5.39}$$

which follows from the scale invariance of $\int \bar{\Psi} k_0 \gamma_0 \Psi$.

The solution $z = 1$ of Eq. (5.36), for all v, indicates the emergence of Lorentz invariance at the quantum critical point. Moreover, g is scale invariant since it can be scaled out of the large N_f field theory (5.32), using $\phi \to \phi/g$, $m^2 \to g^2 m^2$. From this it follows that

$$\Delta_\phi = 2-2D-4\frac{D-1}{\alpha_D D N_f}. \tag{5.40}$$

Effectively, Eq. (5.32) describes the (g_*, λ_*) GNY critical fixed point of Eq. (5.1), at which g and λ are irrelevant perturbations. The correlation length exponent ν is determined by the flow of the single relevant perturbation at the critical fixed point,

$$\frac{dm^2}{d\ell} = \nu^{-1} m^2, \tag{5.41}$$

and can therefore be extracted from Eq. (5.38). The resulting critical exponents in $D = d+1$ dimensions, to leading order in N_f, are

$$\eta_\Psi = \frac{2(2-D)}{D N_f}\frac{\sin(\frac{\pi D}{2})}{\pi}\frac{\Gamma(D-1)}{\Gamma(\frac{D}{2})^2}, \tag{5.42}$$

$$\eta_\phi = \frac{8}{D N_f}\frac{\sin(\frac{\pi D}{2})}{\pi}\frac{\Gamma(D)}{\Gamma(\frac{D}{2})^2}, \tag{5.43}$$

$$\nu^{-1} = D-2+\frac{D-2}{N_f}\frac{\sin(\frac{\pi D}{2})}{\pi}\frac{\Gamma(D+1)}{\Gamma(\frac{D+2}{2})^2}, \tag{5.44}$$

which have been extracted using $[\bar{\Psi}\Psi] = -(D+1)$ and $[\phi\phi] = -2(D-1)$. These exponents are in agreement with previous results using the large N_f conformal bootstrap [86, 87, 92] and the critical point large N_f formalism [89, 90, 91].

5.7 Comparison with the ϵ-expansion

Finally we draw some connections to the ϵ expansion below the upper critical dimension for Dirac fermions. The famous expansion, first proposed by Wilson and Fisher [55], has been extremely successful in describing classical and quantum phase transitions, especially in purely bosonic systems, e.g. in the $O(N)$ ϕ^4 model.

We allow the space-time dimension to be a continuous variable and formulate the expansion below the upper critical dimension of the GNY theory, i.e. $D = 4-\epsilon$. To zeroth order in ϵ, the bare bosonic propagator $G_\phi^{-1}(k) \sim k^2$ satisfies the condition (5.25) for cutoff independence, $n_\phi = 2 - \epsilon$. The $\mathcal{O}(\epsilon)$ corrections to perturbative loop diagrams are cutoff dependent, but do not enter RG equations at any order in ϵ. The GNY RG equations from the ϵ-expansion are therefore independent of the cutoff scheme.

Naturally, for $D = 4 - \epsilon$ the critical exponents η_Ψ (5.42), η_ϕ (5.43) and ν (5.44) agree to leading order in N_f with those obtained from the ϵ-expansion, order by order in ϵ. The ϵ-expansion, however, can also be formulated using the scheme outlined in Fig. 5.3, and results in the RG equations already evaluated at the (g_*, λ_*) critical fixed point.

As a first step, the $1/\epsilon$ pole of the RPA propagator (5.29) must be extracted. The prefactor to the pole can also be obtained from the logarithmic divergence of Π in $D = 4$. Then the remaining diagrams are evaluated using

$$G_\phi^{-1}(k) = \frac{1}{\epsilon}\frac{g^2}{16\pi^2}(k_0^2 + v^2\boldsymbol{k}^2) + m^2. \tag{5.45}$$

It can be verified that the quantum loop corrections calculated in this manner agree with those obtained by perturbative means, after solving for the fixed point $(g_*, \lambda_*) \sim \mathcal{O}(\epsilon)$.

Although somewhat trivial for GNY theories, this methodology can act as an independent check of large N_f critical exponents obtained from the ϵ expansion. It has cutoff scheme independence encoded through the RPA propagator, which is crucial when considering anisotropic systems such as

those considered in the following text. It is also a shortcut to accessing the critical fixed point, which is valuable when dealing with a complicated set of RG equations.

5.8 Discussion

We have investigated the universal critical behaviour of Dirac semimetals at quantum phase transitions that are driven by strong local interactions. We have developed a soft cutoff RG approach that can be used to calculate exact critical exponents to leading order $1/N_f$ in experimentally relevant spatial dimensions.

At the heart of the problem is the phenomenon of Landau damping of order parameter fluctuations by gapless fermion excitations. This leads to non-analytic bosonic self-energy corrections which dominate over the bare boson propagator in the IR long-wavelength limit. Landau damping is therefore essential for the universal critical behaviour of the system. The phenomenon of Landau damping is inherently non-perturbative and not captured by perturbative RG schemes that are based upon the successive decimation of UV modes [40].

As demonstrated within our soft cutoff approach, not accounting for Landau damping, or more generally, using an incorrect IR boson propagator, leads to non-universal results that depend on the choice of the UV cutoff scheme. In turn, enforcing that the quantum corrections do not depend on the cutoff function and on which frequency and momentum directions the cutoff acts upon, the correct IR scaling of the Landau damped boson propagator can be deduced. These scaling constraints are satisfied by the fully dressed RPA boson propagator.

Our soft cutoff approach unifies all possible cutoff schemes, including those based on cylindrical and spherical hard cutoff momentum shells. Our work therefore demonstrates that *any RG scheme* is valid and will produce the same universal results, given that the correct IR boson propagator is used. This should resolve controversies over the "correct" RG shell schemes when there are quantitative discrepancies in the literature, such as in the case of double-Weyl semimetals [74, 75].

Using the soft cutoff RG with the non-perturbative RPA boson propagator, we have computed the exact critical exponents to leading order $1/N_f$ for relativistic Dirac fermions as well as for two-dimensional anisotropic semi-

Dirac fermions, coupled to an Ising order parameter field. The soft cutoff method has a clear advantage over hard cutoff schemes, as it significantly simplifies the calculation of diagrams beyond one-loop order. For the well studied relativistic case, the soft cutoff RG indeed reproduces the exact critical exponents obtained by conformal bootstrap [86, 87, 88] and other field-theoretical techniques [89, 90, 91].

There are a number of interesting questions that could be answered with the methodology presented in this Chapter, one of which is the case of anisotropic nodal-point semimetals which is presented in the next chapter. Further afield, starting with relativistic dynamics, the presence of emergent gauge fields coupled to order parameter fields [97, 101] can alter the dynamical scaling at quantum critical points. In this case, the divergencies associated with non-invertible, damped gauge field propagators can be repaired with non-analytic gauge fixing, as is implemented in pseduo-QED [102]. There are instances where broken symmetry states on lattices allow for cubic terms in the order parameter fields in the low energy effective field theory [70, 103, 104, 101]. In principal, following the Landau criterion, these can render quantum phase transitions first order. However gapless fermion excitations are expected to render such cubic terms irrelevant. In these problems, damping effects away from upper critical dimensions have not been accounted for.

In topological nodal systems the fermions are fundamental in the region of the nodal points. The fermion dynamics must therefore be analytic, implying that non-analytic fermion self energy corrections are absent. Consequently the large N_f expansion is controlled, as N_f does not appear in the fermion propagator. This is in contrast to the case of metallic quantum critical systems, in which the fermions are strongly renormalized by the infinite sea of excitations, resulting in non-analytic fermion self energy corrections. These terms are typically more relevant than the bare fermion dynamics, and render the large N_f uncontrolled [84]. Entirely non-perturbative solutions of the Schwinger-Dyson equations are then required [105]. Using our soft cutoff formalism, it might be possible to derive scaling constraints for both bosonic and fermionic self energies. This could potentially provide an important step towards the discovery of such non-perturbative solutions.

Chapter 6

RG aproach to anisotropic nodal semimetals

The original work presented in this Chapter first appeared in *Fermionic criticality of anisotropic nodal point semimetals away from the upper critical dimension: Exact exponents to leading order in* $\frac{1}{N_f}$, M. D. Uryszek, F. Krüger, E. Christou, Physical Review Research, **2**, 043265 (2020)[38].

6.1 Introduction

A Dirac semimetal can transition into a gapped insulating state either by breaking the protecting symmetry or by tuning the band structure through a topological phase transition where nodal points with opposite chirality merge. Such a topological phase transition was observed in black phosphorous [106, 107], and is predicted to occur in strained honeycomb lattices [108] and VO_2–TiO_2 heterostructures [108, 109]. At the transition point the dispersion becomes quadratic along the momentum direction that the nodal points merge, whilst it remains relativistic along the other direction [16, 17]. Such quasiparticles were termed semi-Dirac fermions [108, 18]. Analogous hybrid-quasiparticles exist at topological quantum phase transitions in noncentrosymmetric three-dimensional materials [110, 39]. Further ahead semimetals with a quadratic band touching point (QBT) [19] in 2D have been found in bilayer graphene[20], and topological crystalline insulators, which are a counterpart of topological insulators in materials without spin orbit coupling [21]. While in 3D these have been found in pyrchlore iridi-

ates and in many gapless semiconductors[22, 23]. Anisotropic nodal fermions with d_L linear and d_Q quadratic momentum directions in $d = d_L + d_Q$ spatial dimensions interpolate between relativistic Dirac or Weyl fermions and quasiparticles in systems with QBTs.

Strong short-range repulsive interactions are known to lead to a symmetry breaking transitions in semi-Dirac semimetals. In the ordered phase the fermionic spectrum is gapped and therefore it goes hand in hand with a semimetal-to-insulator transition like the ones found in Dirac semimetals. A thorough investigation of phase transitions in anisotropic semimetals is hoped to serve as a stepping stone towards an understanding of quantum criticality in metals with extended Fermi surfaces (partly due to similarity of dispersions between the two systems). More generally the lack of Lorentz invariance (in the anisotropic case) and the different scaling of the density of states near the nodal points leads to distinct fermion-induced criticality in nodal fermion systems with quadratic [33, 32, 34, 35] and semi-Dirac [111, 112, 37, 36] band-touching points. The latter are particularly interesting because the intrinsic electronic structure gives rise to highly anisotropic order-parameter correlations with different correlation-length exponents along linear and quadratic momentum directions.

Symmetry breaking transitions of semi-Dirac fermions were tackled previously in literature using different complementary expansions to obtain analytic control in renormalisation-group (RG) calculations. In Ref. [112], the problem was analysed in two spatial dimensions but with a generalized dispersion k_x^{2n} in the non-relativistic direction, facilitating a controlled ascent from one dimension ($n \to \infty$). More traditional approaches include a $1/N_f$ expansion in the number of fermion flavours [37] and an ϵ expansion below the line of upper critical dimensions $2d_L + d_Q = 4$, expanding in the number of quadratic directions, $d_L = 1$, $d_Q = 2 - \epsilon_Q$ [36]. At the same time, the anisotropic dispersion of semi-Dirac fermions makes this problem difficult. Under conventional momentum-shell RG, the bosonic order-parameter propagator develops unphysical divergencies, irrespective of the expansion scheme [36, 37]. This is because along the linear momentum directions, the loop corrections to the propagator, obtained by successive integration of modes from a shell near the UV cutoff, are irrelevant in an RG sense. The related divergencies need to be regularized by an additional IR contribution to the bosonic propagator that is not generated or renormalized under the Wilsonian RG. Instead it needs to be computed separately by integrating the fermion polarization diagram over the entire frequency and momentum range up to the

infinitesimal shell [39, 42, 36, 37, 113, 40, 41].

In order to identify the universal critical behaviour of a general d_L-d_Q nodal-fermion system, it is of crucial importance to use the correct bosonic IR propagator. However, due to the inherent anisotropy, the evaluation of the fermionic polarization diagram that determines the bosonic self energy $\Pi(\boldsymbol{q}, \Omega)$ is rather involved [40]. As one might anticipate, $\Pi(\boldsymbol{q}, \Omega)$ is non-analytic and highly anisotropic, and often approximations or interpolations between different asymptotic forms are used [40, 41, 37, 36], potentially leading to non-universal results. This problem is apparent in recent studies of the effects of long-range Coulomb interactions between semi-Dirac fermions [40, 41]. While the Coulomb interaction in two dimensions is represented by a bare gauge-boson propagator $G_\phi^{-1} \sim |\boldsymbol{q}|$, the long-wavelength behaviour is completely dominated by the non-analytic bosonic self energy $\Pi(\boldsymbol{q}, \Omega)$, giving rise to marginal Fermi-liquid behavior at smallest energies, with various anomalous physical properties [40]. Using an incomplete IR propagator, e.g. neglecting the dynamic part of $\Pi(\boldsymbol{q}, \Omega)$, leads to fundamentally different results [41].

In this chapter we consider the quantum criticality of the family of anisotropic nodal-point semimetals, using a soft cutoff RG approach [93, 94, 95, 96, 97] within the large N_f expansion as utilised in the previous chapter. With the use of the dressed order-parameter propagator, we compute the exact critical exponents for anisotropic semi-Dirac ($d_L = 1$, $d_Q = 1$) fermions to leading order in $1/N_f$, and to all loop orders.

Unlike in the Dirac case, the bosonic propagator in anisotropic d_L-d_Q nodal-point semimetals remains non-analytic, and therefore not perturbatively renormalisable, even at the upper critical dimension line $2d_L + d_Q = 4$ [36]. This has important consequences for the ϵ expansion. Approaching semi-Dirac fermions ($d_L = d_Q = 1$) by expanding in the number of quadratic dimensions, $d_Q = 2 - \epsilon_Q$, $d_L = 1$, one obtains leading corrections to critical exponents that are non-analytic and of the form $\sim \epsilon_Q \ln \epsilon_Q$ [36]. Here we show that the non-analytic dependence changes with the starting point on the upper critical line. Expanding in the number of linear dimensions, $d_Q = 1$, $d_L = (3 - \epsilon_L)/2$, we find leading $\sim \sqrt{\epsilon_L}$ corrections, putting the uniqueness of the ϵ expansion into question.

The outline of this chapter is as follows: In Secs. 6.2 and 6.3 we reintroduce the action for the family of anisotropic nodal-point semimetals and tackle the tree-level scaling. In Sec. 6.4 we show that the dressed RPA boson propagator satisfies the condition of cutoff independence, while the

RG equations for a general system with d_L and d_Q linear and quadratic directions are presented in Sec.6.5. In Sec. 6.6 the RPA bubble is evaluated in approximate and exact forms and then used to calculate the exact $1/N_f$ critical exponents to linear order. Finally in Sec. 6.7 the ϵ-expansion is tackled and the results are discussed in Sec. 6.8.

6.2 Action

We now present the full action for the family of anisotropic nodal-point semimetals with d_L linear and d_Q quadratic momentum directions. For general $d_L + d_Q + 1$ space-time dimensions, it takes the following form

$$S = S_\Psi + S_\phi + S_g + S_\lambda, \tag{6.1}$$

$$S_\Psi = \int dk\ \bar{\Psi}(k) \left(k_0\gamma_0 + \boldsymbol{k}_L \cdot \boldsymbol{\gamma}_L + (iv_Q^2|\boldsymbol{k}_Q|^2 + \Delta) \right) \Psi(k) \tag{6.2}$$

$$S_\phi = \frac{1}{2} \int dk\ G_\phi^{-1}(k)|\phi(k)|^2 \tag{6.3}$$

$$S_g = \frac{g}{\sqrt{N_f}} \int dkdq\ \phi(q)\bar{\Psi}\left(k+q\right)\Psi(k) \tag{6.4}$$

$$S_\lambda = \lambda \int \prod_{i=1,2,3,4} dk_i\ \phi(k_1)\phi(k_2)\phi(k_2)\phi(k_4)\delta(k_1+k_2+k_3+k_4) \tag{6.5}$$

where as before the integration measure,

$$\int dk = \prod_{i=0}^{d_L+d_Q} \int_{-\infty}^{\infty} \frac{dk_i}{2\pi} \tag{6.6}$$

where we have anticipated the use of the soft-cut off formulation which has eliminated the need for the hard cut off Λ from the upper limit of the momentum integral. We have defined k_0 to be Matsubara frequency, $\boldsymbol{k}_L = (k_1, \cdots, k_{d_L})$ and $\boldsymbol{k}_Q = (k_{d_L+1}, \cdots, k_{d_L+d_Q})$ to be the vectors of the liner and quadratic directions respectively. The parameter v_Q is related to the curvature of the quadratic dispersion. The linear momenta couple to $\boldsymbol{\gamma}_L = (\gamma_1, \ldots, \gamma_{d_L})$, which together with γ_0 and γ_Q form a set of mutually anti-commuting gamma matrices, $\{\gamma_\mu, \gamma_\nu\} = 2\delta_{\mu\nu}$. The tuning parameter Δ controls the topological transition from a nodal surface semimetal ($\Delta < 0$)

to a trivial band insulator ($\Delta > 0$). We have once again generalised to N_f-component Grassmanian fields $\Psi = (\Psi_1, \cdots, \Psi_{N_f})$. Note that for $d_Q = 0$ the model reduces to the large-N_f GNY theory defined in Eq. (5.1).

6.3 Tree-level Scaling

We start by a scaling analysis of the Yukawa-type field theory for d_L-d_Q fermions, given in Eq. (6.1). To account for the different scaling of linear and quadratic momenta, we define *two* scaling exponents, z_L and z_Q, such that

$$k_0 = k_0' e^{-z_L \delta\ell}, \ \boldsymbol{k}_L = \boldsymbol{k}_L' e^{-z_L \delta\ell}, \ \boldsymbol{k}_Q = \boldsymbol{k}_Q' e^{-z_Q \delta\ell}, \tag{6.7}$$

under rescaling. This allows us to unify the different scaling conventions in previous studies of anisotropic systems: ($z_L = 2$, $z_Q = 1$) [39, 41, 37, 36] and ($z_L = 1$, $z_Q = 1/2$) [40, 111, 112].

Note that we have rescaled frequency and linear momenta with the same exponent. In general, one should consider different exponents z_0 and z_L and allow for a renormalisation of the Fermi velocity v_L along the linear momentum direction. However, exactly as for the purely relativistic case, there is an emergent Lorentz invariance in the k_0-$\boldsymbol{k}_L$ subspace at the critical fixed point. For that reason we have set $z_0 = z_L$ and $v_L = 1$, without loss of generality.

At tree-level, the gapless fermionic quasiparticle energy $E(\boldsymbol{k})$ at the multi-critical point ($\Delta = 0$, $m^2 = 0$, $\langle\phi\rangle = 0$) scales as

$$E(\boldsymbol{k}) = E(\boldsymbol{k}') e^{-z_L \delta\ell}, \tag{6.8}$$

under the condition that $[v_Q^2] + 2z_Q = z_L$. The latter is satisfied if v_Q is scale invariant, $[v_Q] = 0$, and $z_Q/z_L = 1/2$. The RG procedure could therefore be established by integrating out modes from the $D = d_L + d_Q + 1$ dimensional shell

$$\Lambda e^{-z_L \delta\ell} \leq \sqrt{k_0^2 + E^2(\boldsymbol{k})} \leq \Lambda \tag{6.9}$$

below the UV cutoff Λ. The additional factor of z_L in the exponent suggests that one should consider $z_L \delta\ell$ as the "unit length" and define the rescaling of the fields as

$$\Psi(k) = \Psi'(k') e^{-\Delta_\Psi z_L \delta\ell/2} \tag{6.10}$$

$$\phi(k) = \phi'(k') e^{-\Delta_\phi z_L \delta\ell/2} \tag{6.11}$$

where $\Delta_\Psi = [\bar{\Psi}\Psi] + \eta_\Psi$ and $\Delta_\phi = [\phi\phi] + \eta_\phi$ are the critical dimensions of the fermionic and bosonic fields, respectively. With these conventions the universal critical behaviour will only depend on the ratio z_Q/z_L. Scale invariance of the free-fermion action at tree-level requires that

$$[\bar{\Psi}\Psi] = -\left(2 + d_L + d_Q/2\right). \tag{6.12}$$

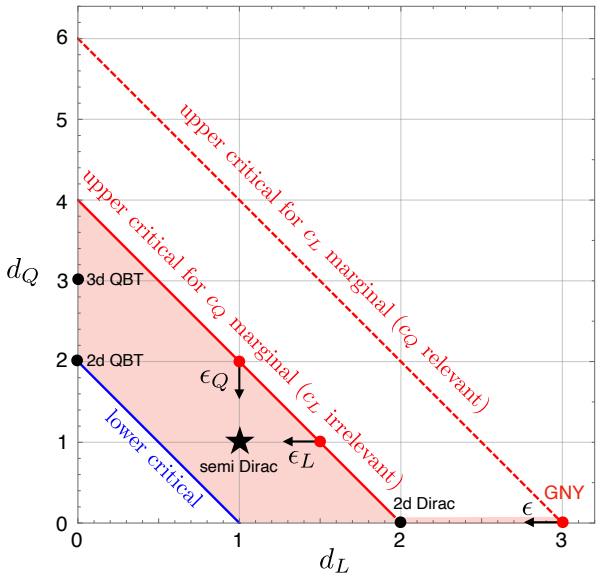

Figure 6.1: Lower and upper critical dimension lines of nodal point semimetals with d_L linear and d_Q quadratic momentum directions. For $d_Q > 0$ the line of upper critical dimensions $2d_L + d_Q = 4$ (red solid line) is obtained from the condition that c_Q is scale invariant. The dashed red line is obtained from the condition that c_L is scale invariant and therefore terminates at the upper critical dimension $d_L = d_{\rm uc} = 3$ of the GNY theory. The universal critical behaviour of semi-Dirac fermions ($d_L = d_Q = 1$) could be approached by ϵ expansions in both the number of linear and quadratic dimensions.

We now turn our attention to the bosonic sector. Since the bare order parameter propagator

$$G^{-1}_{\phi,0}(k) = c_L\left(k_0^2 + \boldsymbol{k}_L^2\right) + c_Q \boldsymbol{k}_Q^2, \tag{6.13}$$

does not show the same anisotropic momentum scaling as the fermionic quasiparticles, but instead depends quadratically on both $\boldsymbol{k}_L$ and $\boldsymbol{k}_Q$, scale invariance is violated at the bare, non-interacting level.

For systems with a finite number of quadratic band touching directions, $d_Q > 0$, it is natural to choose the boson scaling

$$[\phi\phi] = -(2 + d_L + d_Q/2), \tag{6.14}$$

such that c_Q is marginal, but c_L is irrelevant. The resulting tree-level scaling dimension of the Yukawa coupling is given by

$$[g] = \frac{1}{4}(4 - 2d_L - d_Q), \tag{6.15}$$

defining an upper critical line $2d_L + d_Q = 4$ of marginal interactions, shown in Fig. 6.1. Note that this line does not contain the upper-critical dimension $d_L = d_{\text{uc}} = 3$ of the GNY theory ($d_Q = 0$). This point is the termination of the upper critical line $2d_L + d_Q = 6$ obtained from $[c_L] = 0$ and $[g] = 0$. Note that in this case c_Q relevant. Lastly we see that the ϕ^4 term is irrelevant ($[\lambda] < 0$), and it will be ignored henceforth.

6.4 Cutoff independence and dressed RPA boson propagator

The lack of scale invariance of the bare bosonic order parameter propagator $G^{-1}_{\phi,0}(k)$ (6.13) in d_L-d_Q fermion systems is intimately linked to the fundamental problem that perturbative RG procedures do not correctly account for the long-wavelength fluctuations of the order parameter, e.g. they neglect the phenomenon of Landau damping.

The irrelevance of c_L suggests an IR divergence on approach to the critical fixed point. Previously it was argued that this unphysical divergence should be regulated with the asymptotic self-energy correction $\Pi(k_0, \boldsymbol{k}_L, \boldsymbol{k}_Q = 0)$ along the linear momentum and frequency directions [36, 37].

Within our soft cutoff approach it is clear, however, that below the upper critical line such a partially dressed boson propagator leads to quantum corrections that are dependent upon the the UV cutoff scheme and hence non-universal. By enforcing that the results are independent of the cutoff scheme we can deduce the correct IR scaling of the dressed boson propagator.

Since the dressed boson propagator should inherit the different scaling of momenta along linear and quadratic directions, we make the *Ansatz*

$$G_\phi(k) = \frac{G_\phi(\hat{k})}{\varepsilon^{n_\phi}}, \tag{6.16}$$

where we have defined the $(d_L + 2)$ dimensional vector

$$\varepsilon_\mu = (k_0, \ldots, k_{d_L}, \boldsymbol{k}_Q^2), \tag{6.17}$$

and $\varepsilon^2 = \varepsilon_\mu \varepsilon_\mu$, using implicit summation over μ.

In the soft cutoff approach we dress boson and fermion propagators with a completely general cutoff function A,

$$G_{\Psi,\phi}(k) \to G_{\Psi,\phi}(k) A\left(\frac{a_\mu \varepsilon_\mu^2}{\Lambda^2}\right), \tag{6.18}$$

which only needs to satisfy the boundary conditions $A(0) = 1$ and $\lim_{z\to\infty} A(z) = 0$. The hard cutoff is included as the special case where A is a step function, $A(z) = \Theta(1 - z)$. We can also include coefficients a_μ to allow for different cutoff schemes, e.g. $a_\mu = 1$ for $\mu = 0, \cdots, d_L + d_Q$ corresponds to the spherical scheme of Eq. (6.9), while in the cylindrical scheme, $a_0 = 0$, $a_{\mu\neq 0} = 1$, the cutoff only acts on the spatial momenta.

Cutoff independence means that the quantum corrections do not depend upon the the UV scale Λ, the cutoff function A, and the choice of coefficients a_μ. As discussed in detail in Sec. 5.5, this is the case if the integrands of the loop corrections scale as $1/\varepsilon$, since all cutoff dependence vanishes due to the radial integral identity (5.26) for $y = \varepsilon$. For the d_L-d_Q system this is only the case if the dressed boson propagators scales with the exponent

$$n_\phi = d_L + d_Q/2 - 1. \tag{6.19}$$

As in the case of relativistic Weyl or Dirac fermions, the fully dressed RPA boson propagator $G_\phi^{-1}(k) = G_{\phi,0}^{-1}(k) + \Pi(k)$ satisfies the condition (6.19) of cutoff independence in the long-wavelength limit. It is not possible, however, to obtain a closed expression for the bosonic self energy $\Pi(k)$. The asymptotic forms of $\Pi(k)$ for $2 < 2d_L + d_Q \leq 4$ and $d_Q > 0$ along the linear and quadratic directions is given by

$$\Pi(k) \sim \begin{cases} (k_0^2 + \boldsymbol{k}_L^2)^{\frac{1}{4}(2d_L+d_Q-2)} & \text{for } \boldsymbol{k}_Q = 0 \\ \boldsymbol{k}_Q^{(2d_L+d_Q-2)} & \text{for } k_0, \boldsymbol{k}_L = 0 \end{cases} \tag{6.20}$$

Below the upper critical line $2d_L + d_Q = 4$, the self energy $\Pi(k)$ dominates over the bare terms in the propagator in the $k \to 0$ limit and therefore determines the universal critical behaviour. The resulting propagator $G_\phi^{-1}(k)$ is inherently anisotropic, reflecting the different scaling of momenta, and non-analytic, showing that is is inaccessible by perturbative means. It strongly scales with the dimensions d_L, d_Q of the system, $G_\phi^{-1} \sim \varepsilon^{d_L+d_Q/2-1}$, satisfying the condition (6.19) and resulting in cutoff independent quantum corrections.

Note that the boson propagator G_ϕ^{-1} in anisotropic nodal fermion systems remains non-analytic even along the line of upper critical dimensions. Although in this case the conventional scaling $\sim \boldsymbol{k}_Q^2$ along the quadratic directions is recovered, the IR scaling along the linear directions, $G_\phi^{-1} \sim \sqrt{k_0^2 + \boldsymbol{k}_L^2}$ remains non-analytic.

6.5 Large N_f RG equations for general d_L, d_Q

We use the soft cutoff procedure with the dressed RPA boson propagator, Fig. 5.3(a), to compute the quantum corrections shown in Fig. 5.3(b)-(d). In this section, we derive the general form of the corrections, introducing symbolic expressions for the different loop integrals. These integrals depend on the values of d_L and d_Q, through the dimensionality of the loop integral and, more importantly, through the non-perturbative boson propagator, which strongly scales with dimension. Combining quantum corrections and re-scaling contributions, we derive general RG equations, which we solve to obtain expressions for critical exponents of order $1/N_f$ in terms of the loop integrals. These integrals will be evaluated for semi-Dirac fermions ($d_L = d_Q = 1$) in Sec. 6.6.

The cutoff independent quantum corrections are obtained by taking the logarithmic derivatives of the diagrams in Fig. 5.3, with $z_L \ell = \log(\Lambda/\Lambda_0)$, where the extra factor of z_L comes from the redefinition of "unit length". Expanding the fermionic self energy diagram, Fig. 5.3(b), to leading order in frequency, momenta and Δ, we obtain

$$\frac{d}{d\ell}\Sigma = -i\, z_L \left[\delta\Sigma_L \left(k_0\gamma_0 + \boldsymbol{k}_L \cdot \boldsymbol{\gamma}_L\right) + \left(\delta\Sigma_Q\, v_Q^2 \boldsymbol{k}_Q^2 + \delta\Sigma_\Delta\, \Delta\right)\gamma_Q\right], \qquad (6.21)$$

with certain loop integrals $\delta\Sigma_L, \delta\Sigma_Q, \delta\Sigma_\Delta \sim 1/N_f$ that will be computed later. Likewise, the quantum corrections corresponding to the diagrams in

Figs. 5.3(c) and (d), which renormalise the Yukawa coupling g and order-parameter mass m^2, respectively, can be written in the general form

$$\frac{d}{d\ell}\Xi = z_L \delta\Xi \frac{g}{\sqrt{N_f}}, \quad \frac{d}{d\ell}\tilde{\Pi}(0) = z_L \delta\tilde{\Pi}\, m^2. \tag{6.22}$$

Here $\delta\Xi, \delta\tilde{\Pi} \sim 1/N_f$ are one and two-loop integrals over internal momenta. Combining these quantum corrections with the rescaling given in Eqs. (6.7), (6.10) and (6.11), we obtain the following set of RG equations,

$$\frac{d\ln v_Q^2}{d\tilde{\ell}} = \delta\Sigma_Q - 1 - d_L - (2+d_Q)\frac{z_Q}{z_L} - \Delta_\Psi, \tag{6.23}$$

$$\frac{d\ln g}{d\tilde{\ell}} = \delta\Xi - 2\left(1 + d_L + d_Q\frac{z_Q}{z_L}\right) - \Delta_\Psi - \frac{\Delta_\phi}{2}, \tag{6.24}$$

$$\frac{d\ln \Delta}{d\tilde{\ell}} = \delta\Sigma_\Delta - 1 - d_L - d_Q\frac{z_Q}{z_L} - \Delta_\Psi = \nu_\Delta^{-1}, \tag{6.25}$$

$$\frac{d\ln m^2}{d\tilde{\ell}} = \delta\tilde{\Pi} - 1 - d_L - d_Q\frac{z_Q}{z_L} - \Delta_\phi = \nu_\phi^{-1}, \tag{6.26}$$

where we have defined $\tilde{\ell} = z_L\ell$. The critical dimensions of the fermion and boson fields consist of the tree-level scaling $[\ldots]$, given in Eqs. (6.12) and (6.14), and the anomalous dimensions η, $\Delta_\Psi = [\bar{\Psi}\Psi] + \eta_\Psi$, $\Delta_\phi = [\phi\phi] + \eta_\phi$. Note that the RG flow of the two relevant coupling constants Δ and m^2 defines the correlation length exponents ν_Δ and ν_ϕ of the multi-critical point. In addition to the above RG equations, we have to satisfy the constraint

$$\Delta_\Psi = \delta\Sigma_L - 2 - d_L - d_Q\frac{z_Q}{z_L}, \tag{6.27}$$

which follows form the condition that the the coefficient of the linear terms $k_0\gamma_0 + \boldsymbol{k}_L\cdot\boldsymbol{\gamma}_L$ of the fermion propagator remains constant under the RG.

From the RG equations it is straightforward to extract general expressions for critical exponents in terms of the loop integrals. Inserting Eq. (6.27) into Eq. (6.23) and demanding that v_Q does not flow under the RG, we obtain

$$\frac{z_Q}{z_L} = \frac{1}{2} - \frac{1}{2}\left(\delta\Sigma_L - \delta\Sigma_Q\right) \tag{6.28}$$

for the ratio of scaling exponents of momenta along quadratic and linear directions. As to be expected, $1/N_f$ corrections to the "tree-level" value of $1/2$

arise because of different fermionic self-energy corrections along quadratic and linear directions. Using this result along with the tree-level scaling dimension of the fermion field (6.12), we obtain the anomalous dimension of the fermion field,

$$\eta_\Psi = \delta\Sigma_L + \frac{d_Q}{2}\left(\delta\Sigma_L - \delta\Sigma_Q\right). \tag{6.29}$$

In order to determine the critical dimension Δ_ϕ of the boson field and the related anomalous dimension η_ϕ, we can use the same argument as for the large-N_f GNY theory: since it is possible, to scale out the Yukawa coupling g by the simple transformation $\phi \to \phi/g$ and $m^2 \to g^2 m^2$, the coupling g should not renormalise. From Eq. (6.24) and the already determined critical exponents we obtain the anomalous dimension

$$\eta_\phi = 2 - d_L - \frac{d_Q}{2} + 2\left(\delta\Xi - \delta\Sigma_L\right) + d_Q\left(\delta\Sigma_L - \delta\Sigma_Q\right) \tag{6.30}$$

of the boson fields. Note that η_ϕ has a contribution of order $(1/N_f)^0$ that vanishes along the upper critical dimension line $2d_L + d_Q = 4$. In the following we redefine the order parameter scaling such that the anomalous dimension is solely composed of quantum corrections, and the $(1/N_f)^0$ contribution is absorbed into the tree-level scaling

$$[\phi\phi] = -(2d_L + d_Q), \tag{6.31}$$

$$\eta_\phi = 2\left(\delta\Xi - \delta\Sigma_L\right) + d_Q\left(\delta\Sigma_L - \delta\Sigma_Q\right). \tag{6.32}$$

And finally, from Eqs. (6.25) and (6.26), we extract the two correlation length exponents

$$\nu_\Delta^{-1} = 1 + \delta\Sigma_\Delta - \delta\Sigma_L, \tag{6.33}$$

$$\nu_\phi^{-1} = -1 + d_L + \frac{d_Q}{2} + \delta\tilde{\Pi} - 2(\delta\Xi - \delta\Sigma_L) - \frac{d_Q}{2}\left(\delta\Sigma_L - \delta\Sigma_Q\right), \tag{6.34}$$

of the multi-critical fixed point, where ν_ϕ, ν_Δ correspond to the symmetry breaking transition and the topological phase transition, respectively.

6.6 Exact $1/N_f$ exponents for semi-Dirac fermions $(d_L = 1, d_Q = 1)$

In order to calculate the quantum corrections $\delta\Sigma_L$, $\delta\Sigma_Q$, $\delta\Sigma_\Delta$, $\delta\Xi$, and $\delta\tilde{\Pi}$ for semi-Dirac fermions, we first need to compute the dressed IR boson propagator $G_\phi^{-1}(k) = \Pi(k) + m^2$. Unlike for relativistic fermions, it is not possible

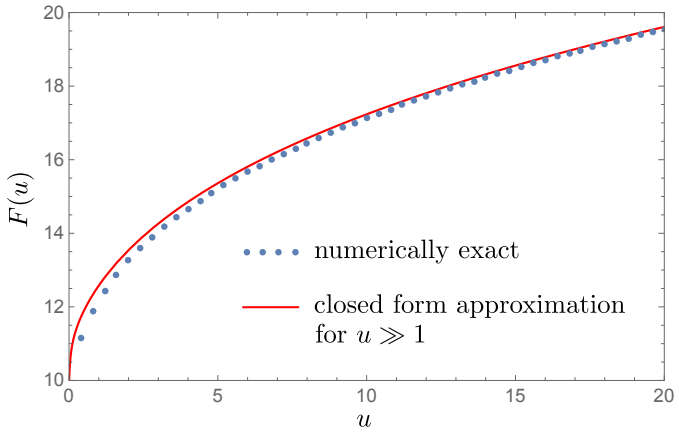

Figure 6.2: The function $F(u)$ determining the bosonic self energy (6.35). The blue dots show the exact result from numerical integration of Eq. 6.36, the red solid line the closed expression obtained in the regime $u \gg 1$.

to analytically evaluate the fermionic polarization $\Pi(k)$ for anisotropic nodal fermions [39, 40, 36]. As shown in Appendix C.1, the bosonic self energy for $d_L = d_Q = 1$ can be written in the form

$$\Pi(k) = \frac{g^2}{8\pi^2} |k_Q| \, F\left(\frac{k_0^2 + k_L^2}{v_Q^4 k_Q^4}\right), \tag{6.35}$$

where the function F is defined as the integral

$$F(u) = \int_0^1 dt \int_{-\infty}^{\infty} dp \frac{(p+1)^4 - p^2(p+1)^2 + (1-t)u}{(p+1)^4 t + p^4(1-t) + t(1-t)u}. \tag{6.36}$$

Notice that in this form, $\Pi(k)$ still satisfies the condition (6.19) for cutoff independence, $n_\phi = d_L + d_Q/2 - 1 = 1/2$, since $|k_Q| \sim \varepsilon^{1/2}$ while the argument of the function F is independent of ε.

The dominant contributions to the quantum corrections come from the regime where $k_Q \to 0$ for finite k_0, k_L, corresponding to large values of the argument u. In this regime, it is possible to obtain a closed asymptotic form for $F(u)$, resulting in the approximate boson self energy

$$\Pi(q) \approx g^2 \left[\frac{a_L(q_0^2 + q_L^2)}{(q_0^2 + q_L^2 + b_Q^4 q_Q^4)^{\frac{3}{4}}} + \frac{a_Q q_Q^2}{(q_0^2 + q_L^2 + b_Q^4 q_Q^4)^{\frac{1}{4}}} \right], \tag{6.37}$$

with $a_L = \Gamma(5/4)^2/\sqrt{2}\pi^{3/2}$, $a_Q = 5\Gamma(3/4)^2/16\sqrt{2}\pi^{3/2}$, and $b_Q = 8a_Q$.

The function $F(u)$ obtained from numerically evaluating the integral (6.36) and the closed asymptotic approximation for large u, leading to Eq. (6.37), are shown in Fig. 6.2.

As shown in Appendix C.2, all quantum corrections can be written as one-dimensional integrals over the function $F(u)$, e.g.

$$\delta\Sigma_L = \frac{1}{N_f}\int_0^\infty du\, \frac{1}{(1+u)^2 F(u)} = \frac{0.0797}{N_f}, \tag{6.38}$$

where we have used the exact form of $F(u)$ to obtain the numerical value. The other quantum corrections are $\delta\Sigma_Q = 0.0214/N_f$, $\delta\Sigma_\Delta = 0.2755/N_f$, $\delta\Xi = -0.4350/N_f$, $\delta\tilde{\Pi} = -0.10541/N_f$. The resulting exact critical exponents, describing the multi-critical fixed point of semi-Dirac fermions, are

$$\frac{z_Q}{z_L} = \frac{1}{2} - \frac{0.0292}{N_f} \tag{6.39}$$

$$\eta_\Psi = \frac{0.1089}{N_f}, \quad \eta_\phi = -\frac{0.9712}{N_f} \tag{6.40}$$

$$\nu_\phi^{-1} = \frac{1}{2} - \frac{0.0537}{N_f}, \quad \nu_\Delta^{-1} = 1 + \frac{0.1958}{N_f}. \tag{6.41}$$

Numerical values of the quantum corrections obtained with the approximate closed form of $F(u)$, corresponding to the approximate propagator (6.37), are given in Appendix C.2. These values deviate by less than 3.5% from the exact ones, except for $\delta\Sigma_Q$ where the deviation is about 17%. The larger deviation for $\delta\Sigma_Q$ is due to the fact that the corresponding integral has considerably more weight for small u.

6.7 Expansion around an upper critical line

In this subsection we formulate an ϵ-expansion below the upper critical line $2d_L + d_Q = 4$ of anisotropic d_L-d_Q nodal fermion systems. In principle, such expansions should allow for a controlled descent to strongly interacting systems of interest, such as the semi-Dirac fermion system with $d_L = d_Q = 1$.

Unlike in the purely Dirac case there is now a freedom in the choice of the starting point on the upper critical line. Here we focus on two natural starting points which correspond to a descent towards semi-Dirac fermions

by expanding in the number of (i) linear and (ii) quadratic dimensions, as illustrated in Fig. 6.1. This corresponds to (i) $d_L = (3-\epsilon_L)/2,\ d_Q = 1$ and (ii) $d_L = 1,\ d_Q = 2-\epsilon_Q$, where semi-Dirac fermions are reached for $\epsilon_L = 1$ and $\epsilon_Q = 1$, respectively. Note that the expansion (ii) in the number of quadratically dispersing directions was used in Ref. [36].

As explained in Sec. 6.4, the bare order parameter propagator, $G^{-1}_{\phi,0}(q) \sim q^2$, does not satisfy the condition for cutoff independence, even at the upper critical line. A fully perturbative RG calculation as the one used in the $D = 4-\epsilon$ expansion for GNY theory is therefore insufficient. Instead, the phenomenon of Landau damping remains of crucial importance at the upper critical line, giving rise to a non-analytic bosonic self-energy correction $\Pi(q_0, \boldsymbol{q}_L, \boldsymbol{q}_Q = 0) \sim (q_0^2 + \boldsymbol{q}_L^2)^{1/2}$ along the linear directions. As expected from the condition of cutoff independence, the scaling of the self-energy along the quadratic directions approaches the form $\Pi(q_0 = 0, \boldsymbol{q}_L = 0, \boldsymbol{q}_Q) \sim \boldsymbol{q}_Q^2$.

However, the coefficient diverges logarithmically on approach of the upper critical line. As shown in Appendix D.1, it is possible to extract the leading $1/\epsilon$ pole associated with this divergence. Since the fermionic polarization diagram cannot be calculated for general $q = (q_0, \boldsymbol{q}_L, \boldsymbol{q}_Q)$ we approximate the dressed IR boson propagator by the sum of the two asymptotic forms of the self energy along linear and quadratic directions.

For the expansion (i) in the linear dimensions, $d_L = (3-\epsilon_L)/2,\ d_Q = 1$, we obtain

$$G_\phi^{-1}(q) = \frac{g^2\pi^{1/4}}{32\Gamma(3/4)}(q_0^2 + \boldsymbol{q}_L^2)^{1/2} + \frac{1}{\epsilon_L}\frac{g^2}{2\pi^{5/4}\Gamma(1/4)}\boldsymbol{q}_Q^2, \tag{6.42}$$

while for the expansion (ii) in the quadratic directions, $d_L = 1,\ d_Q = 2-\epsilon_Q$, the result is

$$G_\phi^{-1}(q) = \frac{g^2}{64}(q_0^2 + \boldsymbol{q}_L^2)^{1/2} + \frac{1}{\epsilon_Q}\frac{g^2}{8\pi^2}\boldsymbol{q}_Q^2. \tag{6.43}$$

Details of the derivation can be found in Appendix D.1. Note that the propagators satisfy the condition (6.19) of cutoff independence.

To demonstrate the fundamental differences between the ϵ_L and ϵ_Q expansions, it is sufficient to calculate the ratio of the scaling dimensions z_Q/z_L and the anomalous dimensions η_Ψ and η_ϕ for the two cases. These critical exponents are expressed in Eqs. (6.28,6.29,6.32) in terms of the quantum corrections $\delta\Sigma_L$, $\delta\Sigma_Q$, which arise from the expansion of the fermion self energy [Fig. 5.3(b)], and $\delta\Xi$ from the vertex correction [Fig. 5.3(c)]. The

Table 6.1: Critical exponents z_Q/z_L, η_Ψ and η_ϕ for two distinct ϵ-expansions around the upper critical line $2d_L + d_Q = 4$. Here $\alpha_1^{-1} = (2\pi)^{1/4}\Gamma(9/4)$ and $\alpha_2 = \pi^2/8$, for brevity.

	$d_L = (3-\epsilon_L)/2,\ d_Q = 1$	$d_Q = 2-\epsilon_Q,\ d_L = 1$
$\frac{z_Q}{z_L}$	$\frac{1}{2} + \alpha_1 \frac{\sqrt{\epsilon_L}}{N_f} - \frac{3\epsilon_L}{2N_f}$	$\frac{1}{2} - \frac{\epsilon_Q}{2N_f}\log(\alpha_2\epsilon_Q) - \frac{5\epsilon_Q}{4N_f}$
η_Ψ	$-\alpha_1 \frac{\sqrt{\epsilon_L}}{2N_f} + \frac{3\epsilon_L}{2N_f}$	$\frac{\epsilon_Q}{N_f}\log(\alpha_2\epsilon_Q) + \frac{3\epsilon_Q}{N_f}$
η_ϕ	$-\alpha_1 \frac{8\sqrt{\epsilon_L}}{N_f} + \frac{5\epsilon_L}{N_f}$	$\frac{4\epsilon_Q}{N_f}\log(\alpha_2\epsilon_Q) + \frac{4\epsilon_Q}{N_f}$

corresponding one-loop integrals are computed in Appendix D.2, using the the soft cutoff approach with the dressed IR boson propagators Eqs. (6.42) and (6.43). The resulting critical exponents are summarized in Table 6.1.

For the expansion along the number of quadratic dimensions, $d_L = 1$, $d_Q = 2 - \epsilon_Q$, we find that the quantum corrections computed with the soft-cutoff RG and the non-perturbative boson propagator (6.43) are in perfect agreement with those obtained in Ref. [36], when evaluated at the interacting fixed point. To leading order in $\epsilon_Q \log \epsilon_Q$ the critical exponents also agree, once the different definitions of the critical dimension of the bosonic field and the number of fermionic flavours have been accounted for. Further details can be found in Appendix D.5.

While the leading quantum corrections are non-analytic for both the ϵ_L and ϵ_Q expansions, the functional dependencies $\sim \sqrt{\epsilon_L}$ and $\sim \epsilon_Q \log \epsilon_Q$ are completely different, potentially signalling an intrinsic problem with ϵ expansions in d_L-d_Q nodal fermion systems. This is further supported by the significant disparity between critical exponents obtained from the extrapolation of the two expansions to the semi-Dirac point, $\epsilon_L = 1$ and $\epsilon_Q = 1$.

6.8 Discussion

We have investigated the quantum phase transition from an anisotropic nodal semimetal to a CDW insulator. Unlike in the isotropic case, the bare bosonic propagator is already not scale invariant at the non-interacting level which suggests an IR divergence near the critical fixed point. This prompted previ-

ous works [37] to use an IR regulator with an asymptotic bosonic self-energy correction along the irrelevant momentum directions. We showed that similarly to the Dirac case, the non-perturbative RPA resummation of fermionic loops results in the correct IR scaling of the bosonic propagator. However due to the inherent anisotropy closed form solutions for the general $d = d_L + d_Q$ case were not possible. We presented the general RG equations paying close attention to the effect of two different "dynamical critical exponents". Focussing on the semi-Dirac case, we computed the RPA contribution in exact and approximate forms, and calculated the exact critical exponents to leading order in $1/N_f$. Finally we commented on the connections between the ϵ-expansion and the soft cutoff large-N_f approach presented here.

We briefly compare some of our exact critical exponents for semi-Dirac fermions,

$$\eta_\Psi = \frac{0.1089}{N_f}, \quad \eta_\phi = -\frac{0.9712}{N_f}, \quad \nu_\phi^{-1} = \frac{1}{2} - \frac{0.0537}{N_f}.$$

with those reported in the literature. As discussed in Appendix D.5 one needs to account for different definitions of the number of fermion flavours N_f and scaling exponents z_L and z_Q.

Ref. [37] employed one-loop perturbative RG with the bosonic IR divergence in c_L (6.13) regulated by the RPA re-summation. Although a stable interacting critical fixed point was located, the results are inherently cutoff dependent as the partially dressed boson propagator does not satisfy the scaling constraint (6.19) for cutoff independence. Moreover, the two-loop diagrams that contribute to the mass renormalization and hence the correlation length exponent ν_ϕ at order $1/N_f$ were neglected. Consequently, there are significant discrepancies in the exponents $\eta_\Psi = 0.0229/N_f$, $\eta_\phi = -0.1004/N_f$ and $\nu_\phi^{-1} = 1/2 + 0.2466/N_f$.

Ref. [111] obtained cutoff independent fermion self energy quantum corrections, using an approximation for the bosonic self energy $\Pi(q)$ that satisfied the scaling constraint (6.19). However, the approximation did not capture the full anisotropy, resulting in $\delta\Sigma_Q$ that is only 12% of that found here (6.38). In addition, the renormalisation of z_L/z_Q was not accounted for in scaling, resulting in $\eta_\Psi = 0.0870/N_f$. Other exponents and quantum corrections were not computed.

We have compared ϵ expansions that descended on the semi-Dirac point by expanding in the number of (i) linear $d_L = (3 - \epsilon_L)/2$, $d_Q = 1$ and (ii) quadratic $d_L = (3 - \epsilon_L)/2$, $d_Q = 1$ dimensions. In both cases we found

quantum corrections and critical exponents that are non-analytic in ϵ. However the functional dependencies $\sqrt{\epsilon_L}$ and $\epsilon_Q \log \epsilon_Q$ are completely different. This calls into question the validity, uniqueness, and extent of perturbative control of this approach for anisotropic nodal fermion systems, in contrast to relativistic GNY and bosonic ϕ^4 theories. Further analysis, and exploration beyond one-loop order is required to make concrete conclusions. Finally, it would be interesting to study the crossover behaviour from perturbative ϵ to integer d_L-d_Q systems, similar to recent work on quantum critical metals [114]. There it was found that low energy and integer dimension limits do not commute.

The scaling constraints we have derived from the requirement of cutoff independence highlight the important role of non-perturbative effects in quantum critical systems. Interestingly, it has been known for some time that the non-perturbative screening of long-range Coulomb interactions in relativistic nodal systems is crucial [99, 100, 79], and formally equivalent to Landau damping. However, such effects are typically neglected when studying spontaneous symmetry breaking from short range interactions. As a result, cutoff independence is often violated in the literature when studying the quantum criticality of two dimensional systems [37, 70, 103, 101, 115]. Screening is also important in anisotropic semi-Dirac systems at low energies. Our analysis shows that the entire polarization function is relevant, leading us to agree with Ref. [40] regarding Coulomb quantum criticality of semi-Dirac fermions: the dynamical part of the polarization should not be neglected, contrary to what was argued in Ref. [41].

There are a number of interesting avenues for future research into strongly interacting nodal systems away from their upper critical dimension. Closely linked to semi Dirac fermions are two and three dimensional nodal line semimetals. These are are described by the same effective field theory (6.1) but at finite $\Delta < 0$, away from the topological phase transition point. The criticality of such systems due to spontaneous symmetry breaking was previously studied within perturbative RG [115], not taking into account the effects of Landau damping. In nodal line semimetals Landau damping is expected to have even stronger effects than in the nodal point case, due to the greatly enhanced electronic density of states at low energies. It would also be interesting to revisit nematic quantum phase transitions in quadratic band touching systems, previously studied within perturbative RG near the upper critical dimension [34, 32]. The bare tensorial order parameter propagator of these theories does not satisfy the condition of cutoff independence

in physically relevant dimensions, highlighting that non-perturbative effects are crucial for the universal critical behaviour.

Chapter 7

Disordered CDW transition on the honeycomb lattice

The original work presented in this Chapter first appeared in *Interplay of interactions and disorder at the charge density wave transition of two-dimensional Dirac semimetals*, M. D. Uryszek, F. Krüger, Physical Review B, **105**, 075143 (2022) [116].

7.1 Introduction

In any realistic condensed matter system disorder is present, hence its understanding is paramount. Quenched, non-dynamical disorder has been widely studied in the non-interacting limit of systems that exhibit two-dimensional Dirac fermions, e.g. degenerate (or zero-gap) semiconductors [117, 118], graphene [119, 120, 121, 122, 123, 124, 125], and d-wave superconductors [126, 127, 128].

A lot of interest was triggered by the first graphene experiments [129, 130, 131] which showed a minimal conductivity of the order of the conductance quantum e^2/h over a wide range of temperatures. It was shown theoretically that the transport properties depend crucially on the type of disorder [120] but that for randomness which preserves one of the chiral symmetries of the clean Hamiltonian the conductivity is equal to the minimal value [120, 121], suggesting that the transport is not affected by localization and remains ballistic. However, this universal result is based on a self-consistent Born approximation, which is not applicable to massless Dirac fermions in two spatial

dimensions [119, 126, 127]. More recently, it was argued that over the experimentally accessible temperature range, graphene is in the Drude–Boltzmann diffusive transport regime and that density inhomogeneities from remote charge impurities render the Dirac points effectively inaccessible to experiments [122, 123]. Using a self consistent RPA-Boltzmann approach, the authors showed that the conductivity is indeed of order e^2/h but with a non-universal pre-factor that depends on the disorder distribution. Remote charge impurities can be viewed as random chemical potential shifts that give rise to puddles of electron and hole-doped regions in the graphene layer. Building on that picture, the scaling of the conductivity was obtained within a random resistor network model that describes the percolation of p- and n-type regions [124].

As the minimal conductivity puzzle shows, there is a lot of rich physics already at the non-interacting level. However, an accurate description of a Dirac semimetal also must include the effects of electron-electron interactions, on top of the disorder. For weak Coulomb interactions the clean two-dimensional Dirac fixed point is unstable against generic disorder and the RG flow is dominated by the randomness in the chemical potential [132, 133, 134], similar to the non-interacting case [119] and consistent with the picture of local electron and hole "puddles". On the other hand, in the regime of moderate to strong Coulomb interactions, it was found that fluctuations associated with such random potential disorder are parametrically cut off by screening and that instead the runaway flow is dominated by vector potential disorder [135]. Such disorder from elastic lattice deformations ("ripples") [120] and topological lattice defects [136, 137, 138].

The situation is very different in three-dimensional Dirac/Weyl semimetals with long-range Coulomb interactions. In these systems the semi-metallic phase is stable against short-range correlated disorder. Above a critical disorder strength, the semi-metallic phase undergoes a quantum phase transition into a disorder controlled diffusive metallic phase with a finite density of states at the Fermi level [139, 140, 141, 142]. It remains a controversial issue whether the disorder transition is rounded out by non-perturbative, rare region effects [143, 144, 145] or not [146, 147].

Under a sufficiently strong short-ranged electron-electron interaction a Dirac semimetal will undergo a quantum phase transition into a symmetry broken state where the fermionic spectrum is gapped. Such a transition is best described using a composite fermion-boson approach, resulting from a Hubbard-Stratonovich decoupling of the fermionic interaction vertex in

the relevant channel with a dynamical order parameter field. In the case of Dirac fermions the resulting field theory is known as the Gross-Neveu-Yukawa (GNY) model which describes chiral symmetry breaking and spontaneous mass generation in high energy physics [49, 50]. The symmetry broken phase is dependent on the nature of the microscopic interactions; for the half-filled Hubbard model on the honeycomb lattice with competing interactions a vast array of phases were found [61], including antiferromagnetism, different types of charge order, Kekule phases and topological Quantum Hall states.

The effects of weak quenched disorder on the semimetal-to-superconductor transition, described by the XY GNY model, were studied using ϵ expansions below the upper critical dimension [2, 3]. It was found that chemical potential disorder is strongly irrelevant at the clean quantum-critical point in $D = 4-\epsilon$ space-time dimensions but that disorder in the superconducting order parameter mass plays a crucial role. Such bosonic disorder would arise from randomness in the attractive fermion interaction after Hubbard-Stratonovich decoupling. In the supersymmetric case of a single two-component Dirac field coupled to the XY order parameter, there is a marginal flow away from the clean critical point to strong disorder [2, 3]. However, if degeneracies such as spin or valley pseudo-spin are included, the clean fixed point becomes stable against weak bosonic mass disorder and a finite-disorder multi-critical point with non-integer dynamical exponent ($z > 1$) can be identified within the double ϵ expansion [3]. Similar finite disorder fixed points were established in the chiral Ising and Heisenberg GNY models with bosonic random-mass disorder, using triple ϵ expansion [148].

In this work we revisit the effects of disorder on the quantum criticality of two dimensional Dirac/Weyl fermions. For simplicity, we focus on quantum phase transitions that, in the absence of disorder, are described by the chiral Ising GNY theory. An example is the CDW transition of electrons on the half-filled honeycomb lattice that is driven by a repulsive nearest-neighbour interaction and characterized by an imbalance of charge on the two sublattices. Our work departs in two important aspects from previous studies [2, 3, 148]. Firstly, we omit an ϵ expansion and compute the quantum corrections in two spatial dimensions. Away from the upper critical dimension, the Landau damping of long-wavelength order-parameter fluctuations is a non-perturbative effect. It renders the order parameter propagator non-analytic in the IR limit, thereby changing the universal critical behaviour [38, 85]. This physics is not captured by the ϵ expansion since the boson propagator remains analytic at the upper critical dimension. Secondly, we

consider disorder on the level of the original fermionic theory, e.g. in the form of a random potential from point-like impurities. In the physical dimension, such fermionic potential disorder is marginal at the clean GNY fixed point.

This chapter is organised as follows, in Sec. 7.2 we lay out the clean GNY action with a damped bosonic propagator. Then in Sec. 7.3 disorder on the fermionic level is introduced and then transformed using the replica theory culminating in the final full disordered action. Then in Sec. 7.4 we perform an RG analysis up to leading order in $1/N_f$ as well as in the disorder strength. We show the existence of a new disordered fixed point and calculate its critical exponents. Finally in Sec. 7.5 we present a summary of our final findings and compare with previous literature.

7.2 Clean Action

The non-interacting imaginary time action for Dirac fermions in two spatial dimensions is given by

$$\mathcal{S}_\psi = \int d^2\boldsymbol{x} \int d\tau\, \Psi^\dagger \left(\partial_\tau + iv\boldsymbol{\partial}\cdot\boldsymbol{\sigma}\right)\Psi, \tag{7.1}$$

over fermionic Grassmann fields $\Psi(\boldsymbol{x},\tau)$. Here $\boldsymbol{\partial} = (\partial_x, \partial_y)$ and $\boldsymbol{\sigma} = (\sigma^x, \sigma^y)$ are the conventional 2×2 Pauli matrices. This action describes non-interacting electrons on the half-filled honeycomb lattice in the long-wavelength, low-energy limit, where in this case the Pauli matrices act on the $\{A, B\}$ sublattice pseudospin subspace. In addition, the fermionic Grassmann fields carry the electron spin flavours and the valley indices from the two distinct Dirac points in the Brillouin zone.

In the following, we do not consider spontaneous symmetry breaking or disorder that lift the spin and valley degeneracies. We further generalize to a total number of N_f components of the fermion fields, $\Psi = (\psi_1, \ldots, \psi_N)$, in order to gain analytic control through an expansion in $1/N_f$. For brevity, we use the short-hand notation $\mathrm{Tr}[\sigma^i\sigma^j] = N_f\delta_{ij}$.

We consider the case where strong short-range interactions drive an instability in the charge channel, which corresponds to a quantum phase transition from a Dirac semimetal to a CDW insulator where the sublattice symmetry is spontaneously broken. Generally this transition belongs to the chiral Ising GNY universality class [49, 50], which is best studied within the Yukawa language where the Dirac fermions couple to a real-valued, scalar dynamical

order parameter $\phi(\boldsymbol{x}, \tau)$.

$$\mathcal{S}_g = \frac{g}{\sqrt{N_f}} \int d^2\boldsymbol{x} \int d\tau \ \phi \Psi^\dagger \sigma^z \Psi. \tag{7.2}$$

where g is the Yukawa "coupling".

As detailed thoroughly in Sec. 5.5, it is imperative to consider the phenomenon of Landau damping of the order parameter fluctuations by gapless electronic particle-hole excitations, when away from the upper critical dimension ($d+1 < 4$). To self-consistently account for these damped dynamics, we use the non-perturbative RPA resummation of fermion loops to obtain the dressed inverse boson propagator. In the long-wavelength limit of small frequency and momenta the damped dynamics dominate over the $(\omega^2 + c^2\boldsymbol{k}^2)$ terms in the bare inverse propagator, which we can then drop. Hence we arrive at the damped clean (non-disordered) GNY theory,

$$\mathcal{S}_{\text{GNY}} = \mathcal{S}_\Psi + \mathcal{S}_g + \mathcal{S}_\phi, \tag{7.3}$$

$$\mathcal{S}_\phi = \frac{1}{2} \int d\omega \int d^2\boldsymbol{k} \ G_\phi^{-1}(\omega, \boldsymbol{k}) |\phi(\omega, \boldsymbol{k})|^2 \tag{7.4}$$

where

$$G_\phi^{-1}(\omega, \boldsymbol{k}) = \frac{g^2}{16v^2} \left(\omega^2 + v^2\boldsymbol{k}^2\right)^{1/2} + m^2 \tag{7.5}$$

where m^2 is the bosonic mass which serves as the tuning parameter for the Dirac semiemtal to CDW insulator phase transition. Similarly to the arguments laid out in previous chapters, we drop the ϕ^4 term which is irrelevant in the RG sense.

7.3 Coupling to Disorder

We will consider different forms of quenched disorder fields $V_i(\boldsymbol{x})$ that arise from non-magnetic charge impurities and are expected to affect the quantum phase transition between the Dirac semimetal and CDW insulator. These fields couple to the fermions in the different channels of the 2×2 sublattice pseudospin space,

$$\mathcal{S}_{\text{dis}} = \sum_{i=0,x,y,z} \int d^2\boldsymbol{x} \int d\tau V_i(\boldsymbol{x}) \Psi^\dagger(\boldsymbol{x}, \tau) \sigma^i \Psi(\boldsymbol{x}, \tau), \tag{7.6}$$

where in addition to the three Pauli matrices we have defined the identity matrix as σ^0. Other forms of disorder which would break degeneracies of the other fermion flavours, e.g. spin or valley degeneracies, are not considered here.

V_0 and V_z are random potentials that couple to the symmetric $(\psi_A^\dagger\psi_A + \psi_B^\dagger\psi_B)$ and anti-symmetric $(\psi_A^\dagger\psi_A - \psi_B^\dagger\psi_B)$ combinations of the local electron densities on the two sites in the unit cell. The latter combination is required as some charge impurities will affect the two sites differently and locally break the symmetry between the two sub-lattices. In the following, we will refer to V_0 as "chemical potential disorder" since it can be viewed as spatial variations of the homogeneous chemical potential $\mu = 0$, and to V_z as "random mass disorder" since it couples in the same way as the electronic mass gap generated by the condensation of the CDW order parameter.

The components $V_\perp := V_x = V_y$ correspond to random gauge (vector) potential disorder. As discussed in the context of graphene, the random gauge potential describes elastic lattice deformations or ripples [135, 149, 150], which will be caused by impurity atoms. The different disorder fields V_i are present in any system with non-magnetic impurities and, as we will show later, there exists a rich interplay between them.

We assume that the random potentials $V_i(\boldsymbol{x})$ are uncorrelated and that they follow Gaussian distributions with zero mean and variances $\Delta_i \geq 0$,

$$\langle V_i(\boldsymbol{x})\rangle_{\text{dis}} = 0, \tag{7.7}$$

$$\langle V_i(\boldsymbol{x}_1)V_j(\boldsymbol{x}_2)\rangle_{\text{dis}} = \Delta_i\delta_{ij}\delta(\boldsymbol{x}_1 - \boldsymbol{x}_2), \tag{7.8}$$

where $\langle\ldots\rangle_{\text{dis}}$ denotes the average over the disorder. The presence of disorder on the level of the quadratic fermion action, Eq. (7.6), does not affect the Hubbard-Stratonovich decoupling of the fermion interaction. The resulting field theory is therefore given by $\mathcal{S}_{\text{GNY}}[\Psi^\dagger, \Psi, \phi] + \mathcal{S}_{\text{dis}}[\Psi^\dagger, \Psi]$. It is important to stress that disorder does not enter in the bosonic sector of the theory, e.g. in the form of random-mass disorder of the CDW order parameter field ϕ.

7.3.1 Replica Field Theory

We are interested in the disorder averaged free energy, which we are able to calculate with the use of the replica trick [151, 152],

$$\langle F\rangle_{\text{dis}} = -T\langle\log\mathcal{Z}\rangle_{\text{dis}} = -T\lim_{n\to 0}\frac{\langle\mathcal{Z}^n\rangle_{\text{dis}} - 1}{n}, \tag{7.9}$$

where $\mathcal{Z} = \int \mathcal{D}[\Psi^\dagger, \Psi, \phi] e^{-(\mathcal{S}_{\rm GNY} + \mathcal{S}_{\rm dis})}$ denotes the partition function. To deal with the n-times replicated partition function in the numerator of the limit, we introduce a "replica" index $a = 1, \cdots, n$,

$$\begin{aligned} \mathcal{Z}^n &= \left(\int \mathcal{D}[\Psi^\dagger, \Psi, \phi] \exp\left(-\mathcal{S}[\Psi^\dagger, \Psi, \phi]\right) \right)^n \\ &= \int \mathcal{D}[\Psi_a^\dagger, \Psi_a, \phi_a] \exp\left(-\sum_{a=1}^{n} \mathcal{S}[\Psi_a^\dagger, \Psi_a, \phi_a] \right) \end{aligned} \tag{7.10}$$

The average over disorder will only affect the disordered part of the action,

$$\langle \mathcal{Z}^n \rangle_{\rm dis} = \int \mathcal{D}[\Psi_a^\dagger, \Psi_a, \phi_a] e^{-\sum_a \mathcal{S}_{\rm GNY}[\Psi_a^\dagger, \Psi_a, \phi_a]} \left\langle e^{-\sum_a \mathcal{S}_{\rm dis}[\Psi_a^\dagger, \Psi_a]} \right\rangle_{\rm dis}. \tag{7.11}$$

Taylor expanding the $\langle \cdots \rangle$ term, we obtain

$$\begin{aligned} \left\langle e^{-\sum_a \mathcal{S}_{\rm dis}[\Psi_a^\dagger, \Psi_a]} \right\rangle_{\rm dis} =& 1 - \left\langle \sum_a \mathcal{S}_{\rm dis}[\Psi_a^\dagger, \Psi_a] \right\rangle_{\rm dis} \\ &+ \frac{1}{2} \left\langle \sum_{a,b} \mathcal{S}_{\rm dis}[\Psi_a^\dagger, \Psi_a] \mathcal{S}_{\rm dis}[\Psi_b^\dagger, \Psi_b] \right\rangle_{\rm dis} + \cdots \end{aligned} \tag{7.12}$$

The disorder average over the first order term evaluates to zero due to Eq.(7.7), while the second term evaluates to,

$$\begin{aligned} &\left\langle \sum_{a,b} \mathcal{S}_{\rm dis}[\Psi_a^\dagger, \Psi_a] \mathcal{S}_{\rm dis}[\Psi_b^\dagger, \Psi_b] \right\rangle_{\rm dis} = \\ &\int_{\boldsymbol{x}} \int_{\tau,\tau'} \Delta_i \left[\Psi_a^\dagger(\boldsymbol{x}, \tau) \sigma^i \Psi_a(\boldsymbol{x}, \tau) \right] \left[\Psi_b^\dagger(\boldsymbol{x}, \tau') \sigma^i \Psi_b(\boldsymbol{x}, \tau') \right] \end{aligned} \tag{7.13}$$

where we have used Eq. (7.7). It's important to note that the replicated disorder part of the action is no longer local in imaginary time. Essentially with the use of the replica trick, we have traded a non-spatially uniform potential $V_i(\boldsymbol{x})$ coupled to a fermion bilinear for a four-fermion interaction that should be easier to deal with in an RG calculation, albeit with a more complicated internal structure.

We then arrive at the final effective replica field theory,

$$\begin{aligned}\mathcal{S} = &\sum_{a=1}^{n} \int d^2\boldsymbol{x} \int d\tau\, \Psi_a^\dagger \left(\partial_\tau + iv\boldsymbol{\partial}\cdot\boldsymbol{\sigma} + \frac{g}{\sqrt{N}}\phi_a\sigma^z \right) \Psi_a \\ &+ \frac{1}{2}\sum_{a=1}^{n} \int_{|\boldsymbol{k}|\leq\Lambda} \frac{d^2\boldsymbol{k}}{(2\pi)^2} \int_{-\infty}^{\infty} \frac{d\omega}{2\pi}\; G_\phi^{-1}(\boldsymbol{k},\omega)|\phi_a(\boldsymbol{k},\omega)|^2 \\ &- \frac{1}{2}\sum_{a,b=1}^{n} \int d^2\boldsymbol{x} \int d\tau \int d\tau' \sum_{i=0,x,y,z} \Delta_i \\ &\times \left[\Psi_a^\dagger(\boldsymbol{x},\tau)\sigma^i\Psi_a(\boldsymbol{x},\tau)\right]\left[\Psi_b^\dagger(\boldsymbol{x},\tau')\sigma^i\Psi_b(\boldsymbol{x},\tau')\right], \end{aligned} \tag{7.14}$$

at zero temperature. Here $G_\phi^{-1}(\omega,\boldsymbol{k})$, defined in Eq.(7.5), is the inverse dressed bosonic propagator that is obtained by the RPA resummation as outlined in Sec. 5.5.

Unlike Refs. [2, 3, 148], we do not include a four-boson disorder vertex. Such a vertex would arise from a replica average of random-mass disorder of the CDW order parameter field ϕ which is not present in our theory. In Appendix E, we show that starting with the bare replica action (7.14), a four-boson disorder vertex is not generated under the RG at two-loop order.

7.4 Renormalisation Group analysis

In the following we perform a momentum-shell RG analysis of the replica action (7.14). We integrate out fast modes with momenta from an infinitesimal shell $\Lambda e^{-d\ell} < |\boldsymbol{k}| < \Lambda$ near the UV momentum cutoff Λ. This is followed by the conventional rescaling of momenta, frequency and fields. To restore the original cutoff we rescale momenta as $\boldsymbol{k} = \boldsymbol{k}' e^{-d\ell}$ while $\omega = \omega' e^{-zd\ell}$ with z the dynamical exponent. The fields are rescaled as

$$\begin{aligned}\Psi(\boldsymbol{k},\omega) &= \Psi'(\boldsymbol{k}',\omega')e^{-\delta_\Psi d\ell/2}, \\ \phi(\boldsymbol{k},\omega) &= \phi'(\boldsymbol{k}',\omega')e^{-\delta_\phi d\ell/2}.\end{aligned} \tag{7.15}$$

We start with a simple tree-level scaling analysis. In the absence of disorder and at the critical point $m^2 = 0$ the field theory remains invariant under the above rescaling for $z = 1$, $\delta_\Psi = -2 - 2z$, and $\delta_\phi = -4$. As the tuning parameter of the quantum phase transition, the order-parameter mass is a

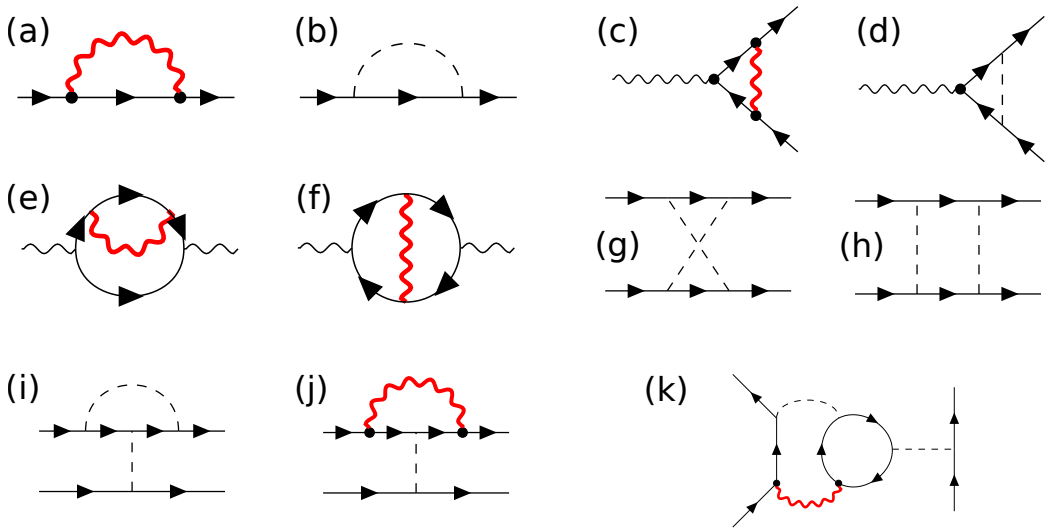

Figure 7.1: Feynman diagrams of $\mathcal{O}(\Delta_i, \frac{1}{N})$ for the large-N theory, Eq. (7.14). (a)-(b) Fermion self energy corrections that renormalise the fermionic propagator. (c)-(d) Renormalisation of the Yukawa vertex. (e)-(f) Renormalisation of the bosonic mass. (g)-(k) Corrections to the fermionic disorder vertex. The dashed line represents the replicated disorder interaction.

relevant perturbation with tree-level scaling dimension $[m^2] = 2 - z$. Due to the interaction driven scaling as detailed in Sec. 5.5, we have neglected the usual ϕ^4 vertex which is irrelevant at the GNY fixed point. Under these scaling conventions the fermionic disorder is vertex is marginal at tree level which motivates a perturbative expansion in the couplings Δ_i of fermionic disorder.

We compute all diagrams, shown in Fig. 7.1, that contribute in the replica limit $n \to 0$ at $\mathcal{O}(\Delta_i, \frac{1}{N})$ in $d = 2$. The full calculation of which can be found in Appendix F.

We first consider the fermionic self-energy corrections due to the Yukawa coupling at second order and the disorder vertex at linear order, which are shown by the two diagrams in Fig. 7.1(a)-(b), respectively. The first diagram leads to a renormalisation of the overall prefactor of the inverse fermion propagator, resulting in an anomalous dimension of the fermion fields. The disorder induced self energy only affects the frequency term and therefore breaks the symmetry between momentum and frequency scaling, leading to

a correction to the dynamical exponent z. The inverse fermion propagator remains invariant under the RG for

$$\delta_\Psi = -4 + \frac{8}{3\pi^2 N} - \frac{1}{2}\left(\tilde{\Delta}_0 + \tilde{\Delta}_z + 2\tilde{\Delta}_\perp\right), \tag{7.16}$$

$$z = 1 + \frac{1}{2}\left(\tilde{\Delta}_0 + \tilde{\Delta}_z + 2\tilde{\Delta}_\perp\right), \tag{7.17}$$

where we have defined the rescaled disorder variances

$$\tilde{\Delta}_i = \frac{\Delta_i}{\pi v^2} \tag{7.18}$$

and $\tilde{\Delta}_\perp := \tilde{\Delta}_x = \tilde{\Delta}_y$. Hence the theory will no longer be Lorentz invariant for any finite disorder fixed point. The renormalisation of the Yukawa vertex is calculated from the diagrams in Fig. 7.1(c)-(d),

$$\frac{dg}{d\ell} = \Bigg[-4 - 2z - \delta_\Psi - \frac{\delta_\phi}{2} - \frac{8}{\pi^2 N} + \frac{1}{4}\left(2\tilde{\Delta}_\perp - \tilde{\Delta}_z - \tilde{\Delta}_0\right)\Bigg] g. \tag{7.19}$$

Since the coupling g can be scaled out of the large-N replica theory, Eq. (7.14), using $\phi \to \phi/g$, $m^2 \to g^2 m^2$, we demand that it is scale invariant. This determines the critical dimension of the order-parameter field ϕ,

$$\delta_\phi = -4 - \frac{64}{3\pi^2 N} - \frac{1}{2}\left(2\tilde{\Delta}_\perp + 3\tilde{\Delta}_z + 3\tilde{\Delta}_0\right), \tag{7.20}$$

where we have eliminated δ_Ψ and z, using Eqs. (7.16) and (7.17). The renormalisation of the order parameter mass m^2 is given by the two-loop diagrams in Fig. 7.1(e)-(f). The resulting RG equation is given by

$$\frac{dm^2}{d\ell} = \left(1 - \frac{32}{3\pi^2 N} + \tilde{\Delta}_z + \tilde{\Delta}_0\right) m^2, \tag{7.21}$$

where the dependence on disorder arises through z (7.17) and δ_ϕ (7.20). At any finite disorder fixed point the order parameter correlation length exponent ν, defined through the identification $dm^2/d\ell = \nu^{-1} m^2$, will therefore differ from the one in the clean system.

Finally, the coupled RG equations for the different types of disorder are obtained from the diagrams in Fig. 7.1(g)-(k),

$$\begin{aligned}
\frac{d\tilde{\Delta}_0}{d\ell} &= \tilde{\Delta}_0\left(\tilde{\Delta}_0+\tilde{\Delta}_z+2\tilde{\Delta}_\perp-\frac{32}{9\pi^2 N}\right)+2\tilde{\Delta}_\perp\tilde{\Delta}_z,\\
\frac{d\tilde{\Delta}_\perp}{d\ell} &= -\tilde{\Delta}_\perp\left(\frac{\tilde{\Delta}_z}{6}+\frac{32}{9\pi^2 N}\right)+\tilde{\Delta}_0\tilde{\Delta}_z,\\
\frac{d\tilde{\Delta}_z}{d\ell} &= \tilde{\Delta}_z\left(\frac{5\tilde{\Delta}_\perp}{3}-\tilde{\Delta}_z-\tilde{\Delta}_0-\frac{32}{3\pi^2 N}\right)+2\tilde{\Delta}_\perp\tilde{\Delta}_0.
\end{aligned} \tag{7.22}$$

In the non-interacting limit, corresponding to diagrams in Fig. 7.1 that only include the disorder vertex, the RG equations for the disorder variances agree with previous results [153, 133, 120, 124].

7.4.1 RG flow and fixed points

We start by summarizing the critical exponents for the interaction-driven semimetal to CDW insulator transition of the clean system at $T=0$ in $d=2$. The critical exponents of order $1/N$ at the clean interacting critical fixed point, which we denote by P_{clean}, are obtained from Eqs. (7.16), (7.17), (7.20) and (7.21) by setting $\tilde{\Delta}_0=\tilde{\Delta}_\perp=\tilde{\Delta}_z=0$. In the absence of disorder the theory satisfies Lorentz invariance with dynamical exponent $z=1$. The anomalous critical dimensions of the fields, defined through $\delta_\Psi=-4+\eta_\Psi$, $\delta_\phi=-4+\eta_\phi$, and the correlation length exponent ν reduce to

$$\begin{aligned}
\eta_\Psi^{\text{clean}}=\frac{8}{3\pi^2 N},\quad \eta_\phi^{\text{clean}}=-\frac{64}{3\pi^2 N},\\
\nu_{\text{clean}}=1+\frac{32}{3\pi^2 N}.
\end{aligned} \tag{7.23}$$

These exponents are in agreement with those obtained from soft cutoff RG [38] and with previous results using the large N conformal bootstrap [86, 87, 92] and the critical point large N formalism [89, 90, 91]. At P_{clean}, the order parameter mass m^2 is the only relevant parameter, representing the tuning parameter of the quantum phase transition.

In order to analyse whether the clean system CDW critical point is stable against weak charge-impurity disorder, we numerically integrate the coupled RG equations for $\tilde{\Delta}_0$, $\tilde{\Delta}_\perp$ and $\tilde{\Delta}_z$ (7.22). The resulting RG flow of the three

disorder variances on the critical manifold $m^2 = 0$ is shown in Fig. 7.2. For small disorder, in the regime bounded by the transparent purple surface, the flow is towards the clean system critical point P_{clean}, demonstrating that the CDW quantum critical point is stable against weak disorder. This is in line with the Harris criterion which states that a non-disordered fixed point is stable if $\nu_{\text{clean}} \geq 2/d$, where d is the dimensionality of the system [154, 155].

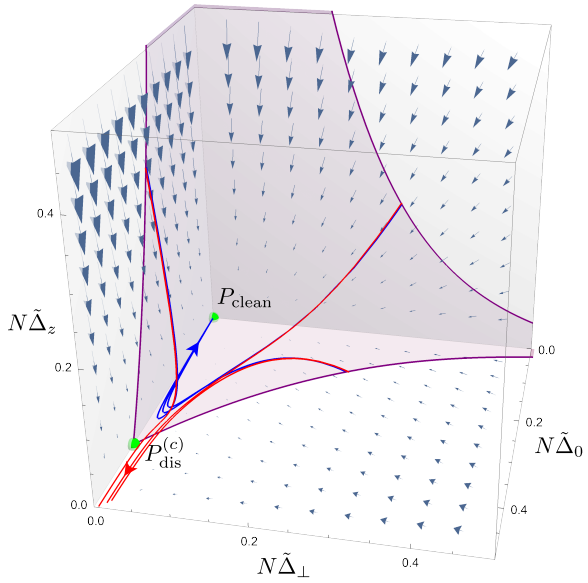

Figure 7.2: RG flow in the disorder subspace on the critical manifold $m^2 = 0$, as defined by Eqs. (7.22). Within the region bounded by the transparent surface disorder renormalizes to zero, showing that the CDW critical point P_{clean} is stable against small disorder. Near this boundary surface the RG flow is towards a finite disorder fixed point $P_{\text{dis}}^{(c)}$ at which only chemical potential disorder is relevant.

Close to the boundary surface, the RG flow is controlled by the only finite disorder fixed point in the accessible region of positive variances,

$$P_{\text{dis}}^{(c)} : \left(\tilde{\Delta}_0^{(c)}, \tilde{\Delta}_\perp^{(c)}, \tilde{\Delta}_z^{(c)}\right) = \left(\frac{32}{9\pi^2 N_f}, 0, 0\right). \tag{7.24}$$

$P_{\text{dis}}^{(c)}$ is unstable along the $\tilde{\Delta}_0$ direction but stable against $\tilde{\Delta}_\perp$ and $\tilde{\Delta}_z$. This is consistent with the RG flow for initial values $\tilde{\Delta}_i(0)$ that are very close to

the separating surface in Fig. 7.2. Shown are three pairs of trajectories with initial values that are slightly inside (blue) and outside (red) of the region bounded by the surface. The trajectories closely track the surface and split very close to $P_{\rm dis}^{(c)}$, where the flow is either to the clean fixed point, $\tilde{\Delta}_0 \to 0$ or strong chemical potential disorder, $\tilde{\Delta}_0 \to \infty$.

Our RG analysis shows that the transition to a glassy state is always driven by potential disorder, even if the other forms of disorder initially dominate. Since the random gauge field and random mass disorders are irrelevant at $P_{\rm dis}^{(c)}$ we neglect them in the following. The RG equations for the chemical potential disorder $\tilde{\Delta}_0$ and the order parameter mass m^2 then reduce to

$$\frac{d\tilde{\Delta}_0}{d\ell} = \tilde{\Delta}_0 \left(\tilde{\Delta}_0 - \frac{32}{9\pi^2 N_f} \right), \tag{7.25}$$

$$\frac{dm^2}{d\ell} = \left(1 - \frac{32}{3\pi^2 N_f} + \tilde{\Delta}_0 \right) m^2. \tag{7.26}$$

Inserting the critical disorder strength $\tilde{\Delta}_0^{(c)} = \frac{32}{9\pi^2 N_f}$ into Eqs. (7.16), (7.17), (7.20) and (7.26) we obtain the critical exponents at the finite disorder multi-critical point $P_{\rm dis}^{(c)}$,

$$\begin{aligned} \eta_\Psi^{\rm dirty} &= \frac{8}{9\pi^2 N_f}, \quad \eta_\phi^{\rm dirty} = -\frac{80}{3\pi^2 N_f}, \\ \nu_{\rm dirty} &= 1 + \frac{64}{9\pi^2 N_f}, \quad z_{\rm dirty} = 1 + \frac{16}{9\pi^2 N_f}. \end{aligned} \tag{7.27}$$

At both the clean system semimetal to CDW insulator transition and at the finite disorder multicritical point the fermion anomalous dimension η_Ψ is greater than zero. This implies that at the quantum critical points (QCPs) the fermion Green's function has branch cuts rather than quasiparticle poles, and the fermionic liquid is therefore a non-Fermi liquid. Approaching the QCPs from the metallic side, $V < V_c$ and $V_c - V \to 0$, the quasiparticle residue has to vanish with some characteristic exponent. On the CDW side, the condensation of the order parameter leads to the formation of a gap M in the fermion spectrum, which increases as a power of $V - V_c > 0$.

In order to extract these exponents we perform a scaling analysis of the fermionic spectral function. Details can be found in Ref. [31]. Here we only give the results. Approaching the quantum phase transition from the metallic

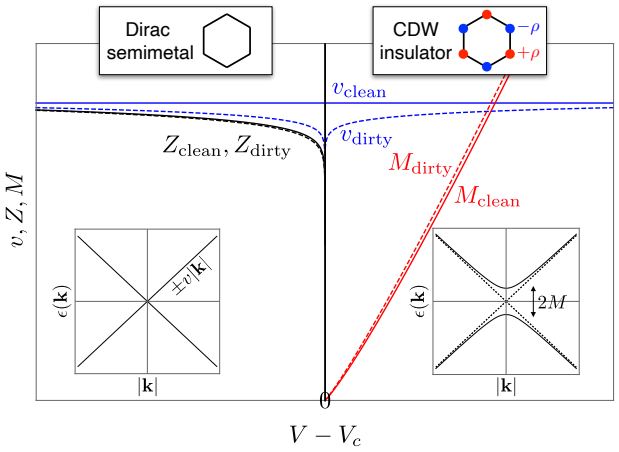

Figure 7.3: Behaviour of the the quasiparticle pole strength Z, the Fermi velocity v and the gap M in the fermion spectrum at the clean semimetal/CDW insulator transition and at the finite disorder multicritical point, as a function of the nearest neighbour repulsion $V - V_c$. Here we evaluated the critical exponents for $N_f = 8$, corresponding to Dirac electrons on the honeycomb lattice with valley and spin degeneracies.

side, the quasiparticle pole strength vanishes as

$$Z \sim (V_c - V)^{(z-1+\eta_\Psi)\nu} = (V_c - V)^{\frac{8}{3\pi^2 N}}, \tag{7.28}$$

where to order $1/N_f$ the critical exponents are the same for the clean and dirty fixed points $P_{\rm clean}$ and $P_{\rm dirty}$. The Fermi velocity behaves as

$$v \sim |V_c - V|^{(z-1)\nu} = \begin{cases} \text{const} & \text{at } P_{\rm clean} \\ |V_c - V|^{\frac{16}{9\pi^2 N}} & \text{at } P_{\rm dirty} \end{cases} \tag{7.29}$$

Finally, on the CDW insulator side of the quantum phase transition the gap in the electron spectrum increases as

$$M \sim (V - V_c)^{z\nu} = \begin{cases} (V - V_c)^{1+\frac{32}{3\pi^2 N}} & \text{at } P_{\rm clean} \\ (V - V_c)^{1+\frac{80}{9\pi^2 N}} & \text{at } P_{\rm dirty} \end{cases} \tag{7.30}$$

The behaviour of Z, v and M near the clean and finite-disorder QCPs is illustrated in Fig. 7.3.

In order to estimate the phase boundary between the CDW insulator and the disordered phase in the close proximity of $P_{\rm dirty}$ for $V > V_c$ and $\tilde{\Delta}_0 > \tilde{\Delta}_0^{(c)}$ we compare the CDW induced gap M in the electron spectrum with the standard deviation $\sqrt{\tilde{\Delta}_0}$ of the chemical potential disorder. Close to $P_{\rm dirty}$, the disorder increase exponentially under the RG,

$$\tilde{\Delta}_0(\ell) - \tilde{\Delta}_0^{(c)} \simeq \left(\tilde{\Delta}_0 - \tilde{\Delta}_0^{(c)}\right) e^{\nu_\Delta^{-1}\ell} \text{ with } \nu_\Delta^{-1} = \frac{32}{9\pi^2 N}.$$

We evaluate the disorder variance at the "correlation length" $\xi \sim e^{\ell^*} \sim (V - V_c)^{-\nu}$, where $m^2(\ell^*) \simeq -1$. Equating the resulting standard deviation with the gap M near $P_{\rm dirty}$, Eq. (7.30), we obtain the phase boundary

$$\begin{aligned}\left(\tilde{\Delta}_0 - \tilde{\Delta}_0^{(c)}\right) &\simeq (V - V_c)^{(2z_{\rm dirty}+\nu_\Delta^{-1})\nu_{\rm dirty}} \\ &\simeq (V - V_c)^{2\left(1+\frac{32}{3\pi^2 N_f}\right)}. \end{aligned} \tag{7.31}$$

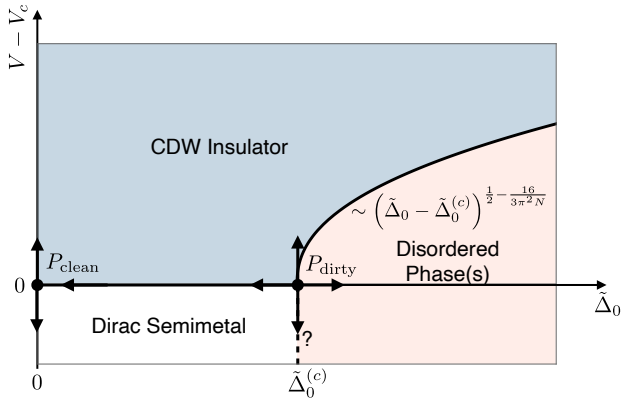

Figure 7.4: Schematic Phase diagram as a function of the interaction strength $V - V_c$ and the variance $\tilde{\Delta}_0$ of the chemical potential disorder.

A schematic phase diagram as a function of the interaction strength $V - V_c \simeq -m^2$ and the chemical potential disorder $\tilde{\Delta}_0$ is shown in Fig. 7.4.

7.5 Discussion

We have investigated the effects of quenched short-ranged disorder on the quantum phase transition between a two-dimensional Dirac semi-metal and a charge density wave (CDW) insulator. In the absence of disorder, the phase transition belongs to the chiral Ising Gross-Neveu-Yukawa (GNY) universality class. In order to achieve analytic control in $d = 2$, far below the upper critical dimension, we have analysed the problem in the limit of a large number N of Dirac fermion flavours. We have used the RPA fermion loop resummation to self-consistently account for the Landau damping of the boson dynamics by electronic particle-hole excitations. As pointed out in the literature [38, 85], this is a non-perturbative effect in two spatial dimensions that changes the IR physics and hence the universal critical behaviour. As we have demonstrated in our work, Landau damping also plays a crucial role in how the critical system responds to disorder.

We have considered three types of electronic disorder that all arise from non-magnetic charge impurities. The random potential from the impurities is decomposed into random mass disorder, which locally breaks the symmetry between the two sublattices, and symmetric random chemical potential disorder. The local lattice deformations caused by impurity atoms is accounted for by random gauge potential disorder [120]. For simplicity, we have neglected correlations between the different types of disorder and assumed that disorder is uncorrelated between different positions in space.

After averaging over disorder, using the replica formalism, we have performed a perturbative RG calculation to leading order in the disorder strength and in $1/N$. Our analysis shows that the clean GNY critical point is stable against weak disorder. This is in stark contrast to non-interacting or weakly interacting two-dimensional Dirac fermions where disorder is a relevant perturbation, resulting in a run-away flow towards strong disorder [119, 132, 133, 134].

Most importantly, we have identified a dirty GNY critical point at a finite value of the chemical potential disorder of order $1/N$. At this multicritcal point, the random mass and random gauge potential disorders are irrelevant. This shows that the transition into a disordered state is driven by chemical potential disorder, even if the other forms of disorder dominate on shorter length and time scales.

The disorder driven phase transition along the line of critical interaction in the two-dimensional system might be similar to the transition in weakly

interacting, three dimensional Weyl/Dirac semimetals [139, 140, 141, 142]. In both cases, the transition is driven by chemical potential disorder which is expected to induce a finite zero-energy density of states in the disordered phase, giving rise to diffusive metallic behaviour. This would be consistent with our naive picture for the transition between the CDW insulator, which forms above the critical interaction strength, and the disordered phase: if the standard deviation of the random chemical potential shifts exceeds the electronic gap induced by the symmetry breaking, the system will develop a finite density of states at the average chemical potential, leading to diffusive metallic behaviour. However, further calculations are required to ascertain the properties of the disordered phase in the strongly interacting, two dimensional system. An investigation of the dependence on the form of the disorder distribution, e.g. whether it is bounded, Gaussian or exhibits long tails, as well as of any potential replica symmetry breaking [156], indicative of glassy behaviour, would be very interesting.

Our renormalisation-group approach does not capture non-perturbative, rare region effects, which have spurned a lot of discussion in the context of three dimensional Weyl/Dirac semimetals. A study by Nandkishore *et al.* [143] first proposed that rare region effects induce a non-vanishing density of states at the Weyl/Dirac points, thereby turning the disorder-driven phase transition into a crossover. This was substantiated by numerical calculations [144, 145] but remains at odds with recent theoretical literature [146, 147]. However, as chemical potential disorder is marginal in two spatial dimensions, and irrelevant in three, it is expected that rare region resonances will have a "sub-leading effect" on the physics of the transition in two dimensions [157].

We have shown that the symmetry-breaking quantum phase transition at the dirty GNY does not belong to the chiral-Ising GNY universality of the clean system. We have computed the critical exponents at the finite-disorder multi-critical point to order $1/N$ and found that the anomalous dimensions of the boson and fermion fields, the correlation length exponent of the CDW order parameter and the dynamical critical exponent differ from those at the clean GNY fixed point. This leads to different critical behaviour of physical observables such as the electronic gap, the Fermi velocity, and the quasiparticle residue near the transition and results in a novel non-Fermi liquid state at the multicritical point.

The interplay between symmetry breaking and disorder was previously studied for the XY GNY [2, 3] and the chiral Ising and Heisenberg GNY models [148], using the replica formalism combined with ϵ expansions. Near

the upper critical dimension fermionic disorder is strongly irrelevant at the clean system quantum critical points. Instead, short-ranged disorder of the bosonic order parameter mass (sometimes referred to as random T_c disorder) gives rise to a finite disorder multicritical point, regardless of the symmetry of the order parameter. At this finite disorder critical point the Lorentz invariance is broken with a dynamical exponent $z > 1$, similar to our dirty GNY fixed point, while the fermionic and bosonic anomalous dimensions remain unchanged, which is not the case in our theory.

The irrelevance of the chemical potential disorder seems to be only valid near the upper critical dimension, hence any extrapolation to the physical dimension of $d = 2$ without the inclusion of it is questionable. Moreover, the non-perturbative Landau damping which is crucial for the universal critical behaviour of the two-dimensional system, is not captured by an ϵ expansion below the upper critical dimension. On the other hand, we have not included bosonic disorder in our theory. Starting from an interacting fermionic model with a random potential, bosonic disorder would not arise from a Hubbard-Stratonovich decoupling of the fermionic interaction vertex. However, as pointed out in Refs. [2] and [3], at two-loop order chemical potential disorder could generate a bosonic disorder vertex in the replica theory. We have presented an explicit calculation in Appendix E, demonstrating that this is not the case.

In future extensions of our work it would be interesting to investigate the effects of long-range correlations of disorder. It is often assumed that impurities and imperfections are screened effectively and that disorder can therefore be taken to be uncorrelated. However, it has been reported that in graphene the correlations between disorder-induced puddles of electron- and hole-doped regions decay algebraically [158, 159, 160]. Such power-law correlations are expected to change the long-wavelength physics and hence the universal critical behaviour. One might also include other types of disorder, e.g. defects that lead to inter-valley scattering, magnetic impurities that break the spin degeneracy, or topological lattice defects that are described by random non-Abelian gauge fields. The interplay of the different types of disorder is expected to lead to rich phase behaviour and novel critical phenomena, in particular if competing fermionic interactions are taken into account.

Chapter 8

Concluding Remarks

We now conclude with a summary of work found in this thesis. For detailed discussion please consult the end of the chapters.

We have investigated the universal critical behaviour of nodal point semimetals at quantum phase transitions that are driven by strong local interactions and/or disorder. Due to the gapless nature of the excitations the critical behaviour cannot be described with a Ginzburg-Landau type of theory, and no longer can the universality class of the transition be defined by the dimensionality of the problem and the symmetry of the order parameter. The natural description involves treating the bosonic and fermionic degrees of freedom on equal footing in a Yukawa-type theory. The transitions investigated in this thesis are the simplest examples of fermionic quantum criticality which should shed some light on criticality in systems with extended Fermi surfaces.

In Chapter 3, we used the path integration formulation of Landau's free energy approach to phase transitions, to show that already at mean-field level the role of fermions is fundamental to the criticality. The mean-field exponents differ from the standard Ising universality class. This was due to the appearance of non-analytic terms in the mean-field free energy which in turn are a consequence of the vanishing density of states at the half-filling point. The density of states took the form of $\rho(\varepsilon) = \varepsilon, \sqrt{\varepsilon}$ for the Dirac and semi-Dirac case respectively, which in turn resulted in disparate critical exponents for the two cases. Moreover we showed that the inherent anisotropy of the semi-Dirac excitations results in different correlation length scaling along the inequivalent directions, which could stabilise emergent modulated order and stripe phases.

In Chapter 5 we utilised the Wilson's momentum shell RG to investigate the criticality of the Gross-Neveu-Yukawa theory with a scalar order parameter, which describes the quantum phase transition from a Dirac semimetal to a charge density wave insulator. We found that using two different cutoff scheme in the momentum shell gave rise to disparities in the resulting RG equations. Specifically using a cylindrical cutoff scheme (which is probably the most natural one) resulted in the breaking of Lorentz invariance, a symmetry that is well known to exist at the interacting fixed point. Such inconsistencies were solved with the use of a soft cutoff scheme that set a constraint on the scaling of the bosonic propagator, which in two spatial dimensions required for it to be non-analytical. A non-perturbative effect which turned out to be a consequence of screening (Landau damping) of order parameter fluctuations by particle-hole excitations. To self-consistently account for this effect an RPA resummation of UV convergent fermionic loops was calculated. We found that with the use of damped boson propagator we obtained critical exponents that were in exact agreement with the literature.

Building on the knowledge developed in the previous chapter, we investigate fermionic quantum criticality of nodal point semimetals with d_L, d_Q linearly and quadratically dispersing directions respectively. The anisotropy makes the problem more interesting as parts of the bare bosonic propagator are RG irrelevant in all dimensions of interest. Once again with the soft cutoff method we illustrated that Landau damping is crucial, and should be included even when at the upper critical line. However a closed form expression of the RPA resummation of fermion loops was not possible, hence we calculated the critical exponents for the case of semi-Dirac only.

Lastly in Chapter 7 we considered the effect of non-magnetic disorder on the Dirac semimetal to charge density wave insulator quantum phase transition. While clean non-interacting graphene is stable against disorder, it was known that the interplay of Coulomb interaction and disorder was far from trivial in the Dirac semimetal. Moreover previous works on the disordered symmetry breaking transitions of Dirac semimetals utilised variations of the famous ϵ-expansion and failed to agree in their results, and even more importantly failed to include the Landau damping effect. Using a combination of replica theory and RG we computed the flow of this disordered GNY model, and found a new disordered interacting fixed point which was characterised by non-zero chemical potential disorder. Interestingly enough the other two disorders considered (vector potential and random mass) were irrelevant to the criticality, even though physically one might expect them to

be interlinked with the chemical potential disorder. However the clean GNY interacting fixed point was found to be stable to any disorder, and that a transition to some sort of a glassy phase occurs past a critical value of the chemical potential disorder.

More generally, we have contributed to the understanding of fermionic quantum criticality, and elucidated the importance of order parameter screening in semimetals which are subject to strong short-range interactions which in turn drive a phase transition into a broken symmetry phase.

Bibliography

[1] S. Chakravarty, B. I. Halperin, and D. R. Nelson, "Two-dimensional quantum heisenberg antiferromagnet at low temperatures," *Phys. Rev. B*, vol. 39, pp. 2344–2371, Feb 1989.

[2] R. Nandkishore, J. Maciejko, D. A. Huse, and S. L. Sondhi, "Superconductivity of disordered dirac fermions," *Phys. Rev. B*, vol. 87, p. 174511, May 2013.

[3] H. Yerzhakov and J. Maciejko, "Disordered fermionic quantum critical points," *Phys. Rev. B*, vol. 98, p. 195142, Nov 2018.

[4] A. V. Chubukov, S. Sachdev, and J. Ye, "Theory of two-dimensional quantum heisenberg antiferromagnets with a nearly critical ground state," *Phys. Rev. B*, vol. 49, pp. 11919–11961, May 1994.

[5] M. Hälg, D. Hüvonen, N. P. Butch, F. Demmel, and A. Zheludev, "Finite-temperature scaling of spin correlations in a partially magnetized heisenberg $s = \frac{1}{2}$ chain," *Phys. Rev. B*, vol. 92, p. 104416, Sep 2015.

[6] S. Sachdev, *Quantum Phase Transitions*. Cambridge University Press, 2 ed., 2011.

[7] V. L. Ginzburg and L. D. Landau, *On the Theory of Superconductivity*, pp. 113–137. Berlin, Heidelberg: Springer Berlin Heidelberg, 2009.

[8] K. G. Wilson, "Renormalization group and critical phenomena. ii. phase-space cell analysis of critical behavior," *Phys. Rev. B*, vol. 4, pp. 3184–3205, Nov 1971.

[9] N. P. Armitage, E. J. Mele, and A. Vishwanath, "Weyl and dirac semimetals in three-dimensional solids," *Rev. Mod. Phys.*, vol. 90, p. 015001, Jan 2018.

[10] B. Yan and C. Felser, "Topological materials: Weyl semimetals," *Annual Review of Condensed Matter Physics*, vol. 8, no. 1, pp. 337–354, 2017.

[11] O. Vafek and A. Vishwanath, "Dirac fermions in solids: From high-tc cuprates and graphene to topological insulators and weyl semimetals," *Annual Review of Condensed Matter Physics*, vol. 5, no. 1, pp. 83–112, 2014.

[12] A. H. Castro Neto, F. Guinea, N. M. R. Peres, K. S. Novoselov, and A. K. Geim, "The electronic properties of graphene," *Rev. Mod. Phys.*, vol. 81, pp. 109–162, Jan 2009.

[13] M. Z. Hasan and C. L. Kane, "Colloquium: Topological insulators," *Rev. Mod. Phys.*, vol. 82, pp. 3045–3067, Nov 2010.

[14] X.-L. Qi and S.-C. Zhang, "Topological insulators and superconductors," *Rev. Mod. Phys.*, vol. 83, pp. 1057–1110, Oct 2011.

[15] X. Wan, A. M. Turner, A. Vishwanath, and S. Y. Savrasov, "Topological semimetal and fermi-arc surface states in the electronic structure of pyrochlore iridates," *Phys. Rev. B*, vol. 83, p. 205101, May 2011.

[16] P. Dietl, F. Piéchon, and G. Montambaux, "New magnetic field dependence of landau levels in a graphenelike structure," *Phys. Rev. Lett.*, vol. 100, p. 236405, Jun 2008.

[17] G. Montambaux, F. Piéchon, J.-N. Fuchs, and M. O. Goerbig, "Merging of dirac points in a two-dimensional crystal," *Phys. Rev. B*, vol. 80, p. 153412, Oct 2009.

[18] S. Banerjee, R. R. P. Singh, V. Pardo, and W. E. Pickett, "Tight-binding modeling and low-energy behavior of the semi-dirac point," *Phys. Rev. Lett.*, vol. 103, p. 016402, Jul 2009.

[19] K. Sun, H. Yao, E. Fradkin, and S. A. Kivelson, "Topological insulators and nematic phases from spontaneous symmetry breaking in 2d fermi

systems with a quadratic band crossing," *Phys. Rev. Lett.*, vol. 103, p. 046811, Jul 2009.

[20] E. McCann and M. Koshino, "The electronic properties of bilayer graphene," *Reports on Progress in Physics*, vol. 76, p. 056503, apr 2013.

[21] L. Fu, "Topological crystalline insulators," *Phys. Rev. Lett.*, vol. 106, p. 106802, Mar 2011.

[22] E.-G. Moon, C. Xu, Y. B. Kim, and L. Balents, "Non-fermi-liquid and topological states with strong spin-orbit coupling," *Phys. Rev. Lett.*, vol. 111, p. 206401, Nov 2013.

[23] W. Witczak-Krempa, G. Chen, Y. B. Kim, and L. Balents, "Correlated quantum phenomena in the strong spin-orbit regime," *Annual Review of Condensed Matter Physics*, vol. 5, no. 1, pp. 57–82, 2014.

[24] A. A. Soluyanov, D. Gresch, Z. Wang, Q. Wu, M. Troyer, X. Dai, and B. A. Bernevig, "Type-ii weyl semimetals," *Nature*, vol. 527, no. 7579, pp. 495–498, 2015.

[25] B. Bradlyn, J. Cano, Z. Wang, M. G. Vergniory, C. Felser, R. J. Cava, and B. A. Bernevig, "Beyond dirac and weyl fermions: Unconventional quasiparticles in conventional crystals," *Science*, vol. 353, no. 6299, 2016.

[26] C. Fang, M. J. Gilbert, X. Dai, and B. A. Bernevig, "Multi-weyl topological semimetals stabilized by point group symmetry," *Phys. Rev. Lett.*, vol. 108, p. 266802, Jun 2012.

[27] P. Tang, Q. Zhou, and S.-C. Zhang, "Multiple types of topological fermions in transition metal silicides," *Phys. Rev. Lett.*, vol. 119, p. 206402, Nov 2017.

[28] N. B. M. Schröter, D. Pei, M. G. Vergniory, Y. Sun, K. Manna, F. de Juan, J. A. Krieger, V. Süss, M. Schmidt, P. Dudin, B. Bradlyn, T. K. Kim, T. Schmitt, C. Cacho, C. Felser, V. N. Strocov, and Y. Chen, "Chiral topological semimetal with multifold band crossings and long fermi arcs," *Nature Physics*, vol. 15, pp. 759–765, Aug 2019.

[29] G. Chang, S.-Y. Xu, B. J. Wieder, D. S. Sanchez, S.-M. Huang, I. Belopolski, T.-R. Chang, S. Zhang, A. Bansil, H. Lin, and M. Z. Hasan, "Unconventional chiral fermions and large topological fermi arcs in rhsi," *Phys. Rev. Lett.*, vol. 119, p. 206401, Nov 2017.

[30] I. F. Herbut, "Interactions and phase transitions on graphene's honeycomb lattice," *Phys. Rev. Lett.*, vol. 97, p. 146401, Oct 2006.

[31] I. F. Herbut, V. Juricic, and B. Roy, "Theory of interacting electrons on the honeycomb lattice," *Phys. Rev. B*, vol. 79, p. 085116, Feb 2009.

[32] I. F. Herbut and L. Janssen, "Topological mott insulator in three-dimensional systems with quadratic band touching," *Phys. Rev. Lett.*, vol. 113, p. 106401, Sep 2014.

[33] Y. Lemonik, I. L. Aleiner, C. Toke, and V. I. Fal'ko, "Spontaneous symmetry breaking and lifshitz transition in bilayer graphene," *Phys. Rev. B*, vol. 82, p. 201408, Nov 2010.

[34] L. Janssen and I. F. Herbut, "Nematic quantum criticality in three-dimensional fermi system with quadratic band touching," *Phys. Rev. B*, vol. 92, p. 045117, Jul 2015.

[35] O. Vafek and K. Yang, "Many-body instability of coulomb interacting bilayer graphene: Renormalization group approach," *Phys. Rev. B*, vol. 81, p. 041401, Jan 2010.

[36] S. Sur and B. Roy, "Unifying interacting nodal semimetals: A new route to strong coupling," *Phys. Rev. Lett.*, vol. 123, p. 207601, Nov 2019.

[37] M. D. Uryszek, E. Christou, A. Jaefari, F. Krüger, and B. Uchoa, "Quantum criticality of semi-dirac fermions in $2+1$ dimensions," *Phys. Rev. B*, vol. 100, p. 155101, Oct 2019.

[38] M. D. Uryszek, F. Krüger, and E. Christou, "Fermionic criticality of anisotropic nodal point semimetals away from the upper critical dimension: Exact exponents to leading order in $\frac{1}{N_f}$," *Phys. Rev. Research*, vol. 2, p. 043265, Nov 2020.

[39] B.-J. Yang, E.-G. Moon, H. Isobe, and N. Nagaosa, "Quantum criticality of topological phase transitions in three-dimensional interacting electronic systems," *Nature Physics*, vol. 10, p. 774, 2014.

[40] H. Isobe, B.-J. Yang, A. Chubukov, J. Schmalian, and N. Nagaosa, "Emergent non-fermi-liquid at the quantum critical point of a topological phase transition in two dimensions," *Phys. Rev. Lett.*, vol. 116, p. 076803, Feb 2016.

[41] G. Y. Cho and E.-G. Moon, "Novel quantum criticality in two dimensional topological phase transitions," *Scientific Reports*, vol. 6, no. 1, p. 19198, 2016.

[42] S. Han, C. Lee, E.-G. Moon, and H. Min, "Emergent anisotropic non-fermi liquid at a topological phase transition in three dimensions," *Phys. Rev. Lett.*, vol. 122, p. 187601, May 2019.

[43] P. R. Wallace, "The band theory of graphite," *Phys. Rev.*, vol. 71, pp. 622–634, May 1947.

[44] C. L. Kane and E. J. Mele, "Quantum spin hall effect in graphene," *Phys. Rev. Lett.*, vol. 95, p. 226801, Nov 2005.

[45] Y. Yao, F. Ye, X.-L. Qi, S.-C. Zhang, and Z. Fang, "Spin-orbit gap of graphene: First-principles calculations," *Phys. Rev. B*, vol. 75, p. 041401, Jan 2007.

[46] M. Gmitra, S. Konschuh, C. Ertler, C. Ambrosch-Draxl, and J. Fabian, "Band-structure topologies of graphene: Spin-orbit coupling effects from first principles," *Phys. Rev. B*, vol. 80, p. 235431, Dec 2009.

[47] N. A. García-Martínez, A. G. Grushin, T. Neupert, B. Valenzuela, and E. V. Castro, "Interaction-driven phases in the half-filled spinless honeycomb lattice from exact diagonalization," *Phys. Rev. B*, vol. 88, p. 245123, Dec 2013.

[48] J. Motruk, A. G. Grushin, F. de Juan, and F. Pollmann, "Interaction-driven phases in the half-filled honeycomb lattice: An infinite density matrix renormalization group study," *Phys. Rev. B*, vol. 92, p. 085147, Aug 2015.

[49] D. J. Gross and A. Neveu, "Dynamical symmetry breaking in asymptotically free field theories," *Phys. Rev. D*, vol. 10, pp. 3235–3253, Nov 1974.

[50] J. Zinn-Justin, "Four-fermion interaction near four dimensions," *Nuclear Physics B*, vol. 367, no. 1, pp. 105 – 122, 1991.

[51] A. Altland and B. D. Simons, *Condensed Matter Field Theory*. Cambridge: Cambridge University Press, 2010.

[52] B. Uchoa and K. Seo, "Superconducting states for semi-dirac fermions at zero and finite magnetic fields," *Phys. Rev. B*, vol. 96, p. 220503, Dec 2017.

[53] K. G. Wilson, "Renormalization group and critical phenomena. i. renormalization group and the kadanoff scaling picture," *Phys. Rev. B*, vol. 4, pp. 3174–3183, Nov 1971.

[54] R. Shankar, "Renormalization-group approach to interacting fermions," *Rev. Mod. Phys.*, vol. 66, pp. 129–192, Jan 1994.

[55] K. G. Wilson and M. E. Fisher, "Critical exponents in 3.99 dimensions," *Phys. Rev. Lett.*, vol. 28, pp. 240–243, Jan 1972.

[56] R. Guida and J. Zinn-Justin, "Critical exponents of the n-vector model," *Journal of Physics A: Mathematical and General*, vol. 31, no. 40, p. 8103, 1998.

[57] M. Campostrini, A. Pelissetto, P. Rossi, and E. Vicari, "25th-order high-temperature expansion results for three-dimensional ising-like systems on the simple-cubic lattice," *Phys. Rev. E*, vol. 65, p. 066127, Jun 2002.

[58] Y. Deng and H. W. J. Blöte, "Simultaneous analysis of several models in the three-dimensional ising universality class," *Phys. Rev. E*, vol. 68, p. 036125, Sep 2003.

[59] M. Hasenbusch, "Finite size scaling study of lattice models in the three-dimensional ising universality class," *Phys. Rev. B*, vol. 82, p. 174433, Nov 2010.

[60] F. Kos, D. Poland, D. Simmons-Duffin, and A. Vichi, "Precision islands in the ising and o (n) models," *Journal of High Energy Physics*, vol. 2016, no. 8, pp. 1–16, 2016.

[61] A. G. Grushin, E. V. Castro, A. Cortijo, F. de Juan, M. A. H. Vozmediano, and B. Valenzuela, "Charge instabilities and topological phases in the extended hubbard model on the honeycomb lattice with enlarged unit cell," *Phys. Rev. B*, vol. 87, p. 085136, Feb 2013.

[62] M. Daghofer and M. Hohenadler, "Phases of correlated spinless fermions on the honeycomb lattice," *Phys. Rev. B*, vol. 89, p. 035103, Jan 2014.

[63] S. Capponi and A. M. Läuchli, "Phase diagram of interacting spinless fermions on the honeycomb lattice: A comprehensive exact diagonalization study," *Phys. Rev. B*, vol. 92, p. 085146, Aug 2015.

[64] D. D. Scherer, M. M. Scherer, and C. Honerkamp, "Correlated spinless fermions on the honeycomb lattice revisited," *Phys. Rev. B*, vol. 92, p. 155137, Oct 2015.

[65] Y. Volpez, D. D. Scherer, and M. M. Scherer, "Electronic instabilities of the extended hubbard model on the honeycomb lattice from functional renormalization," *Phys. Rev. B*, vol. 94, p. 165107, Oct 2016.

[66] M. Kurita, Y. Yamaji, and M. Imada, "Stabilization of topological insulator emerging from electron correlations on honeycomb lattice and its possible relevance in twisted bilayer graphene," *Phys. Rev. B*, vol. 94, p. 125131, Sep 2016.

[67] D. S. de la Peña, J. Lichtenstein, and C. Honerkamp, "Competing electronic instabilities of extended hubbard models on the honeycomb lattice: A functional renormalization group calculation with high-wavevector resolution," *Phys. Rev. B*, vol. 95, p. 085143, Feb 2017.

[68] E. Christou, B. Uchoa, and F. Krüger, "Hidden charge order of interacting dirac fermions on the honeycomb lattice," *Phys. Rev. B*, vol. 98, p. 161120, Oct 2018.

[69] F. F. Assaad and I. F. Herbut, "Pinning the order: The nature of quantum criticality in the hubbard model on honeycomb lattice," *Phys. Rev. X*, vol. 3, p. 031010, Aug 2013.

[70] Z.-X. Li, Y.-F. Jiang, S.-K. Jian, and H. Yao, "Fermion-induced quantum critical points," *Nature Communications*, vol. 8, p. 314, Aug 2017.

[71] J. A. Hertz, "Quantum critical phenomena," *Phys. Rev. B*, vol. 14, pp. 1165–1184, Aug 1976.

[72] A. J. Millis, "Effect of a nonzero temperature on quantum critical points in itinerant fermion systems," *Phys. Rev. B*, vol. 48, pp. 7183–7196, Sep 1993.

[73] A. Abanov and A. Chubukov, "Anomalous scaling at the quantum critical point in itinerant antiferromagnets," *Phys. Rev. Lett.*, vol. 93, p. 255702, Dec 2004.

[74] H.-H. Lai, "Correlation effects in double-weyl semimetals," *Phys. Rev. B*, vol. 91, p. 235131, Jun 2015.

[75] S.-K. Jian and H. Yao, "Correlated double-weyl semimetals with coulomb interactions: Possible applications to $hgcr_2se_4$ and $srsi_2$," *Phys. Rev. B*, vol. 92, p. 045121, Jul 2015.

[76] B. L. Altshuler, L. B. Ioffe, and A. J. Millis, "Low-energy properties of fermions with singular interactions," *Phys. Rev. B*, vol. 50, pp. 14048–14064, Nov 1994.

[77] J. Polchinski, "Low-energy dynamics of the spinon-gauge system," *Nuclear Physics B*, vol. 422, no. 3, pp. 617–633, 1994.

[78] A. Abanov, A. V. Chubukov, and J. Schmalian, "Quantum-critical theory of the spin-fermion model and its application to cuprates: Normal state analysis," *Advances in Physics*, vol. 52, no. 3, pp. 119–218, 2003.

[79] D. T. Son, "Quantum critical point in graphene approached in the limit of infinitely strong coulomb interaction," *Phys. Rev. B*, vol. 75, p. 235423, Jun 2007.

[80] M. A. Metlitski and S. Sachdev, "Quantum phase transitions of metals in two spatial dimensions. ii. spin density wave order," *Phys. Rev. B*, vol. 82, p. 075128, Aug 2010.

[81] D. F. Mross, J. McGreevy, H. Liu, and T. Senthil, "Controlled expansion for certain non-fermi-liquid metals," *Phys. Rev. B*, vol. 82, p. 045121, Jul 2010.

[82] K. B. Efetov, H. Meier, and C. Pépin, "Pseudogap state near a quantum critical point," *Nature Physics*, vol. 9, no. 7, pp. 442–446, 2013.

[83] A. V. Chubukov and P. Wölfle, "Quasiparticle interaction function in a two-dimensional fermi liquid near an antiferromagnetic critical point," *Phys. Rev. B*, vol. 89, p. 045108, Jan 2014.

[84] S.-S. Lee, "Low-energy effective theory of fermi surface coupled with u(1) gauge field in $2+1$ dimensions," *Phys. Rev. B*, vol. 80, p. 165102, Oct 2009.

[85] A. V. Chubukov, C. Pépin, and J. Rech, "Instability of the quantum-critical point of itinerant ferromagnets," *Phys. Rev. Lett.*, vol. 92, p. 147003, Apr 2004.

[86] A. N. Vasil'ev and A. Stepanenko, "The 1/n expansion in the gross-neveu model: Conformal bootstrap calculation of the exponent 1/v to the order 1/n 2," *Theoretical and Mathematical Physics*, vol. 97, no. 3, pp. 1349–1354, 1993.

[87] J. Gracey, "Computation of critical exponent η at o(1/n3) in the four-fermi model in arbitrary dimensions," *International Journal of Modern Physics A*, vol. 9, no. 5, pp. 727–744, 1994.

[88] L. Iliesiu, F. Kos, D. Poland, S. S. Pufu, D. Simmons-Duffin, and R. Yacoby, "Bootstrapping 3d fermions," *Journal of High Energy Physics*, vol. 2016, no. 3, pp. 1–42, 2016.

[89] G. Gat, A. Kovner, B. Rosenstein, and B. Warr, "Four-fermi interaction in (2+1) dimensions beyond leading order in 1/n," *Physics Letters B*, vol. 240, no. 1, pp. 158 – 162, 1990.

[90] J. Gracey, "Calculation of exponent η to o(1/n2) in the o(n) gross neveu model," *International Journal of Modern Physics A*, vol. 06, no. 03, pp. 395–407, 1991.

[91] J. Gracey, "Anomalous mass dimension at o(1/n2) in the o(n) gross-neveu model," *Physics Letters B*, vol. 297, no. 3, pp. 293 – 297, 1992.

[92] L. Iliesiu, F. Kos, D. Poland, S. S. Pufu, and D. Simmons-Duffin, "Bootstrapping 3d fermions with global symmetries," *Journal of High Energy Physics*, vol. 2018, p. 36, Jan 2018.

[93] E. Brezin, J. Le Guillou, and J. Zinn-Justin, "Phase transitions and critical phenomena," in *Phase Transitions and Critical Phenomena* (M. G. C. Domb, ed.), vol. 6, ch. 3, Academic Press, London, 1976.

[94] M. Vojta, Y. Zhang, and S. Sachdev, "Renormalization group analysis of quantum critical points in d-wave superconductors," *International Journal of Modern Physics B*, vol. 14, no. 29n31, pp. 3719–3734, 2000.

[95] M. Vojta, Y. Zhang, and S. Sachdev, "Quantum phase transitions in d-wave superconductors," *Phys. Rev. Lett.*, vol. 85, pp. 4940–4943, Dec 2000.

[96] M. Vojta, Y. Zhang, and S. Sachdev, "Erratum: Quantum phase transitions in d-wave superconductors [phys. rev. lett. 85, 4940 (2000)]," *Phys. Rev. Lett.*, vol. 100, p. 089904, Feb 2008.

[97] Y. Huh and S. Sachdev, "Renormalization group theory of nematic ordering in d-wave superconductors," *Phys. Rev. B*, vol. 78, p. 064512, Aug 2008.

[98] J. Zinn-Justin, *Quantum field theory and critical phenomena*. Clarendon Press, 1996.

[99] J. González, F. Guinea, and M. Vozmediano, "Non-fermi liquid behavior of electrons in the half-filled honeycomb lattice (a renormalization group approach)," *Nuclear Physics B*, vol. 424, no. 3, pp. 595 – 618, 1994.

[100] J. González, F. Guinea, and M. A. H. Vozmediano, "Marginal-fermi-liquid behavior from two-dimensional coulomb interaction," *Phys. Rev. B*, vol. 59, pp. R2474–R2477, Jan 1999.

[101] E. Christou, F. de Juan, and F. Krüger, "Criticality of dirac fermions in the presence of emergent gauge fields," *Phys. Rev. B*, vol. 101, p. 155121, Apr 2020.

[102] E. Marino, "Quantum electrodynamics of particles on a plane and the chern-simons theory," *Nuclear Physics B*, vol. 408, no. 3, pp. 551 – 564, 1993.

[103] S.-K. Jian and H. Yao, "Fermion-induced quantum critical points in two-dimensional dirac semimetals," *Phys. Rev. B*, vol. 96, p. 195162, Nov 2017.

[104] M. M. Scherer and I. F. Herbut, "Gauge-field-assisted kekulé quantum criticality," *Phys. Rev. B*, vol. 94, p. 205136, Nov 2016.

[105] A. Schlief, P. Lunts, and S.-S. Lee, "Exact critical exponents for the antiferromagnetic quantum critical metal in two dimensions," *Phys. Rev. X*, vol. 7, p. 021010, Apr 2017.

[106] J. Kim, S. S. Baik, S. H. Ryu, Y. Sohn, S. Park, B.-G. Park, J. Denlinger, Y. Yi, H. J. Choi, and K. S. Kim, "Observation of tunable band gap and anisotropic dirac semimetal state in black phosphorus," *Science*, vol. 349, no. 6249, pp. 723–726, 2015.

[107] A. S. Rodin, A. Carvalho, and A. H. Castro Neto, "Strain-induced gap modification in black phosphorus," *Phys. Rev. Lett.*, vol. 112, p. 176801, May 2014.

[108] V. Pardo and W. E. Pickett, "Half-metallic semi-dirac-point generated by quantum confinement in tio_2/vo_2 nanostructures," *Phys. Rev. Lett.*, vol. 102, p. 166803, Apr 2009.

[109] H. Huang, Z. Liu, H. Zhang, W. Duan, and D. Vanderbilt, "Emergence of a chern-insulating state from a semi-dirac dispersion," *Phys. Rev. B*, vol. 92, p. 161115, Oct 2015.

[110] B.-J. Yang, M. S. Bahramy, R. Arita, H. Isobe, E.-G. Moon, and N. Nagaosa, "Theory of topological quantum phase transitions in 3d noncentrosymmetric systems," *Phys. Rev. Lett.*, vol. 110, p. 086402, Feb 2013.

[111] J.-R. Wang, G.-Z. Liu, and C.-J. Zhang, "Excitonic pairing and insulating transition in two-dimensional semi-dirac semimetals," *Phys. Rev. B*, vol. 95, p. 075129, Feb 2017.

[112] B. Roy and M. S. Foster, "Quantum multicriticality near the dirac-semimetal to band-insulator critical point in two dimensions: A controlled ascent from one dimension," *Phys. Rev. X*, vol. 8, p. 011049, Mar 2018.

[113] X. Li, J.-R. Wang, and G.-Z. Liu, "Phase transition with trivial quantum criticality in an anisotropic weyl semimetal," *Phys. Rev. B*, vol. 97, p. 184508, May 2018.

[114] A. Schlief, P. Lunts, and S.-S. Lee, "Noncommutativity between the low-energy limit and integer dimension limits in the ϵ expansion: A case study of the antiferromagnetic quantum critical metal," *Phys. Rev. B*, vol. 98, p. 075140, Aug 2018.

[115] G. Jose and B. Uchoa, "Quantum critical scaling of gapped phases in nodal-line semimetals," *Phys. Rev. B*, vol. 101, p. 115123, Mar 2020.

[116] M. D. Uryszek and F. Krüger, "Interplay of interactions and disorder at the charge density wave transition of two-dimensional dirac semimetals," *Phys. Rev. B*, vol. 105, p. 075143, Feb 2022.

[117] E. Fradkin, "Critical behavior of disordered degenerate semiconductors. i. models, symmetries, and formalism," *Phys. Rev. B*, vol. 33, pp. 3257–3262, Mar 1986.

[118] E. Fradkin, "Critical behavior of disordered degenerate semiconductors. ii. spectrum and transport properties in mean-field theory," *Phys. Rev. B*, vol. 33, pp. 3263–3268, Mar 1986.

[119] I. L. Aleiner and K. B. Efetov, "Effect of disorder on transport in graphene," *Phys. Rev. Lett.*, vol. 97, p. 236801, Dec 2006.

[120] P. M. Ostrovsky, I. V. Gornyi, and A. D. Mirlin, "Electron transport in disordered graphene," *Phys. Rev. B*, vol. 74, p. 235443, Dec 2006.

[121] P. M. Ostrovsky, I. V. Gornyi, and A. D. Mirlin, "Quantum criticality and minimal conductivity in graphene with long-range disorder," *Phys. Rev. Lett.*, vol. 98, p. 256801, Jun 2007.

[122] E. H. Hwang, S. Adam, and S. D. Sarma, "Carrier transport in two-dimensional graphene layers," *Phys. Rev. Lett.*, vol. 98, p. 186806, May 2007.

[123] S. Adam, E. H. Hwang, V. M. Galitski, and S. Das Sarma, "A self-consistent theory for graphene transport," *Proceedings of the National Academy of Sciences*, vol. 104, no. 47, pp. 18392–18397, 2007.

[124] V. V. Cheianov, V. I. Fal'ko, B. L. Altshuler, and I. L. Aleiner, "Random resistor network model of minimal conductivity in graphene," *Phys. Rev. Lett.*, vol. 99, p. 176801, Oct 2007.

[125] S. Das Sarma, S. Adam, E. H. Hwang, and E. Rossi, "Electronic transport in two-dimensional graphene," *Rev. Mod. Phys.*, vol. 83, pp. 407–470, May 2011.

[126] A. Nersesyan, A. Tsvelik, and F. Wenger, "Disorder effects in two-dimensional fermi systems with conical spectrum: exact results for the density of states," *Nuclear Physics B*, vol. 438, no. 3, pp. 561–588, 1995.

[127] A. A. Nersesyan, A. M. Tsvelik, and F. Wenger, "Disorder effects in two-dimensional d-wave superconductors," *Phys. Rev. Lett.*, vol. 72, pp. 2628–2631, Apr 1994.

[128] A. Altland, B. Simons, and M. Zirnbauer, "Theories of low-energy quasi-particle states in disordered d-wave superconductors," *Physics Reports*, vol. 359, no. 4, pp. 283–354, 2002.

[129] K. S. Novoselov, A. K. Geim, S. V. Morozov, D. Jiang, Y. Zhang, S. V. Dubonos, I. V. Grigorieva, and A. A. Firsov, "Electric field effect in atomically thin carbon films," *Science*, vol. 306, no. 5696, pp. 666–669, 2004.

[130] K. S. Novoselov, A. K. Geim, S. V. Morozov, D. Jiang, M. I. Katsnelson, I. V. Grigorieva, S. V. Dubonos, and A. A. Firsov, "Two-dimensional gas of massless dirac fermions in graphene," *Nature*, vol. 438, no. 7065, pp. 197–200, 2005.

[131] Y. Zhang, Y.-W. Tan, H. L. Stormer, and P. Kim, "Experimental observation of the quantum hall effect and berry's phase in graphene," *Nature*, vol. 438, no. 7065, pp. 201–204, 2005.

[132] J. Ye and S. Sachdev, "Coulomb interactions at quantum hall critical points of systems in a periodic potential," *Phys. Rev. Lett.*, vol. 80, pp. 5409–5412, Jun 1998.

[133] J. Ye, "Effects of weak disorders on quantum hall critical points," *Phys. Rev. B*, vol. 60, pp. 8290–8303, Sep 1999.

[134] T. Stauber, F. Guinea, and M. A. H. Vozmediano, "Disorder and interaction effects in two-dimensional graphene sheets," *Phys. Rev. B*, vol. 71, p. 041406, Jan 2005.

[135] M. S. Foster and I. L. Aleiner, "Graphene via large n: A renormalization group study," *Phys. Rev. B*, vol. 77, p. 195413, May 2008.

[136] J. González, F. Guinea, and M. Vozmediano, "The electronic spectrum of fullerenes from the dirac equation," *Nuclear Physics B*, vol. 406, no. 3, pp. 771–794, 1993.

[137] P. E. Lammert and V. H. Crespi, "Topological phases in graphitic cones," *Phys. Rev. Lett.*, vol. 85, pp. 5190–5193, Dec 2000.

[138] J. González, F. Guinea, and M. A. H. Vozmediano, "Electron-electron interactions in graphene sheets," *Phys. Rev. B*, vol. 63, p. 134421, Mar 2001.

[139] P. Goswami and S. Chakravarty, "Quantum criticality between topological and band insulators in $3 + 1$ dimensions," *Phys. Rev. Lett.*, vol. 107, p. 196803, Nov 2011.

[140] J. González, "Competition between disorder and interaction effects in three-dimensional weyl semimetals," *Phys. Rev. B*, vol. 96, p. 081104, Aug 2017.

[141] B. Roy and S. Das Sarma, "Diffusive quantum criticality in three-dimensional disordered dirac semimetals," *Phys. Rev. B*, vol. 90, p. 241112, Dec 2014.

[142] J.-R. Wang, W. Li, G. Wang, and C.-J. Zhang, "Global phase diagram of coulomb-interacting anisotropic weyl semimetal with disorder," *Journal of Physics: Condensed Matter*, vol. 33, p. 125601, jan 2021.

[143] R. Nandkishore, D. A. Huse, and S. L. Sondhi, "Rare region effects dominate weakly disordered three-dimensional dirac points," *Phys. Rev. B*, vol. 89, p. 245110, Jun 2014.

[144] J. H. Wilson, D. A. Huse, S. Das Sarma, and J. H. Pixley, "Avoided quantum criticality in exact numerical simulations of a single disordered weyl cone," *Phys. Rev. B*, vol. 102, p. 100201, Sep 2020.

[145] J. H. Pixley, D. A. Huse, and S. Das Sarma, "Rare-region-induced avoided quantum criticality in disordered three-dimensional dirac and weyl semimetals," *Phys. Rev. X*, vol. 6, p. 021042, Jun 2016.

[146] M. Buchhold, S. Diehl, and A. Altland, "Vanishing density of states in weakly disordered weyl semimetals," *Phys. Rev. Lett.*, vol. 121, p. 215301, Nov 2018.

[147] M. Buchhold, S. Diehl, and A. Altland, "Nodal points of weyl semimetals survive the presence of moderate disorder," *Phys. Rev. B*, vol. 98, p. 205134, Nov 2018.

[148] H. Yerzhakov and J. Maciejko, "Random-mass disorder in the critical gross-neveu-yukawa models," *Nuclear Physics B*, vol. 962, p. 115241, 2021.

[149] I. F. Herbut, V. Juricic, and O. Vafek, "Coulomb interaction, ripples, and the minimal conductivity of graphene," *Phys. Rev. Lett.*, vol. 100, p. 046403, Jan 2008.

[150] O. Vafek and M. J. Case, "Renormalization group approach to two-dimensional coulomb interacting dirac fermions with random gauge potential," *Phys. Rev. B*, vol. 77, p. 033410, Jan 2008.

[151] S. F. Edwards and P. W. Anderson, "Theory of spin glasses," *Journal of Physics F: Metal Physics*, vol. 5, pp. 965–974, may 1975.

[152] K. H. Fischer and J. A. Hertz, *Spin Glasses*. Cambridge Studies in Magnetism, Cambridge University Press, 1991.

[153] A. W. W. Ludwig, M. P. A. Fisher, R. Shankar, and G. Grinstein, "Integer quantum hall transition: An alternative approach and exact results," *Phys. Rev. B*, vol. 50, pp. 7526–7552, Sep 1994.

[154] A. B. Harris, "Effect of random defects on the critical behaviour of ising models," *Journal of Physics C: Solid State Physics*, vol. 7, pp. 1671–1692, may 1974.

[155] J. T. Chayes, L. Chayes, D. S. Fisher, and T. Spencer, "Finite-size scaling and correlation lengths for disordered systems," *Phys. Rev. Lett.*, vol. 57, pp. 2999–3002, Dec 1986.

[156] G. Parisi, "Infinite number of order parameters for spin-glasses," *Phys. Rev. Lett.*, vol. 43, pp. 1754–1756, Dec 1979.

[157] J. Pixley and J. H. Wilson, "Rare regions and avoided quantum criticality in disordered weyl semimetals and superconductors," *Annals of Physics*, p. 168455, 2021.

[158] J. Martin, N. Akerman, G. Ulbricht, T. Lohmann, J. H. Smet, K. von Klitzing, and A. Yacoby, "Observation of electron–hole puddles in graphene using a scanning single-electron transistor," *Nature Physics*, vol. 4, no. 2, pp. 144–148, 2008.

[159] A. Deshpande, W. Bao, F. Miao, C. N. Lau, and B. J. LeRoy, "Spatially resolved spectroscopy of monolayer graphene on sio_2," *Phys. Rev. B*, vol. 79, p. 205411, May 2009.

[160] Y. Zhang, V. W. Brar, C. Girit, A. Zettl, and M. F. Crommie, "Origin of spatial charge inhomogeneity in graphene," *Nature Physics*, vol. 5, no. 10, pp. 722–726, 2009.

Appendix A

Useful integral identities

The loop calculations utilize integral identities that follow from the integral representations of the Γ function. Typically, k-integrals are rewritten in hyper-spherical coordinates $k_\mu = y\hat{k}_\mu$ with $\hat{k}_\mu\hat{k}_\mu = 1$,

$$\int_k = \int \frac{d^D k}{(2\pi)^D} = \int \frac{d\hat{\Omega}_k}{(2\pi)^D} \int_0^\infty dy\, y^{D-1}. \tag{A.1}$$

The radial integral identity

$$\int_0^\infty dy \frac{y^{D-1+\alpha}}{(y^\beta + M)^n} = \frac{\Gamma(\frac{D+\alpha}{\beta})\Gamma(n - \frac{D+\alpha}{\beta})}{\beta\,\Gamma(n) M^{n-\frac{D+\alpha}{\beta}}}, \tag{A.2}$$

is valid for $D + \alpha > 0$ and $n\beta > D + \alpha$. The angular integral identity over the D-dimensional unit sphere

$$\int \frac{d\hat{\Omega}_k}{(2\pi)^D} \hat{k}_\mu^{2n} = S_D \frac{\Gamma(\frac{D}{2})\Gamma(\frac{2n+1}{2})}{\sqrt{\pi}\Gamma(\frac{2n+D}{2})}, \tag{A.3}$$

for integer n. Integrals over odd powers of $\hat{k}_\mu$ are zero, by symmetry. Here $\mu = 0, \ldots, D$ is not summed over and

$$S_D = \frac{1}{(2\pi)^{\frac{D}{2}}} \frac{2\pi^{\frac{D}{2}}}{\Gamma(\frac{D}{2})}, \tag{A.4}$$

is the surface area of a D-dimensional unit sphere.

The Feynman parameterization

$$\frac{1}{a^n b^m} = \frac{\Gamma(n+m)}{\Gamma(n)\Gamma(m)} \int_0^1 dt \frac{t^{n-1}(1-t)^{m-1}}{[ta+(1-t)b]^{n+m}}, \tag{A.5}$$

in conjunction with appropriate linear momentum shifts is used to render integrals radially symmetric.

The Feynman parameter integral identity

$$\int_0^1 dt\ t^a (1-t)^b = \frac{\Gamma(a+1)\,\Gamma(b+1)}{\Gamma(a+b+2)}, \tag{A.6}$$

is valid for $a > -1$ and $b > -1$.

Appendix B

GNY diagrams

B.1 RPA boson propagator

We work in units where the Fermi velocity $v = 1$, such that

$$G_\Psi(k) = \frac{ik_\mu \gamma_\mu}{k^2}. \tag{B.1}$$

The fermion loop diagram is displayed in Fig. 5.2(a). We calculate the regularized fermion loop $\Pi(q) \to \Pi(q) - \Pi(0)$,

$$\begin{aligned}\Pi(q) &= \frac{g^2}{N_f}\int_k \text{tr}\,[G_\Psi(k+q)G_\Psi(k) - G_\Psi(k)G_\Psi(k)] \\ &= g^2 \int_k \frac{(k_\mu + q_\mu)q_\mu}{(k+q)^2 k^2},\end{aligned} \tag{B.2}$$

where we have used that $\text{tr}\,\gamma_\mu\gamma_\nu = N_f\delta_{\mu\nu}$. After using the Feynman parametrization (A.5) with $n = m = 1$, $a = (k+q)^2$ and $b = k^2$, and substituting $\tilde{k} = k + tq$, the $\tilde{k}$ integral is radially symmetric,

$$\Pi(q) = g^2 \int_0^1 dt \int_{\tilde{k}} \frac{(1-t)q^2}{[\tilde{k}^2 + t(1-t)q^2)]^2}. \tag{B.3}$$

Evaluating the $\tilde{k}$ integral, using the radial integration formula (A.2), and then carrying out the one-dimensional integral over the Feynman parameter t, using the identity (A.6), we obtain

$$\Pi(q) = \frac{g^2 S_D \alpha_D}{v^{D-1}} (q_0^2 + v^2 \boldsymbol{q}^2)^{\frac{D-2}{2}}, \tag{B.4}$$

where we have reinstated the Fermi velocity v, and defined

$$\alpha_D = -\frac{\pi}{2\sin(\frac{\pi D}{2})}\frac{\Gamma(D/2)^2}{\Gamma(D-1)}. \tag{B.5}$$

The resulting dressed RPA boson propagator is given by

$$\begin{aligned} G_\phi^{-1}(q) &= G_{\phi,0}^{-1}(q) + \Pi(q) \\ &= \frac{g^2 S_D \alpha_D}{v^{D-1}}(q_0^2 + v^2 \boldsymbol{q}^2)^{\frac{D-2}{2}} + m^2, \end{aligned} \tag{B.6}$$

where we neglected the sub-leading momentum and frequency terms from the bare propagator $G_{\phi,0}^{-1}(q)$.

B.2 Soft cutoff one-loop quantum corrections

In the following we work in rescaled units, such that $v = 1$. The dependence on the Fermi velocity will be reinstated in the end. The propagators are augmented by cutoff functions A as described in the main text with $A_k = A(a_\mu k_\mu^2/\Lambda^2)$. The flow of the fermion self energy correction $\Sigma(q)$, Fig. 5.3(b), is

$$\frac{d}{d\ell}\Sigma(q) = -\Lambda\frac{d}{d\Lambda}\frac{g^2}{N_f}\int_k G_\Psi(k+q)G_\phi(k)A_k A_k. \tag{B.7}$$

We extract the relevant linear q term on the critical surface $m^2 = 0$,

$$\frac{d}{d\ell}\Sigma(q) = \frac{iq_\mu\gamma_\nu}{S_D\alpha_D N_f}\Lambda\frac{d}{d\Lambda}\int_k \frac{2k_\mu k_\nu - \delta_{\mu\nu}k^2}{k^{D+2}}A_k^2, \tag{B.8}$$

and rewrite the integral in terms of angular and radial integrals, defining $k = y\hat{k}$,

$$\begin{aligned} \frac{d}{d\ell}\Sigma(q) &= \frac{iq_\mu\gamma_\nu}{S_D\alpha_D N_f}\int_{\hat{\Omega}}\left(2\hat{k}_\mu\hat{k}_\nu - \delta_{\mu\nu}\right) \\ &\quad \times\Lambda\frac{d}{d\Lambda}\int_0^\infty \frac{dy}{y}A^2\left(\frac{f(\hat{\Omega})y^2}{\Lambda^2}\right). \end{aligned} \tag{B.9}$$

While the radial y integral becomes trivial, using the soft cutoff integral identity (5.26), the angular integral can be computed using Eq. (A.3). The final result is

$$\frac{d}{d\ell}\Sigma(q) = -i\frac{D-2}{\alpha_D D N_f}(q_0\gamma_0 + v\boldsymbol{q}\cdot\boldsymbol{\gamma}). \tag{B.10}$$

To compute the flow of the vertex correction Ξ, Fig. 5.3(c), we follow the same steps,

$$\begin{aligned}\frac{d}{d\ell}\Xi &= \Lambda\frac{d}{d\Lambda}\frac{g^3}{\sqrt{N_f}^3}\int_k G_\Psi^2(k)G_\phi(k)A_k^3 \\ &= -\frac{g}{S_D\alpha_D\sqrt{N_f}^3}\Lambda\frac{d}{d\Lambda}\int_{\hat{\Omega}}\int_0^\infty \frac{dy}{y}A^3\left(\frac{f(\hat{\Omega})y^2}{\Lambda^2}\right) \\ &= -\frac{1}{\alpha_D N_f}\frac{g}{\sqrt{N_f}}. \end{aligned} \tag{B.11}$$

B.3 Soft cutoff two-loop quantum corrections

The flow of the two loop boson self energy $\tilde{\Pi}$, Fig. 5.3(d), that renormalizes the boson mass (at zero external momentum) is

$$\begin{aligned}\frac{d}{d\ell}\tilde{\Pi} = \Lambda\frac{d}{d\Lambda}\frac{g^4}{N_f^2}\int_{k,q} G_\phi(q)A_q \times \mathrm{tr}\Big[\\ G_\Psi(k+q)G_\Psi(k+q)G_\Psi(k)G_\Psi(k)A_{k+q}^2A_k^2 \\ + 2G_\Psi(k+q)G_\Psi(k)G_\Psi(k)G_\Psi(k)A_{k+q}A_k^3\Big]. \end{aligned} \tag{B.12}$$

We extract the relevant m^2 contribution

$$\begin{aligned}\frac{d}{d\ell}\tilde{\Pi} = -\frac{m^2}{(S_D\alpha_D)^2N_f}\Lambda\frac{d}{d\Lambda}\int_{k,q}\frac{1}{q^{2D-4}k^2(k+q)^2} \\ \times\Big[A_k^2A_{k+q}^2A_q + \frac{2(k_\mu+q_\mu)k_\mu}{k^2}A_k^3A_{k+q}A_q\Big]. \end{aligned} \tag{B.13}$$

The two loop calculation involves more steps. We use the transformation $q_\mu = y\hat{q}_\mu$, $k_\mu = yx\hat{k}_\mu$, where $\hat{q}_\mu\hat{q}_\mu = 1$ and $\hat{k}_\mu\hat{k}_\mu = 1$, such that

$$\begin{aligned}\frac{d}{d\ell}\tilde{\Pi} = -\frac{m^2}{(S_D\alpha_D)^2N_f}\int\frac{\hat{\Omega}_k}{(2\pi)^D}\int\frac{d\hat{\Omega}_q}{(2\pi)^D}\int_0^\infty dx\, x^{D-1} \\ \times\Lambda\frac{d}{d\Lambda}\int_0^\infty\frac{dy}{y}\frac{1}{x^2(x\hat{k}+\hat{q})^2}\Big[A_{yx\hat{k}}^2A_{y(x\hat{k}+\hat{q})}^2A_{y\hat{q}} \\ + \frac{2(x^2+x\hat{k}_\mu\hat{q}_\mu)}{x^2}A_{yx\hat{k}}^3A_{y(x\hat{k}+\hat{q})}A_{y\hat{q}}\Big]. \end{aligned} \tag{B.14}$$

The y integral is evaluated with the soft cutoff identity (5.26). The integral is rendered radially symmetric in x after the introduction of the Feynman parameter t (A.5), with the shift $\hat{k} \to \hat{k} - t\hat{q}/x$. Then the angular integrals are evaluated resulting in

$$\frac{d}{d\ell}\tilde{\Pi} = -\frac{m^2}{\alpha_D^2 N_f}\int_0^1 dt \int_0^\infty dx\, x^{D-1}\Big\{ \frac{1}{[x^2+t(1-t)]^2} + 4(1-t)\frac{x^2-t(1-t)}{[x^2+t(1-t)]^3}\Big\}. \tag{B.15}$$

The radial x integral and the integral over the Feynman parameter t are evaluated using Eqs. (A.2) and (A.6), respectively. The final result is

$$\frac{d}{d\ell}\tilde{\Pi} = \frac{D-1}{\alpha_D^2 N_f \sin(\frac{\pi D}{2})}\frac{\pi\Gamma(\frac{D}{2})^2}{\Gamma(D-1)}m^2. \tag{B.16}$$

Appendix C

Diagrams for semi-Dirac ($d_L = d_Q = 1$) systems

We work in units where the $v_Q = 1$, and define

$$\varepsilon_\mu(k) = (k_0, k_L, k_Q^2), \tag{C.1}$$

as well as $\gamma_\mu = (\gamma_0, \gamma_L, \gamma_Q)$, such that (at $\Delta = 0$)

$$G_\Psi(k) = i\frac{\varepsilon_\mu(k)\gamma_\mu}{\varepsilon^2(k)} = i\frac{k_0\gamma_0 + k_L\gamma_L + k_Q^2\gamma_Q}{k_0^2 + k_L^2 + k_Q^4}. \tag{C.2}$$

C.1 RPA boson propagator

We compute the boson self energy, which is given by the fermion polarization diagram,

$$\begin{aligned}
\Pi(q) &= \frac{g^2}{N_f}\int_k \text{tr}\,\left[G_\Psi(k+q)G_\Psi(k) - G_\Psi(k)G_\Psi(k)\right] \\
&= g^2\int_k \Big\{q_0(k_0+q_0) + q_L(k_L+q_L) + (k_Q+q_Q)^2 \\
&\quad \times\left[(k_Q+q_Q)^2 - k_Q^2\right]\Big\}\Big/\Big\{(k_0^2+k_L^2+k_Q^4) \\
&\quad \times\left[(k_0+q_0)^2 + (k_L+q_L)^2 + (k_Q+q_Q)^4\right]\Big\},
\end{aligned} \tag{C.3}$$

where we have used that $\text{tr}\gamma_\mu\gamma_\nu = N_f\delta_{\mu\nu}$. This integral can be rendered radially symmetric in (k_0, k_L) by introducing the Feynman parameter t (A.5)

followed by the shift $(k_0, k_L) \to (k_0, k_L) - t(q_0, q_L)$,

$$\Pi(q) = \frac{g^2}{4\pi^2} \int_0^1 dt \int_{-\infty}^{\infty} dk_Q \int_0^{\infty} dy\, y \times \frac{(1-t)(q_0^2+q_L^2) + (k_Q+q_Q)^2\left[(k_Q+q_Q)^2 - k_Q^2\right]}{[y^2 + t(1-t)(q_0^2+q_L^2) + t(k_Q+q_Q)^4 + (1-t)k_Q^4]^2}, \tag{C.4}$$

where $y^2 = k_0^2 + k_L^2$. The radial integral over y can be performed using the radial integral identity (A.2),

$$\Pi(q) = \frac{g^2}{8\pi^2} \int_0^1 dt \int_{-\infty}^{\infty} dk_Q \times \frac{(1-t)(q_0^2+q_L^2) + (k_Q+q_Q)^2\left[(k_Q+q_Q)^2 - k_Q^2\right]}{t(1-t)(q_0^2+q_L^2) + t(k_Q+q_Q)^4 + (1-t)k_Q^4}, \tag{C.5}$$

Substituting $p = k_Q/|q_Q|$, we can write the bosonic self energy in the form

$$\Pi(q) = \frac{g^2}{8\pi^2} |q_Q|\, F\left(\frac{q_0^2+q_L^2}{q_Q^4}\right), \tag{C.6}$$

where

$$F(u) = \int_0^1 dt \int_{-\infty}^{\infty} dp \frac{(p+1)^4 - p^2(p+1)^2 + (1-t)u}{(p+1)^4 t + p^4(1-t) + t(1-t)u}. \tag{C.7}$$

This is evaluated numerically, and is used to obtain numerically exact quantum corrections.

C.2 Soft cutoff one-loop quantum corrections

Using the non-analytic RPA boson propagator

$$G_\phi^{-1}(k) = \frac{g^2}{8\pi^2} |k_Q|\, F\left(\frac{k_0^2+k_L^2}{k_Q^4}\right) + m^2, \tag{C.8}$$

without the sub-leading bare terms, we compute the loop integrals $\delta\Sigma_L$, $\delta\Sigma_Q$, and $\delta\Sigma_\Delta$, which arise in the expansion of the fermion self-energy correction, Eq. (6.21), and $\delta\Xi$, which enters in the quantum correction that renormalizes

the Yukawa coupling, Eq. (6.22). The corresponding diagrams are shown in Figs. 5.3(b) and (c), respectively. The one-loop integrals we need to compute are

$$\delta\Sigma_L = \frac{8\pi^2}{N_f}\Lambda\frac{d}{d\Lambda}\int_k \frac{A_k^2}{|k_Q|F_k}\left(\frac{1}{\varepsilon_k^2} - \frac{k_0^2+k_L^2}{\varepsilon_k^4}\right), \tag{C.9}$$

$$\delta\Sigma_Q = \frac{8\pi^2}{N_f}\Lambda\frac{d}{d\Lambda}\int_k \frac{A_k^2}{|k_Q|F_k}\times \tag{C.10}$$
$$\times\left(\frac{(k_0^2+k_L^2)^2 - 12(k_0^2+k_L^2)k_Q^4 + 3k_Q^8}{\varepsilon_k^6}\right),$$

$$\delta\Sigma_\Delta = \frac{8\pi^2}{N_f}\Lambda\frac{d}{d\Lambda}\int_k \frac{A_k^2}{|k_Q|F_k}\left(\frac{k_0^2+k_L^2-k_Q^4}{\varepsilon_k^4}\right), \tag{C.11}$$

$$\delta\Xi = -\frac{8\pi^2}{N_f}\Lambda\frac{d}{d\Lambda}\int_k \frac{A_k^3}{|k_Q|F_k}\left(\frac{1}{\varepsilon_k^2}\right), \tag{C.12}$$

where we have defined $F_k = F[(k_0^2+k_L^2)/k_Q^4]$, $A_k = A(a_\mu\varepsilon_\mu^2(k)/\Lambda^2)$, and $\varepsilon_k^2 = \varepsilon_\mu(k)\varepsilon_\mu(k)$, for brevity.
Using the transformation

$$k_0 = y\cos\theta, \quad k_L = y\sin\theta, \quad k_Q = \sqrt{y}\tilde{k}_Q, \tag{C.13}$$

the integral over the global radial coordinate y in conjunction with the logarithmic derivative $\Lambda\frac{d}{d\Lambda}$ becomes trivial due to the soft cutoff identity (5.26). After evaluating the angular integral over θ and substitution $u = 1/\tilde{k}_Q^4$, we obtain

$$\delta\Sigma_L = \frac{1}{N_f}\int_0^\infty du\,\frac{1}{(1+u)^2F(u)} = \frac{0.0797}{N_f}, \tag{C.14}$$

$$\delta\Sigma_Q = \frac{1}{N_f}\int_0^\infty du\,\frac{u^2-12u+3}{(1+u)^3F(u)} = \frac{0.0214}{N_f}, \tag{C.15}$$

$$\delta\Sigma_\Delta = \frac{1}{N_f}\int_0^\infty du\,\frac{u-1}{(1+u)^2F(u)} = \frac{0.2755}{N_f}, \tag{C.16}$$

$$\delta\Xi = -\frac{1}{N_f}\int_0^\infty du\,\frac{1}{(1+u)F(u)} = -\frac{0.4350}{N_f}, \tag{C.17}$$

where in the last step we have numerically evaluated the integral over u, using the exact function $F(u)$ (C.7) which is itself a two-dimensional integral.

Alternatively it is possible to compute the corrections with the asymptotic propagator in Eq. (6.37). In this case $F(u)$ is approximated by a closed form expression and only the one dimensional integral over u needs to be performed numerically. The resulting quantum corrections are $\delta\Sigma_L \approx 0.0771/N_f$, $\delta\Sigma_Q \approx 0.0250/N_f$, $\delta\Sigma_\Delta \approx 0.2759/N_f$, $\delta\Xi \approx -0.4300/N_f$.

C.3 Soft cutoff two-loop quantum corrections

The two-loop integrals that contribute to the mass renormalization, Eq. (6.22), are given by

$$\delta\tilde{\Pi} = -\frac{(8\pi^2)^2}{N_f}\Lambda\frac{d}{d\Lambda}\int_{k,q}\frac{1}{\varepsilon_{k+q}^2\varepsilon_k^2\left|q_Q\right|^2 F_q^2}\Big[A_k^2 A_{k+q}^2 A_q + \frac{2\varepsilon_{k+q}^\mu\varepsilon_k^\mu}{\varepsilon_k^2}A_k^3 A_{k+q}A_q\Big]. \tag{C.18}$$

We use the transformation

$$\begin{aligned} q_0 &= y\hat{q}_0, \quad q_L = y\hat{q}_L, \quad q_Q = \sqrt{y}\tilde{q}_Q, \\ k_0 &= yx\hat{k}_0, \quad k_L = yx\hat{k}_L, \quad k_Q = \sqrt{y}\tilde{k}_Q. \end{aligned} \tag{C.19}$$

with $\hat{k}_0^2 + \hat{k}_L^2 = 1$ and $\hat{q}_0^2 + \hat{q}_L^2 = 1$, e.g. $\hat{k}_0 = \cos\theta$, $\hat{k}_L = \sin\theta$, $\hat{q}_0 = \cos\phi$, and $\hat{q}_L = \sin\phi$.

The global radial integral over y is trivial due to the soft cutoff identity (5.26) that reflects the cutoff independence. We then introduce the Feynman parameter t (A.5) to render the x integral radially symmetric, after the shift $x\hat{k}_{0,L} \to x\hat{k}_{0,L} - t\hat{q}_{0,L}$. Evaluating the angular integrals results in

$$\delta\tilde{\Pi} = -\frac{16\pi^2}{N_f}\int_{k_Q,q_Q}\frac{1}{\left|\tilde{q}_Q\right|^2 F(\tilde{q}_Q^{-4})^2}\int_0^1 dt\int_0^\infty dx\, x\Big\{ \frac{1}{[x^2 + t(1-t) + t(\tilde{k}_Q+\tilde{q}_Q)^4 + (1-t)\tilde{k}_Q^4]^2} + \frac{4(1-t)[x^2 - t(1-t) + (\tilde{k}_Q+\tilde{q}_Q)^2\tilde{k}_Q^2]}{[x^2 + t(1-t) + t(\tilde{k}_Q+\tilde{q}_Q)^4 + (1-t)\tilde{k}_Q^4]^3}\Big\}. \tag{C.20}$$

Using the identity (A.2) the radial x integral is evaluated resulting in

$$\delta\tilde{\Pi} = -\frac{2}{N_f}\int_{-\infty}^{\infty} d\tilde{q}_Q \frac{1}{|\tilde{q}_Q|^2\, F(\tilde{q}_Q^{-4})^2}\int_0^1 dt \int_{-\infty}^{\infty} d\tilde{k}_Q \Big\{ \frac{1+2(1-t)}{[t(1-t)+t(\tilde{k}_Q+\tilde{q}_Q)^4+(1-t)\tilde{k}_Q^4]} + \frac{2(1-t)[(\tilde{k}_Q+\tilde{q}_Q)^2\tilde{k}_Q^2 - t(1-t)]}{[t(1-t)+t(\tilde{k}_Q+\tilde{q}_Q)^4+(1-t)\tilde{k}_Q^4]^2} \Big\}. \tag{C.21}$$

Although the Feynman parameter can be evaluated, we find that numerical stability of integration is enhanced if the current three-dimensional form is used. We find that $\delta\Pi = -1.053/N_f$ with the full F, and is approximated as $\delta\Pi \approx -1.037/N_f$ with the asymptotic propagator (6.37).

Appendix D

$\epsilon_{L,Q}$-expansions for anisotropic nodal semimetals

D.1 Derivation of the RPA near the upper critical line

Here we compute the regularized bosonic self energy (C.3) for the two cases: (i) $d_L = (3-\epsilon_L)/2,\ d_Q = 1$ and (ii) $d_L = 1,\ d_Q = 2-\epsilon_Q$. The first steps are carried out for general d_L and d_Q. Using Feynman parametrization (A.5) together with the shift $(k_0, \boldsymbol{k}_L) \to (k_0, \boldsymbol{k}_L) - t(q_0, \boldsymbol{q}_L)$, the integral is rendered radially symmetric in the linear $(k_0, \boldsymbol{k}_L)$ subspace,

$$\Pi(q) = \frac{g^2}{2^{d_L}\pi^{(d_L+1)/2}\Gamma(\frac{d_L+1}{2})} \int_{\boldsymbol{k}_Q} \int_0^1 dt \int_0^\infty dy\, y^{d_L} \frac{(1-t)(q_0^2+\boldsymbol{q}_L^2) + (\boldsymbol{k}_Q+\boldsymbol{q}_Q)^2[(\boldsymbol{k}_Q+\boldsymbol{q}_Q)^2 - \boldsymbol{k}_Q^2]}{[y^2 + t(1-t)(q_0^2+\boldsymbol{q}_L^2) + t(\boldsymbol{k}_Q+\boldsymbol{q}_Q)^4 + (1-t)\boldsymbol{k}_Q^4]^2}, \tag{D.1}$$

where $k_0^2 + \boldsymbol{k}_L^2 = y^2$ and t denotes the Feynman parameter. Note that we have evaluated the angular integral over the $d_L + 1$ dimensional sphere and evaluated the surface area S_{d_L+1} using Eq. (A.4). Using the integral identity

in Eq. (A.2) we can integrate over y,

$$\Pi(q) = \frac{g^2 \sec\left(\frac{d_L\pi}{2}\right)(d_L-1)}{2^{2+d_L}\pi^{(d_L-1)/2}\Gamma\left(\frac{d_L+1}{2}\right)} \int_{\boldsymbol{k}_Q}\int_0^1 dt \Big\{ \\ \left[(\boldsymbol{k}_Q+\boldsymbol{q}_Q)^2(2\boldsymbol{k}_Q\cdot\boldsymbol{q}_Q+\boldsymbol{q}_Q^2)+(q_0^2+\boldsymbol{q}_L^2)(1-t)\right]\times \\ \left[\boldsymbol{k}_Q^2+(2\boldsymbol{k}_Q\cdot\boldsymbol{q}_Q+\boldsymbol{q}_Q^2+(q_0^2+\boldsymbol{q}_L^2)(1-t))t\right]^{(d_L-3)/2}\Big\}. \tag{D.2}$$

This integral cannot be computed in closed form so we look at two limits, first where $\boldsymbol{q}_Q = 0$, and second where $(q_0, \boldsymbol{q}_L) = 0$. The final asymptotic form of the propagator will be approximated by $G_\phi^{-1}(q) = \Pi(q_0, \boldsymbol{q}_L, \boldsymbol{q}_Q = 0) + \Pi(q_0 = 0, \boldsymbol{q}_L = 0, \boldsymbol{q}_Q)$. In the first limit, $\boldsymbol{q}_Q = 0$, the integral does not diverge for any $d_L, d_Q > 0$ and $2d_L + d_Q < 6$, and results in

$$\Pi(q_0, \boldsymbol{q}_L, \boldsymbol{q}_Q = 0) = \\ -g^2 \frac{\pi^{(3-d_L-d_Q)/2}\sec\left(\frac{(2d_L+d_Q)\pi}{4}\right)}{4^{d_L+d_Q}\Gamma\left(\frac{2+d_Q}{4}\right)\Gamma\left(\frac{2d_L+d_Q}{4}\right)}(q_0^2+\boldsymbol{q}_L^2)^{\frac{2d_L+d_Q-2}{4}}. \tag{D.3}$$

Evaluating this expression for the two starting points (i) $d_L = 3/2$, $d_Q = 1$ and (ii) $d_L = 1$, $d_Q = 2$ on the upper critical line results in the linear terms in Eqs. (6.42) and (6.43).

The integral in the second limit, $(q_0, \boldsymbol{q}_L) = 0$, is however typically divergent on the upper critical line, but upon an evaluation in $2d_L + d_Q = 4 - \epsilon_{L,Q}$ we can obtain the leading $\epsilon_{L,Q}$ behavior, i.e. the $1/\epsilon_{L,Q}$ pole. This divergence can be recovered upon first making the spherical transformation $|\boldsymbol{k}_Q|^4 = r^2$, and then expanding the integral in the limit of large r in $d_Q + 2d_L = 4 - \epsilon_{L,Q}$. The leading term $\sim |\boldsymbol{q}_Q|^{2-\epsilon_{L,Q}}/r^{1+\epsilon_{L,Q}}$ is extracted, and upon the evaluation of the integral results in

$$\Pi(q_0 = 0, \boldsymbol{q}_L = 0, \boldsymbol{q}_Q) = \\ \frac{(2d_L+d_Q-2)\pi^{(1-d_L-d_Q)/2}\sec\left(\frac{d_L\pi}{2}\right)}{d_Q 2^{d_L+d_Q}(2d_L+d_Q-4)\Gamma\left(\frac{d_L-1}{2}\right)\Gamma\left(\frac{d_Q}{2}\right)}|\boldsymbol{q}_Q|^{2d_L+d_Q-2}. \tag{D.4}$$

Evaluating the pre-factor for (i) $d_L = (3-\epsilon_L)/2$, $d_Q = 1$ and (ii) $d_L = 1$, $d_Q = 2 - \epsilon_Q$ and extracting the leading $1/\epsilon_L$ and $1/\epsilon_Q$ divergencies, we obtain the quadratic terms in Eqs. (6.42) and (6.43).

D.2 Fermion self-energy and the Vertex correction

We proceed to compute the one-loop diagrams in Figs. 5.3(b) and (c), using the soft cutoff approach. Expanding the fermion self energy diagram to leading order in external frequency and momenta we obtain the quantum corrections to the linear and quadratic momentum directions as well as to the Yukawa vertex for a general d_L-d_Q system,

$$\delta\Sigma_L = \frac{g^2}{N_f}\Lambda\frac{d}{d\Lambda}\int_k \left(\frac{1}{\varepsilon_k^2} - \frac{2(k_0^2+\boldsymbol{k}_L^2)}{(d_L+1)\varepsilon_k^4}\right) G_\phi(k) A_k^2, \tag{D.5}$$

$$\delta\Sigma_Q = \frac{g^2}{N_f}\Lambda\frac{d}{d\Lambda}\int_k \Bigg\{ \frac{G_\phi(k)A_k^2}{\varepsilon_k^6}, \left(\frac{4\boldsymbol{k}_Q^8 - 12(k_0^2+\boldsymbol{k}_L^2)\boldsymbol{k}_Q^4}{d_Q} + (k_0^2+\boldsymbol{k}_L^2)^2 - \boldsymbol{k}_Q^8\right)\Bigg\}, \tag{D.6}$$

$$\delta\Xi = -\frac{g^2}{N_f}\Lambda\frac{d}{d\Lambda}\int_k \frac{G_\phi(k)A_k^3}{\varepsilon_k^2}, \tag{D.7}$$

Here $G_\phi(k)$ is the IR order parameter propagator defined in Eq. (6.42) for the ϵ_L expansion and in Eq. (6.43) for the ϵ_Q expansion.

D.3 ϵ_L-expansion

We compute the above integrals in $d_L = 3/2$, $d_Q = 1$ dimensions with the boson propagator $G_\phi(k)$ in Eq. (6.42). Defining the radial coordinate y in the $d_L + 1 = 5/2$ dimensional $(k_0, \boldsymbol{k}_L)$ subspace, $k_0^2 + \boldsymbol{k}_L^2 = y^2$, and substituting $k_Q = \sqrt{y}x$, the y integrals can be evaluated with the soft cutoff identity (5.26), reflecting the cutoff independence. The angular integral simply gives a factor $S_{5/2} = (8\pi^{5/4})/\Gamma(1/4)$. The remaining one-dimensional x integrals can be computed analytically. Keeping the leading $\sim \sqrt{\epsilon_L}$ and first subleading $\sim \epsilon_L$ contributions for small ϵ_L, we obtain the quantum corrections

$$\begin{aligned}\delta\Sigma_L &= \frac{64\epsilon_L}{5\pi N_f}\int_0^\infty \frac{(1+5x^4)dx}{(1+x^4)^2\left(16\sqrt{2}\,x^2 + \sqrt{\pi}\,\Gamma\left(\frac{1}{4}\right)^2\epsilon_L\right)} \\ &= \frac{2^{3/4}}{5\pi^{1/4}\Gamma\left(\frac{5}{4}\right)}\frac{\sqrt{\epsilon_L}}{N_f},\end{aligned} \tag{D.8}$$

$$\begin{aligned}\delta\Sigma_Q &= \frac{64\epsilon_L}{\pi N_f}\int_0^\infty \frac{(1-12x^4+3x^8)dx}{(1+x^4)^3\left(16\sqrt{2}\,x^2+\sqrt{\pi}\,\Gamma\left(\frac{1}{4}\right)^2\epsilon_L\right)} \\ &= \frac{2^{3/4}}{\pi^{1/4}\Gamma\left(\frac{5}{4}\right)}\frac{\sqrt{\epsilon_L}}{N_f}-\frac{3\epsilon_L}{N_f}, \end{aligned} \tag{D.9}$$

$$\begin{aligned}\delta\Xi &= -\frac{64\epsilon_L}{\pi N_f}\int_0^\infty \frac{dx}{(1+x^4)\left(16\sqrt{2}\,x^2+\sqrt{\pi}\,\Gamma\left(\frac{1}{4}\right)^2\epsilon_L\right)} \\ &= -\frac{2^{3/4}}{\pi^{1/4}\Gamma\left(\frac{5}{4}\right)}\frac{\sqrt{\epsilon_L}}{N_f}+\frac{\epsilon_L}{N_f}. \end{aligned} \tag{D.10}$$

D.4 ϵ_Q-expansion

For the expansion in the number of quadratic dimensions, we compute the integrals in Eqs. (D.5)-(D.7) in $d_L = 1,\ d_Q = 2$, using the IR boson propagator given in Eq. (6.43). Defining $k_0^2 + k_L^2 = y^2$ and $\boldsymbol{k}_Q^2 = yx^2$, the y integral and the angular integrals are again trivial. Keeping the leading $\sim \epsilon_Q \log \epsilon_Q$ and first sub-leading $\sim \epsilon_Q$ contributions for small ϵ_Q, the final x integrals result in

$$\begin{aligned}\delta\Sigma_L &= \frac{16\epsilon_Q}{N_f}\int_0^\infty dx\frac{x^5}{(1+x^4)^2(8x^2+\pi^2\epsilon_Q)} \\ &= \frac{\epsilon_Q}{2N_f}, \end{aligned} \tag{D.11}$$

$$\begin{aligned}\delta\Sigma_Q &= \frac{16\epsilon_Q}{N_f}\int_0^\infty dx\frac{x(1-6x^4+x^8)}{(1+x^4)^3(8x^2+\pi^2\epsilon_Q)} \\ &= -\frac{\epsilon_Q}{N_f}\log\left(\frac{\pi^2\epsilon_Q}{8}\right)-\frac{2\epsilon_Q}{N_f}, \end{aligned} \tag{D.12}$$

$$\begin{aligned}\delta\Xi &= -\frac{16\epsilon_Q}{N_f}\int_0^\infty dx\frac{x}{(1+x^4)(8x^2+\pi^2\epsilon_Q)} \\ &= \frac{\epsilon_Q}{N_f}\log\left(\frac{\pi^2\epsilon_Q}{8}\right). \end{aligned} \tag{D.13}$$

D.5 Comparing scaling and critical exponents

When comparing to critical exponents found in the literature one must be careful about the variation in definitions of the number of fermion components N_f, and the unit length scale $z_L = 1$ or $z_Q = 1$. We discuss how to do so here.

Throughout the literature, various n-component fermions are considered, depending on the symmetry of the initial Hamiltonian. For analytic control, the generalization to N_n flavors is made. The conversion to our convention is then $N_f = nN_n$.

We have defined a unified scaling relying on the "unit length" $z_L\delta\ell$,

$$X(k) = X'(k')e^{-\Delta_X z_L \delta\ell/2}, \tag{D.14}$$

where $X = \Psi, \phi$ and $\Delta_X = [X^\dagger X] + \eta_X$ are the total scaling dimensions. Here η_X contains all order $1/N_f$ corrections by definition. We did so because in the literature there are variations in the definition of the unit length scale, either using: (i) linear $z_L = 1$ and (ii) quadratic $z_Q = 1$ momentum directions. As we found in the main text, the ratio z_L/z_Q renormalizes and so, for example, fixing $z_L = 1$ causes z_Q to renormalize with $1/N_f$ corrections.

We seek to compare to previous results in the literature, where in general the scaling is defined as

$$X(k) = X'(k')e^{-\tilde{\Delta}_X \delta\ell/2}, \tag{D.15}$$

and typically either $z_L = 1$ is fixed, or $z_Q = 1$ is fixed. When the linear momentum has been defined as the unit length scale, $\tilde{\Delta}_X = \Delta_X$, as $z_L = 1$ is fixed. Where as, for the quadratic momentum defining the unit length scale, $\tilde{\Delta}_X = z_L\Delta_X$, as $z_Q = 1$ but z_L is not fixed.

In the case $z_Q = 1$ there are subtleties in the conversion between anomalous dimensions η_X and $\tilde{\eta}_X$. To leading order in N_f we define $z_L = z_L^{(0)} + z_L^{(1)}/N_f$, then expand $\tilde{\Delta}_X = z_L\Delta_X$ and equate $1/N_f$ terms resulting in the relation

$$\eta_X = \frac{\tilde{\eta}_X}{z_L^{(0)}} - \frac{z_L^{(1)}\widetilde{[X^\dagger X]}}{(z_L^{(0)})^2 N_f}. \tag{D.16}$$

There can be other variations in scaling definitions, for example Ref. [36] defined $\tilde{\Delta}_X = \widetilde{[X^\dagger X]} + 2\hat{\eta}_X$, such that $\tilde{\eta}_X = 2\hat{\eta}_X$. We use the comparison of the order parameter anomalous dimension as a relevant example.

Appendix E

Genertion of Bosonic disorder at two-loops

Here we address the question if the electronic disorder, which are defined on the level of the quadratic fermion action [see Eq. (7.6)], can generate random mass disorder of the bosonic order parameter field at two loop order, as suggested in Refs. [2] and [3]. In the disorder averaged replica theory the electronic disorder is described by a disorder vertex that is quartic in the fermionic Grassmann fields, couples different replicas, and is non-local in imaginary time [see Eq. (7.14)]. Similarly, bosonic random mass disorder gives rise to a disorder vertex

$$S_{\phi}^{\mathrm{dis}} = -\frac{\sigma^2}{2} \sum_{a,b=1}^{n} \int d^2\boldsymbol{x} \int d\tau \int d\tau' \phi_a^2(\boldsymbol{x},\tau)\phi_b^2(\boldsymbol{x},\tau') \tag{E.1}$$

in the replica field theory, where σ^2 is the variance of the bosonic random mass disorder distribution. This vertex would be generated by the two-loop diagram shown in Fig. E.1 where the external momenta in the loop integrals are set to zero. This results in

$$\sigma^2 \sim \frac{g^4}{N^2} \sum_{i=0,x,y,z} D_i^2 \Delta_i \tag{E.2}$$

with

$$D_i = \int_{\boldsymbol{k},\omega} \mathrm{Tr}\left[G_{\Psi}(\boldsymbol{k},\omega)\sigma^z G_{\Psi}(\boldsymbol{k},\omega)\sigma^z G_{\Psi}(\boldsymbol{k},\omega)\sigma^i\right]. \tag{E.3}$$

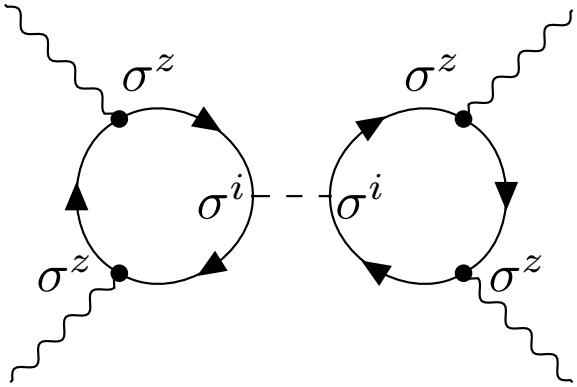

Figure E.1: The two-loop diagram that according to Refs.[2, 3] generates the bosonic disorder vertex.

It is straightforward to see that electronic random mass disorder Δ_z does not contribute since the trace over the product of Pauli matrices vanishes in this case, $D_z = 0$. In the other channels we obtain the integrals

$$D_0 = -N \int_{\boldsymbol{k},\omega} \frac{i\omega}{(\omega^2 + v^2\boldsymbol{k}^2)^2},$$
$$D_x = -N \int_{\boldsymbol{k},\omega} \frac{vk_x}{(\omega^2 + v^2\boldsymbol{k}^2)^2},$$
$$D_y = -N \int_{\boldsymbol{k},\omega} \frac{vk_y}{(\omega^2 + v^2\boldsymbol{k}^2)^2},$$

after taking the trace. These integrals are either odd in the frequency or momenta and therefore evaluate to zero. This shows that for the chiral Ising GNY theory with purely electronic disorder, the bosonic disorder vertex is not generated at two-loop order.

There are certain higher-loop diagrams that vanish for similar reasons, or after taking the Replica limit $n \to 0$. However, we don't see a general argument for why boson mass disorder can't be generated at higher-loop order. As stated in the main text, there are other ways to generate boson mass disorder, e.g. by considering disorder in the nearest neighbour fermion interaction before Hubbard-Stratonovich decoupling.

We stress that the two-loop diagrams only vanish if external frequencies and momenta are set to zero. But only such diagrams result in a boson vertex

of the form $\phi_a^2\phi_b^2$ corresponding to Replica averaged random mass disorder. Expanding out external momenta is equivalent to a gradient expansion and gives rise to additional boson vertices such $(\nabla\phi_a)^2\phi_b^2$ or $(\nabla\phi_a)^2(\nabla\phi_b)^2$, which are irrelevant under the RG.

Appendix F

Diagrams for the disordered CDW phase transtion

For the calculation of diagrams in Fig. 7.1, the following fermionic propagator is used,

$$G_\Psi(\omega, \boldsymbol{k}) = \frac{i\omega + v\boldsymbol{k}\cdot\boldsymbol{\sigma}}{\omega^2 + v^2\boldsymbol{k}^2}, \tag{F.1}$$

the momentum vector $\boldsymbol{k} = (k_x, k_y)$ is two dimensional while ω denotes the Matsubara frequency. We also use the damped bosonic propagator, the derivation of which can be found in Appendix B.1,

$$G_\phi^{-1}(\omega, \boldsymbol{k}) = \frac{g^2}{16v^2}\left(\omega^2 + v^2\boldsymbol{k}^2\right)^{1/2} + m^2. \tag{F.2}$$

In what follows, for ease of notation we define,

$$\int_{\boldsymbol{k}} = \int_{\Lambda e^{-d\ell}<|\boldsymbol{k}|<\Lambda} \frac{d^2\boldsymbol{k}}{(2\pi)^2}, \quad \int_\omega = \int_{-\infty}^{\infty} \frac{d\omega}{2\pi}, \quad \int_{\vec{k}} = \int_\omega \int_{\boldsymbol{k}} \tag{F.3}$$

F.1 One-loop corrections

Henceforth a diagram depicted in Fig. 7.1 with a subscript (x) will be denoted by $\mathrm{D}_{(\mathrm{x})}$.

The flow of the clean fermionic self-energy has been previously derived in Appendix B.2 in Eqs. (B.7)-(B.10). The first "dirty" diagram we tackle is the fermionic self-energy depicted in Fig. 7.1(b), which is given by,

$$\mathrm{D}_{(\mathrm{b})} = -\Delta_i \int_{\boldsymbol{k}} \sigma^i G_\Psi(\omega, \boldsymbol{k}) \sigma^i \tag{F.4}$$

Unlike the clean fermionic self-energy only the frequency prefactor in the fermionic sector is renormalised. This means that disorder will break the emergent Lorentz invariance of the pure GNY model. To obtain the correction we expand in ω and retain the leading contribution,

$$\begin{aligned} \mathrm{D}_{(\mathrm{b})} &= \frac{\Delta_i}{v^2}\int_{\boldsymbol{q}} \frac{-i\omega + v\boldsymbol{q}\cdot\boldsymbol{\sigma}}{\boldsymbol{q}^2} \\ &= \frac{\Delta_0 + 2\Delta_\perp + \Delta_z}{2\pi v^2} d\ell\ (-i\omega) \end{aligned} \tag{F.5}$$

The renormalisation of the Yukawa vertex coming from the four-fermion disorder term is depicted in Fig. 7.1(d),

$$\begin{aligned} \mathrm{D}_{(\mathrm{d})} &= \frac{g}{\sqrt{N}}\frac{\Delta_i}{2}\int_{\boldsymbol{k}} \sigma^i G_\Psi(0,\boldsymbol{k})\sigma^z G_\Psi(0,\boldsymbol{k})\sigma^i \\ &= \frac{2\Delta_\perp - \Delta_0 - \Delta_z}{4\pi v^2} d\ell \left(\frac{g}{\sqrt{N_f}}\right) \end{aligned} \tag{F.6}$$

where in the first line we had already set the external momenta to be zero as the Yukawa interaction is a contact one and has no momentum dependence. The integral is then trivial and the result is portrayed in the second line. The differing signs of the disorders come from the fact that the gauge field disorder anti-commutes with σ^z while the other two orders commute.

The four-fermion disorder vertex is renormalised by diagrams in Fig. 7.1(g)-(k). Tackling (g) and (h) first, we obtain

$$\begin{aligned} \mathrm{D}_{(\mathrm{g})} &= -\frac{\Delta_i\Delta_j}{2}\int_{\boldsymbol{k}} \left\{\sigma^i G_\Psi(0,-\boldsymbol{k})\sigma^j\right\} \otimes \left\{\sigma^i G_\Psi(0,\boldsymbol{k})\sigma^j\right\} \\ \mathrm{D}_{(\mathrm{h})} &= -\frac{\Delta_i\Delta_j}{2}\int_{\boldsymbol{k}} \left\{\sigma^j G_\Psi(0,-\boldsymbol{k})\sigma^i\right\} \otimes \left\{\sigma^i G_\Psi(0,\boldsymbol{k})\sigma^j\right\} \end{aligned} \tag{F.7}$$

where in the bare disorder term a Δ_i couples to $\sigma^i \otimes \sigma^i$. The sum of the two diagrams then can be computed,

$$\begin{aligned} \mathrm{D}_{(\mathrm{g})} + \mathrm{D}_{(\mathrm{h})} = \frac{d\ell}{\pi v^2}\Big[&2\Delta_\perp\Delta_z \sigma^0\otimes\sigma^0 + \Delta_0\Delta_z(\sigma^x\otimes\sigma^x + \sigma^y\otimes\sigma^y) + \\ &+ 2\Delta_0\Delta_\perp \sigma^z\otimes\sigma^z\Big] \end{aligned} \tag{F.8}$$

The remaining two one-loop diagrams that renormalise the bare disorder term, are depicted in (i) and (j). The former only contains disorder vertices,

$$\begin{aligned}\mathrm{D}_{(\mathrm{i})} &= -\Delta_i\Delta_j \int_{\boldsymbol{k}} \sigma^j G_\Psi(0,\boldsymbol{k})\sigma^i G_\Psi(0,\boldsymbol{k})\sigma^j \\ &= \frac{d\ell}{\pi v^2}\Big[\Delta_0\left(\Delta_0+\Delta_z+2\Delta_\perp\right)\sigma^0\otimes\sigma^0 + \\ &\qquad + \Delta_z\left(2\Delta_\perp-\Delta_0-\Delta_z\right)\sigma^z\otimes\sigma^z\Big]. \end{aligned} \tag{F.9}$$

We see that the gauge disorder $\Delta_\perp$ is not renormalised by this diagram as there is no $\sigma^{x,y}\otimes\sigma^{x,y}$ term. Lastly diagram (j) which mixes the Landau damped propagator and the disorder vertex.

$$\begin{aligned}\mathrm{D}_{(\mathrm{j})} &= \frac{g^2\Delta_i}{3N}\int_{\vec{k}} G_\phi(\vec{k})\ \sigma^z G_\Psi(\vec{k})\sigma^i G_\Psi(\vec{k})\sigma^z \\ &= \frac{16}{9\pi^2 N} d\ell\left(\Delta_0\sigma^0\otimes\sigma^0+\Delta_\perp(\sigma^x\otimes\sigma^x+\sigma^y\otimes\sigma^y)-3\Delta_z\sigma^z\otimes\sigma^z\right)\end{aligned} \tag{F.10}$$

F.2 Two-loop correction

The inclusion of the two-loop diagram in Fig.7.1(k) is justified on the basis that it is $\mathcal{O}(\Delta^2)$ hence contributes at the same order as the rest of the disorder diagrams considered thus far. The extra factor of $1/N_f$ is cancelled by the fermionic loop and the the damped bosonic propagator similarly cancels out the Yukawa coupling g. It's functional form is given by,

$$\begin{aligned}\mathrm{D}_{(\mathrm{k})} &= \Delta_i\Delta_j\left(\frac{g^2}{N_f}\right)\int_{\boldsymbol{k},\boldsymbol{q}}\int_\omega G_\phi(0,\boldsymbol{q})\Big\{\sigma^i G_\Psi(0,\boldsymbol{q})\sigma^z\Big\}\otimes\sigma^j \\ &\quad\times \mathrm{Tr}\Big[\sigma^i G_\Psi(\omega,\boldsymbol{k})\sigma^z G_\Psi(\omega,\boldsymbol{k}+\boldsymbol{q})\sigma^j G_\Psi(\omega,\boldsymbol{k}+\boldsymbol{q})\Big].\end{aligned} \tag{F.11}$$

Due to the nature of the diagram it is easier to compute it using a soft cut-off approach or by simply exracting the leading log divergence, as opposed to using Wilson's momentum shell scheme. With the help of of identities outlined in Appendix A, we arrive at the following result,

$$\mathrm{D}_{(\mathrm{k})} = -\frac{d\ell}{6\pi v^2}\Big[\Delta_\perp\Delta_z(\sigma^x\otimes\sigma^x+\sigma^y\otimes\sigma^y)+2\Delta_\perp\Delta_z\sigma^z\otimes\sigma^z\Big]. \tag{F.12}$$

F.3 RG equations

Finally we arrive at the final set of RG equations for the "frequency" coupling c_ω which will help us set the fermionic critical dimension δ_Ψ, the fermionic velocity v which constrains the dynamical exponent z, the Yukawa coupling g through which we calculate the bosonic critical dimension δ_ϕ, and all the disorder variances,

$$\frac{d\log c_\omega}{d\ell} = -(2+2z+\delta_\Psi) + \frac{8}{3\pi^2 N_f} + \frac{\Delta_0 + 2\Delta_\perp + \Delta_z}{2\pi v^2} \tag{F.13}$$

$$\frac{d\log v}{d\ell} = -(3+z+\delta_\Psi) + \frac{8}{3\pi^2 N_f} \tag{F.14}$$

$$\frac{d\log g}{d\ell} = -\left(4+2z+\delta_\Psi+\frac{\delta_\phi}{2}\right) - \frac{8}{\pi^2 N_f} + \frac{2\Delta_\perp - \Delta_0 - \Delta_z}{4\pi v^2} \tag{F.15}$$

$$\frac{d\Delta_0}{d\ell} = \Delta_0\left[-(6+2z+2\delta_\Psi) + \frac{\Delta_0+\Delta_z+2\Delta_\perp}{\pi v^2} + \frac{16}{9\pi^2 N_f}\right] + \frac{2\Delta_\perp\Delta_z}{\pi v^2} \tag{F.16}$$

$$\frac{d\Delta_\perp}{d\ell} = \Delta_\perp\left[-(6+2z+2\delta_\Psi) + \frac{16}{9\pi^2 N_f} - \frac{\Delta_z}{6\pi v^2}\right] + \frac{\Delta_0\Delta_z}{\pi v^2} \tag{F.17}$$

$$\frac{d\Delta_z}{d\ell} = \Delta_z\left[-(6+2z+2\delta_\Psi) + \frac{2\Delta_\perp - \Delta_0 - \Delta_z}{\pi v^2} - \frac{16}{3\pi^2 N_f} - \frac{\Delta_\perp}{3\pi v^2}\right] + \frac{2\Delta_0\Delta_\perp}{\pi v^2}. \tag{F.18}$$

It is trivial to check that the form of δ_Ψ, z and δ_ϕ given in Eqs. (7.16), (7.17), and (7.20) respectively result in the reduced set of RG equations delinenated in Eq. (7.22).